DEVELOPMENT OF A NOVEL HIGH TEMPERATURE FAN HUB DESIGN

A THESIS SUBMITTED IN PARTIAL FULFILMENT OF THE REQUIREMENTS OF THE DEGREE OF MASTERS BY REASEARCH AT THE UNIVERSITY OF HUDDERSFIELD

By

James Swinton

Director of Research: Dr Taimoor Asim

School of Computing and Engineering

University of Huddersfield

UK

May 2018

ABSTRACT

As the process temperature of a fan system increases, the amount of heat that gets transmitted to the bearings and/or motor increases. If this is not accounted for, it can lead to catastrophic failure. The main heat conduction path is through the shaft, and certain mechanisms must be considered when looking for new solutions. These include; how heat is transmitted through the shaft or increasing the thermal resistance of the shaft, and dissipating heat as it is conducted through the shaft. These aspects must always be considered in addition to the impact of the manufacturing complexity. In the present study, an existing heat dissipation arrangement is reviewed and replaced by a new hub which reduces the time taken to machine the part, and ultimately the overall cost of the product. Techniques are employed to determine in detail the manufacturability of the existing design and determining what should be done to reduce the overall cost to manufacture. Finite Element Analysis (FEA) based techniques have been adopted to simulate the stresses the model experiences under the operating loads. Computation Fluid Dynamics (CFD) based techniques have been used to numerically simulate the designs under operating conditions, and the resulting heat transfer through the shaft compared with respect to the heat dissipation properties are analysed. Currently, a special hub is utilised for high temperature applications such as within industrial ovens and furnaces in order to dissipate heat. The hub connects the impeller to the motor shaft, the impeller would be subjected to the high temperatures whilst the motor would remain below 70°C. According to Fourier's law heat transfer will take place through the shaft. The material the shaft is manufactured from and its geometric properties both affect the shafts overall temperature. Should the temperature become too high at the point along the shaft where the motor bearings sit, permeant damage will occur and result in bearing failure. The current hub utilised is designed to reduce the heat within the shaft through the use of fins. The is current hub design is quite labour intensive to produce leading to potentially unnecessary costs. Subsequently a new hub has been created that can be easily machined, thus reducing the overall manufacturing time leading to cost savings. The results demonstrate that although the new hub is less effective at dissipating heat, it provides a substantial cost reduction compared to the existing design, while substantially reducing the impact of the design on various aspects of production.

ACKNOWLEDGEMENTS

I would like to thank my supervisor Dr Taimoor Asim for this continued support throughout this process, his knowledge and patience has helped me no end. I would also like to thank Halifax Fan Ltd who provided me with the means to carry out the experimental testing.

CONTENTS

LIST OF FIGURES

LIST OF TABLES

Nomenclature

a_r	Acceleration (m/s-²)
A	Cross Sectional Area (m²)
E	Energy (J)
F_a	Force (N)
h	Enthalpy (kJ/kg)
k	Thermal Conductivity of Material (W/m K)
k_{eff}	Effective Conductivity
p	Pressure (Static) (Pa)
q	Heat Transfer (W)
r	Radius (m)
T	Temperature (°K)
V	Volume (m3)
ρ	Density (kg/m3)
ω	Angular Velocity (rad/s)
σ	Stress (N/m²)

CHAPTER 1 INTRODUCTION

Fans are used as integral parts of systems in a wide range of industries. This chapter provides an introductory discussion into the types of fans used within industry. Certain measures must be taken to prevent damage to the fan equipment when operating in harsh environments. This chapter also discusses the techniques applied to reduce the heat transfer in a system. Furthermore, this chapter looks at the design for manufacture methods that can be utilised to simplify a product with respect to its fabrication and assembly.

1.1. Introduction to fans

Mechanical fans are used to move air through a system, this is achieved through the use of a rotating assembly made up of blades. These blades usually sit within a housing that directs the airflow to improve performance. The rotation of the blades is usually generated by an electric motor, however different power sources can be used, such as internal combustion engines and hydraulic motors amongst others. Fans produce high volume air flow and low pressure, in comparison to a compressor that produces high pressure and reasonably low volumes of fluid. The first known use of a fan to provide a cooling effect to an area, in a similar way to a modern air conditioning unit, was during the 8th century. It wasn't unit the 17th century that the principles such as vacuum and airflow were established, that led to the potential for what a fan could achieve. One of the first successful recorded uses of a fan system was to draw air out from within coalmines. The adoption of steam as a power source powered the early fan systems. Once electric motors become widely available they took over as the preferred method of power. The global market for industrial fans is expected to grow in the coming years. The two main trends within the current marketplace are, technological drivers and environmental drivers. The technological drivers include, the implementation of new technology to minimise production costs. The requirement for an increase in high specification fans putting an emphasis on high quality and specialist products. In Europe the requirement for quieter fans governed by EU directives and the trend towards EC motors over traditional AC motors. The Environmental drivers governed by the Ecodesign directive, requires products to operate with greater efficiencies [1].

1.2. Types of fans used within industry

Fans are used in various applications such as, aeration, dryers, dust control, fume control, incineration, material conveying, odour control, oven exhaust, process cooling, process heat and vacuum systems are a few examples. The applications are required throughout the world, in industries such as, Chemical, Pharmaceutical, Petroleum, Oil and Gas, Power Generation and Nuclear. Fan companies have to manufacture a product that produces a high efficiency to compete within the marketplace. The two main types of fans used within industry are axial and centrifugal fans.

1.2.1 Axial Fans

Axial fans create high quantities of airflow however, the airflow created is of low pressure and require a low power input for operation. A simple example of axial fans are used as table fans. Ceiling fans, mounted in the centre of a room are axial fans that run at low speeds to provide a cooling effect. Within automobiles axial fans are used to cool the engine as part of the radiator system to prevent overheating. Axial fans can be used for cooling in small confined spaces such as inside a computer and other electrical appliances where the components need to be kept cool to prevent overheating. Axial fans are used within air-conditioning units in large spaces throughout the world.

Figure 1-1 shows how the air flows through an axial fan [2]. The air moves over the motor from the inlet with no change of direction before passing out of the outlet. In order to move air through the fan in this manner there must be a pressure difference. The impeller design must be suitable to achieve the required flow rate and efficiency. To understand this pressure difference an understanding of how the blades work must be established.

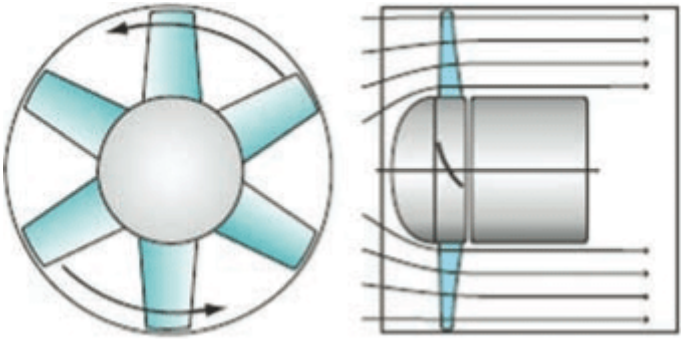

Figure 1-1, Example of an axial fan [2]

To understand the parameters of axial fans blade element theory is utilised [3]. Blade element theory divides an impeller into separate sections along its length. These sections look at the thrust and torque produced from the balance of lift and drag forces along the length. The axial and angular momentum is balanced out during these calculations. The overall resultant of the forces from these calculations can be used to predict the overall impeller performance. Whilst the theory does not account for 3D velocity of flow caused by the tip and the vortices. The thrust predictions from the theory result in a typical increase in efficiency of between 5 to 10%. However, the theory is still a reliable method for optimising the pitch of the impeller blades and for calculating the predictions of thrust and torque for a range of operating conditions.

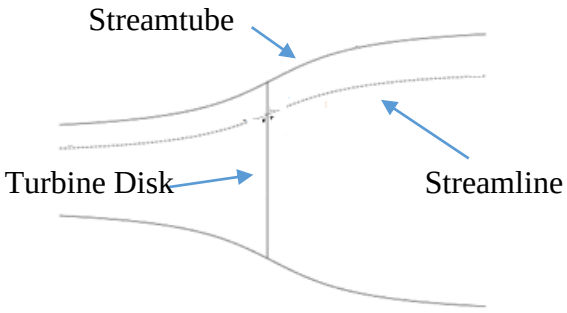

Figure 1-2, Enclosed disk in Streamtube

The theory is applied in conjunction with the slipstream theory, also known as momentum theory, which studies an enclosed turbine disk figure 1-2. The tube enclosure is assumed infinitely long in the upstream and downstream directions and all the fluid through the system passes through the turbine disk. The theory adopts some simplifications, however is useful when determining the momentum within the system. Further research can be carried out to study the rotation in the slipstream.

1.2.2 Centrifugal Fans

Figure 1-3 depicts how the air passes through the centrifugal fan. The air passes through the inlet into impeller then changes 90° within the fan casing before passing though the outlet. This is the defining characteristic of a centrifugal fan and through modification to its geometry such as to the impeller width, different pressures are able to be achieved. In general, centrifugal fans require higher power, steadier flow and higher flow rate than axial fans. Typical applications include high-pressure environments such as drying and air-conditioning. The enclosed casing section makes them a preferred choice for pollution and filtration systems. Centrifugal fans can

be used within a range of industries. Modifying the materials used for manufacture enables operation in high temperature or highly corrosive environments. An example of this is the Mineral/Aggregate industry. Fans need to be manufactured from wear resistant steels to cope with the abrasive dust that present in such an industry. Centrifugal fans can be used within the nuclear industry. For successful operation the fans are required to be gas tight to extract hazardous nuclear material. The material extracted is corrosive and toxic. These aspects are considered at the design stage and special specifications for the welding and internal surface finish are required.

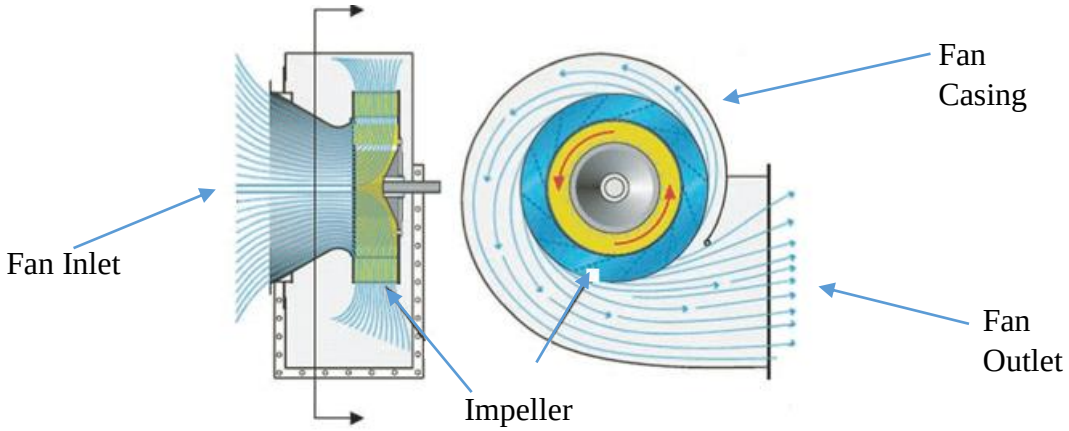

Figure 1-3, Example of a centrifugal fan [2]

Figure 1-4 depicts two types of centrifugal fan arrangement. The design principles remain the same. However, there are many variations with options such as, belt drives, variable speed drives, types of bearings and the different blade profiles allowing the fan type be used for various applications. The preference for belt driven centrifugal fans instead of conventional direct drive fans, where the impeller is mounted directly onto the motor shaft. Is due to the high stresses from the impeller that could damage the bearings in a motor. Belt drives can be used to change the impeller speed however modern technologies have enabled the variable speed drives to become much more commonplace and a simpler solution.

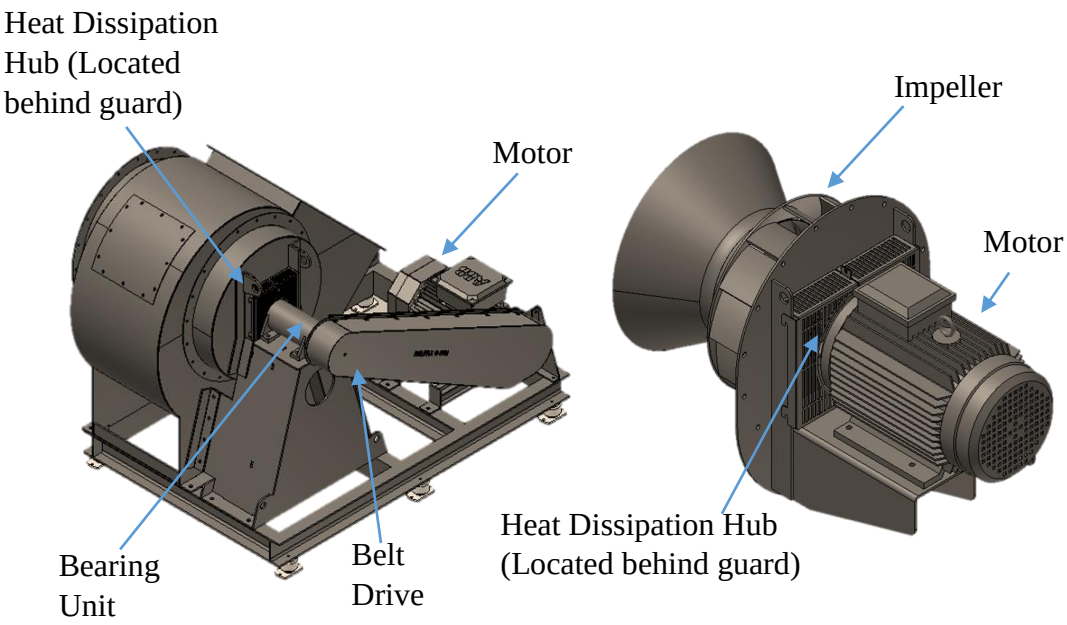

Figure 1-4, Two types of centrifugal fan, belt driven and direct drive

The variations in blade profiles enable different characteristics to be achieved. Similarly to axial fans, blade element theory is the baseline for understanding how blades effect the volume flow rate. For example, forward curved blades are used for low levels of noise and low volume flow rate with a high static pressure. In comparison backward curved blades are used for applications that require a lower pressure but higher flow rate. Different configurations of both axial and centrifugal fans can be designed to incorporate an external bearing unit to reduce the stresses on the motor shaft. However, if the medium passing through the fan were at an elevated temperature the shaft connected to the impeller will transmit some of the heat. The application of fans in high temperature environments requires the control of this heat transfer through its components. In particular, through the shaft as this connects the impeller to the prime mover which moves the high temperature gas through the system. This can cause heat transfer through the shaft and heat the motor bearings. If the phenomenon of heat transfer is not understood and equipment is designed incorrectly the outcomes can be less than desirable.

1.3. Stresses on rotating equipment

The stresses that a rotating piece of equipment such as an impeller are subjected to, arise from centrifugal forces [4]. Presents how the particles on a thin rotating disc radius r with a constant angular velocity ω are subjected to centripetal acceleration a_r in the form of:

$$a_r = -r\omega \tag{1.1}$$

The negative is due to the acceleration in the radial direction towards the centre of the disc. These accelerations create stresses in the disc through creation of inertial forces F_a and taking ρ as density:

$$F_a = -\rho r\omega^2 \tag{1.2}$$

The axisymmetric forces on the disc and the stresses due to the acceleration can be expressed in the following equation using the axisymmetric equation of equilibrium in a plane which accounts for the strain displacement relation and the stress strain laws:

$$\frac{\partial \sigma_{rr}}{\partial r} + \frac{1}{r}(\sigma_{rr} - \sigma_{\theta\theta}) = 0 \quad (1.3)$$

Replacing for the acceleration term to give the following equation of motion:

$$\frac{\partial \sigma_{rr}}{\partial r} + \frac{1}{r}(\sigma_{rr} - \sigma_{\theta\theta}) = -\rho r \omega^2 \quad (1.4)$$

1.4. Methods of reducing heat transfer in rotating machinery used at high temperatures

Both types of fans can be used in a number of the different industries, however when the fans are used at high temperatures, for successful and safe operation additional considerations must be taken into account during the design stages. As the process temperature of a fan system increases, the amount of heat transmitted to the bearings and/or motor increases. If this heat transfer is not accounted for it can lead to the bearing temperature increasing and potentially leading to catastrophic failure. The main heat conduction path is through the shaft, and certain mechanisms must be considered when looking for new solutions. These include; how heat is transmitted through the shaft or increasing the thermal resistance of the shaft, and dissipating heat as it is conducted through the shaft. These aspects must always be considered in addition to the impact of the manufacturing complexity.

Figure 1-5 illustrates a method of using an additional impeller within the system to reduce the temperature in a bearing unit. As the drive shaft rotates to move the impeller as required, the cooling impeller will also rotate and draw heat away from the shaft. Figure 1-6 shows two examples of designs used to reduce the shaft temperature in systems where heat from within the fan can travel along the shaft. One uses enclosures around the bearings that allow for ambient air to provide a cooling effect on the bearings. The other illustrates a system in which water is used to exchange heat from the shaft to reduce the bearing temperature. All three systems in figures 1-5 and 1-6 use Fouriers law of heat transfer to understand how using external air or water can reduce the heat in the shaft.

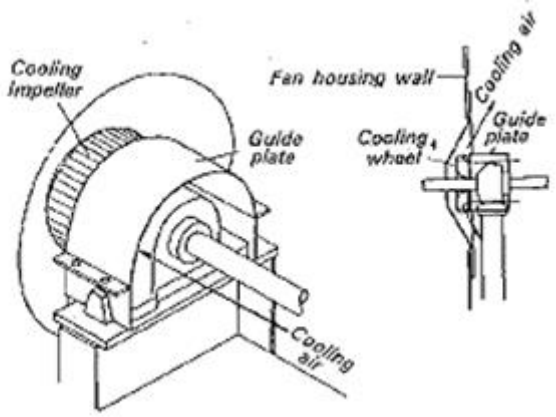

Figure 1-5, Example of a cooling impeller used to reduce the temperature in a rotating system [5]

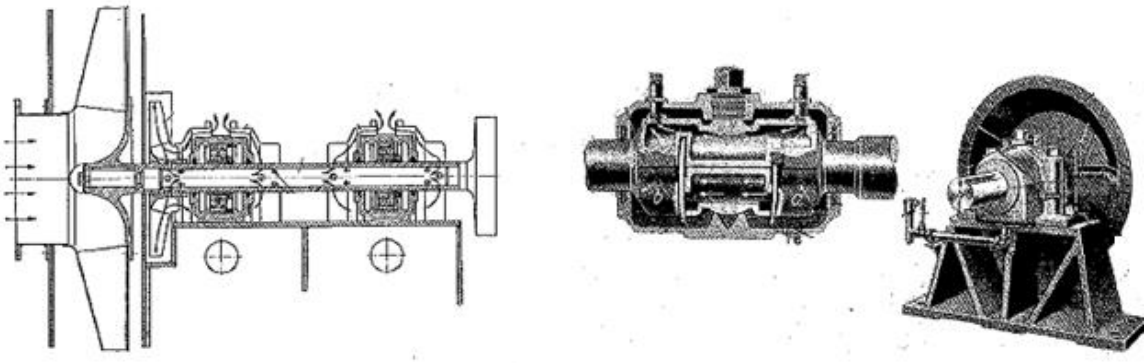

Figure 1-6, Devices used to reduce heat in shaft bearings [5]

1.5. Hub baseline design

The hub design currently utilised to dissipate heat away from the shaft of fans used in industries such as those already mentioned is depicted in figure 1-7. The hub body, hub outer and fins are manufactured from mild steel. The main features of the hub are the welded fin sections that connect the hub outer to the hub body. The design of the fins are to transfer heat away from the shaft, to reduce the heat transfer effect. The other features include, the flange section used to connect the hub to the impeller and the aluminium cooling disc. The cooling disc uses fins to allow further heat dissipation away from the shaft. This design will be referred to as the baseline model for the remainder of this study.

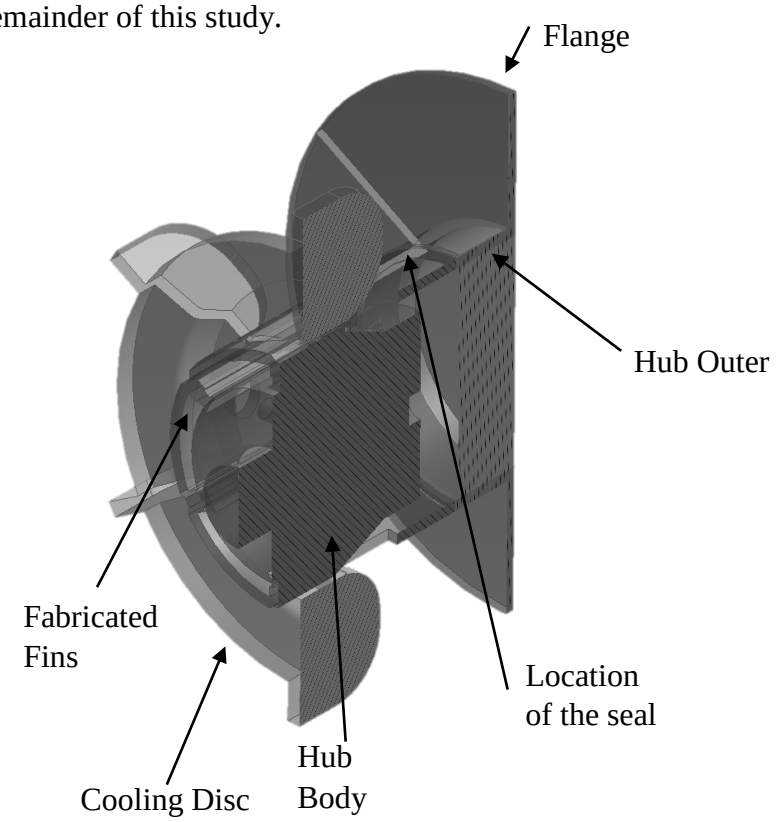

Figure 1-7, Hub baseline design

1.5. Heat Transfer Theory

The phenomenon of heat transfer through the shaft of the fan occurs due to conduction governed by Fourier's law. As stated by Bergman et. al. [6], the heat transfer rate is dependent on the variables, temperature difference (ΔT), shaft length (Δx), cross-sectional area (A) and the thermal conductivity of the material (k). The relationship is defined as;

$$q_x = -kA\frac{\Delta T}{\Delta x} \tag{1.5}$$

As Δx approaches zero,

$$\frac{\Delta T}{\Delta x} \rightarrow \frac{dT}{dx} \tag{1.6}$$

The relationship becomes:

$$q_x = -kA\frac{dT}{dx} \tag{1.7}$$

This is the general one dimensional form of Fourier's law. The negative sign is used as heat flows in the positive x direction when temperature decreases in the direction also.

The thermal conductivity indicates the rate at which energy is transferred by diffusion, it varies with molecular and atomic structure. Solids are comprised of free electrons and atoms joined together in a lattice. Thermal energy can be transported in two ways; the movement of any free electrons and vibration waves in the lattice. In pure metals, free electron movement is understood to be the main factor in which energy is transferred, whereas in nonconductive and semi conductive elements energy is transferred across the lattice vibrations.

1.6. Designing for manufacture

The purpose of designing for manufacture is to reduce the overall cost of a product, whilst at the same time improving the time taken to make, thus creating a product that can be priced competitively and operate effectively. Traditionally a sequential method is used when designing a product stating that the manufacturing costs are spilt into, Labour (direct and indirect): 2-15%, Materials and processes: 50-80% and Overheads: 15-45% [7]. Additionally, research finds that the costs to design a product require 10% of the budget but 80% of the manufacturing costs are determined by the products design. This would mean that the design of a product cannot affect the manufacturing costs of a product by more than 20%. This shows the limitations in the traditional sequential design approach. Figure 1-8, depicts the design for manufacture method as a flow chart. In comparison to the sequential method the design for manufacture method is more detailed. Companies of considerable size and stature have adopted this way of developing products, tailoring the guidelines to suit their particular needs. There are examples where companies have achieved: reductions in assembly by 61%, 53% reduction in assembly tasks, reducing defects from assembly by 68% and decreasing time to market by as much as 50% [7].

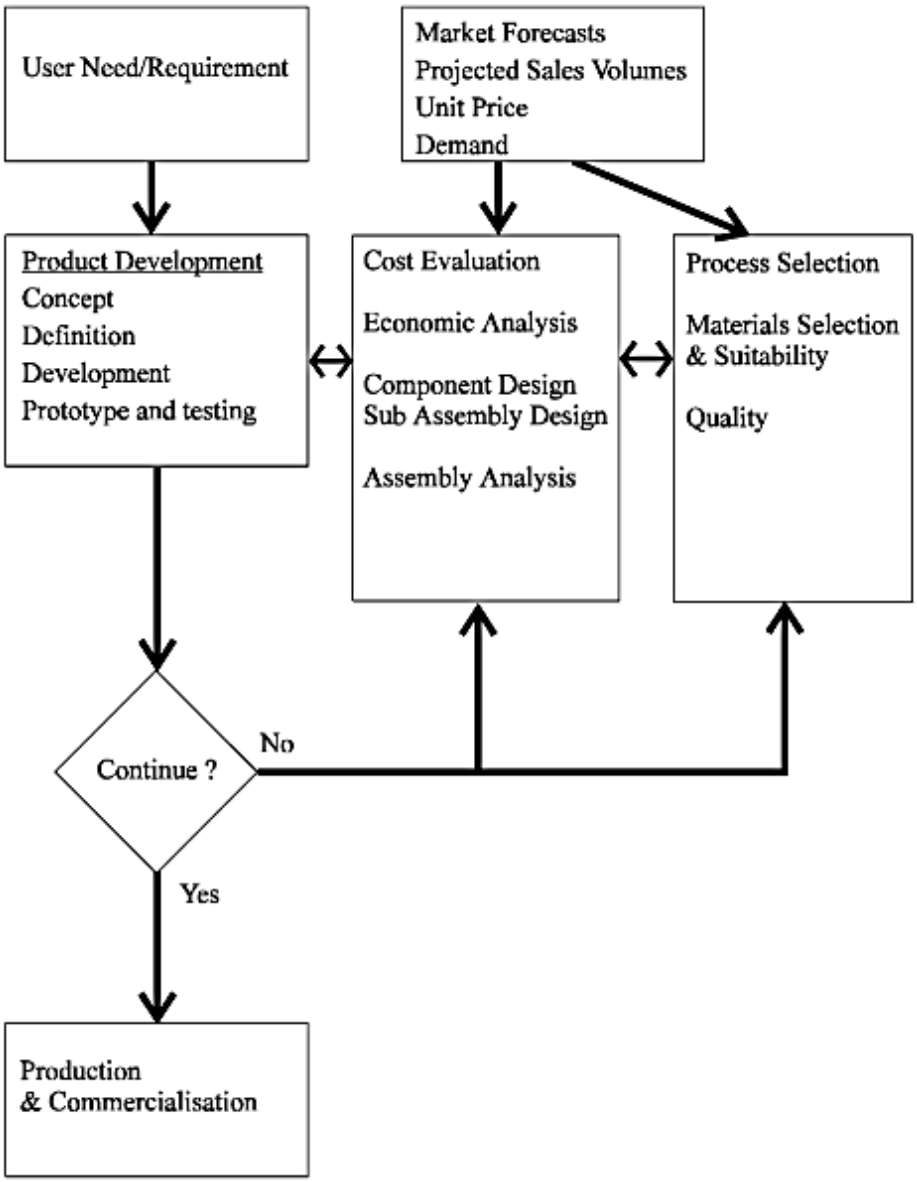

Figure 1-8, Design for manufacture method flow chart [7].

1.7. Motivation of the work

The baseline model utilised for industrial high temperature fan applications to dissipate heat from the shaft. It is known to operate effectively in high temperature environments. This is achieved through its design but also when used in conjunction with a cooling disc. However, the design of the hub is known to be difficult to manufacture and has a large number of individual parts. One way to reduce the assembly and fabrication time would be to reduce the number of parts required for manufacture. Moreover, the creation of a new hub will involve analysing its stress and thermal properties to establish its suitability. To achieve this an understanding of high temperature applications, stress analysis and design for manufacture is required. The present study will look to create a new hub that is easier to manufacture and is suitable for use in high temperature environments.

1.8. Research aims

The primary aim of the study is to create with respect to the design for manufacture principles, a new high temperature heat dissipation hub used within a fan system. The aim of the study is to look at the thermal efficiency of an existing hub design using CFD and determine its effectivity. Moreover, a stress analysis is to be carried out to determine the effect the operational loads has on the model. Subsequently how long it takes to manufacture the hub and the costs associated with this are to be analysed. From this a novel design will be created to reduce the manufacturing time and costs but also assess the products capabilities with regard to dissipating heat. The research aims are to;

1. To investigate the structural and thermal characterises of a high temperature fan hub.
2. To develop a novel design of high temperature fan hub based on design of manufacture.

1.9. Organisation of thesis

Chapter 1 provides an overview of fans, their applications and the problems faced when operating at high temperatures. From this discussions are led into the motivation for carrying out this study is given, identifying the areas to cover in chapter 2

Chapter 2 consists of a literature review carried out in the areas of structural design analysis, thermal design analysis and mechanical design analysis. This forms the scope of research and the research objectives.

Chapter 3 documents the experimental and numerical simulations carried out.

Chapter 4 discusses the results gained from the simulations and the experimental analysis.

Chapter 5 uses design for manufacture methods to create a new hub design that is then compared to the baseline model with respect to the numerical and experimental work carried out.

Chapter 6 concludes the findings from the study, stating the achievements made and recommendations for future work.

CHAPTER 2 LITERATURE REVIEW

After gathering information on methods of reducing the heat in a rotating assembly and designing for manufacture in the previous chapter, this chapter presents a detailed literature review to highlight the gaps in the current knowledge of the existing literature. Exploring published works on high temperature fans, furnaces and other rotating machinery operating at high temperatures. Moreover, works relating to the method of design for manufacture are explored. From this literature review the research objectives for this study have been identified.

2.1. Introduction

The requirement to understand heat transfer through a body is crucial as an under appreciation can potentially lead to failure of components. Environments that demand such an understanding are found within a range of industries. The industries that use technologies such as furnaces, boilers, turbines, ovens and industries such as process utilities that use compressed air, water cooling and industrial gases. Design for manufacture and design for manufacturing assembly are two methods that are adopted when trying to reduce the overall cost of a product. This is carried out throughout the industry using various methods.

2.2. Structural Design Analysis

Rotating impellers are subject to centrifugal forces. If these forces are not understood there is the potential they can lead to failure especially if the impeller is at elevated temperatures. To understand this and put preventative measures in place the theory must be understood. Sharma et. al. [8] explores the thermoelastic field in a thin circular disc. The forces due to the inertia from the disc's rotation and a thermal load are assessed. They base their research on the axisymmetric equations and the thermoelastic theory to solve the problem using a finite element analysis. The study finds that the thermostatic field is significantly affected by the temperature applied to the model. Going forward this data will be used to optimise the disc design to create a circular cutting disc or grinder.

Wong et. al. [9] uses the finite element analysis method to improve an axial impeller blade geometry with respect to the stresses it is subjected to. Predictions for stress and displacement are made and successfully achieved using Finite Element Analysis FEA. The impeller blades used within the study are complex and take significant time to design. The use of FEA enabled time and cost savings as predictions for stress and displacements can be achieved computationally, instead of designers creating physical models for experimental testing. The author was able to achieve an optimum hollow blade profile with the option to manufacture the blade from a variety of materials. Some of the different impeller designs created are depicted in figure 2-1.

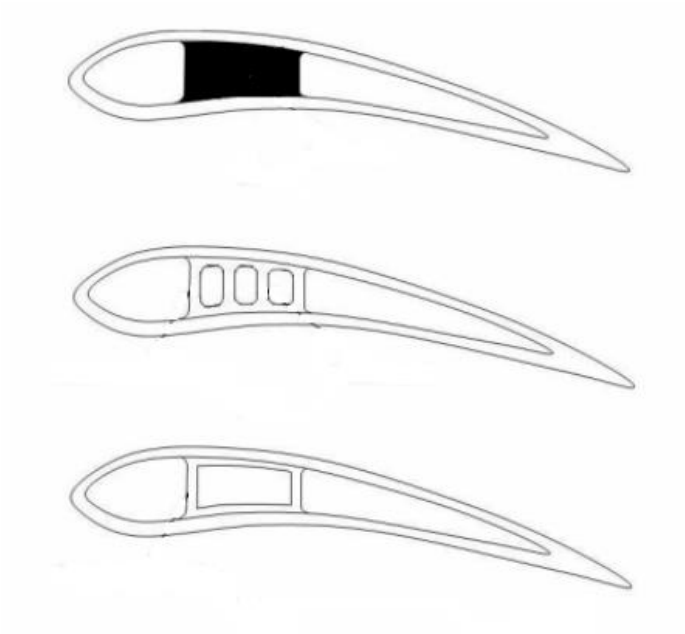

Figure 2-1, Different blade structures investigated

Poirier et. al. [10] explored how cutting discs are limited by their critical speed, which is affected by heating the disc. To try reduce this, shape memory alloys are investigated using FEA to attempt to stiffen the disc as the heating effect occurs. The study finds the composite memory alloys are better suited than the conventional steel used. The author incorporated the shape memory alloys in the disc design and achieved a thinner disc can be used whilst operating with similar fundamental frequencies.

Rajanand et. al. [11] uses FEA as part of a design methodology to analyse the impeller of a centrifugal pump. The impeller is currently manufactured from mild steel. Assessing the impeller at normal operating rotational speeds using FEA alternative materials can be selected to improve fatigue strength and wear resistance. The analysis carried out determined that the maximum displacement of the mild steel impeller is 0.002839 mm, this is deemed acceptable. The maximum stress was calculated as 12.043MPa well below the maximum allowable stress for mild steel. The results found that the low levels of stress and displacement mean a change in the impellers material to stainless steel can be achieved. This gives the overall impeller a reduction in weight of 1.28% reducing bearing loads.

2.3. Thermal Design Analysis

Researchers have analysed how changes to the shaft speed, fin arrangement and fin thickness affects the heat transfer through a system and away from a shaft. Zainullin et. al. [12] carried out experimental investigations on a furnace fan to determine how changing fan speed and enclosing the shaft from its surroundings affects the heat transfer from the shaft. This type of problem is faced by industries utilising fans within furnaces. In which the cooling effect must be great enough to prevent damage to the fan components, in particular the bearings. Furthermore, the measures used to achieve the desired cooling effect must not result in a process that produces a product of lower quality. The results indicate a heat transfer coefficient of 40-60% higher for a shaft that was open and rotating compared to an enclosed stationary shaft. Furthermore as the shaft speed increases from 100 to 600rpm, the bearing temperatures

fall considerably. Figure 2-2 shows the arrangement of the test apparatus used for the experimentation. The layout of the apparatus is very useful in understanding how the experimentation was carried out and aspects of it can be used for this studies experimental work. Table 2-1 details the apparatus used. There are a number of aspects to the apparatus that this study could use to test the baseline model experimentally. One aspect that would be improved upon is the number of temperature readings taken. Zainullin et. al. only takes two readings on the shaft, whilst this might be adequate for their work it would useful to know the temperature on other areas of the apparatus also.

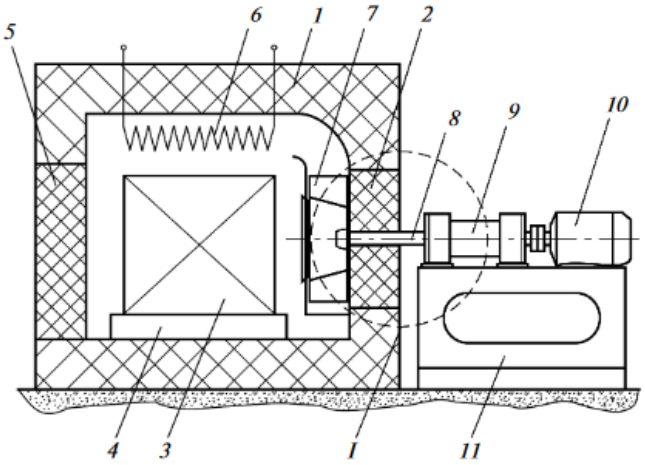

Figure 2-2, Apparatus used [12]

Table 2-1 Breakdown of the components used for experimentation [12]

Label Number	Component
1	Heat-insulated housing
2	Heat insulating wall (Plug Section)
3	Heated Body
4	Body Support
5	Charging gate
6	Heater
7	Fan Impeller
8	Shaft
9	Bearings
10	Electric Motor
11	Pedestal

Using finned sections mounted to a shaft Aziz et. al. [13] investigated solutions for rotating radial fins to determine the thermal performance of the fins by losing heat by convection to its surroundings. The study theoretically analysed using homotopy to determine the effect fin thickness has on the results. Figure 2-3 depicts the effect the conventional fin parameter, C1 has on the temperature distribution of a rectangular fin design. The increase in C1 reflects an increase in the heat transfer coefficient. The paper goes on to determine that as the rotational

speed increases the temperature distribution in the fins also increases. Moreover, as the rotation increases the heat transfer coefficient increases and the temperature in the fins decreases.

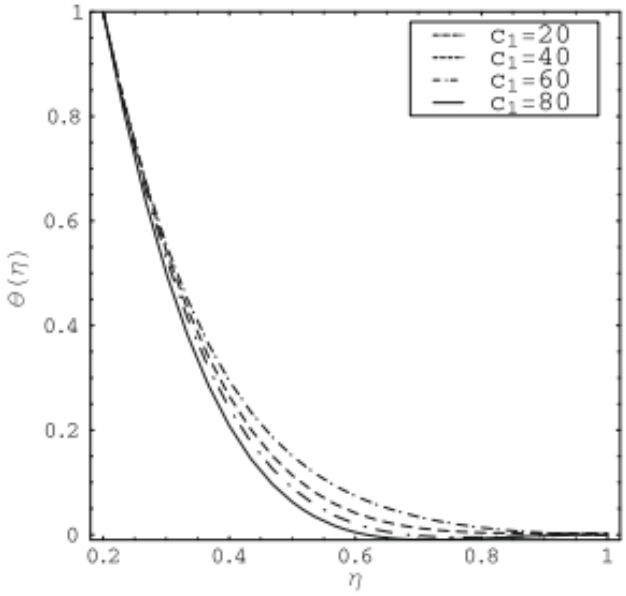

Figure 2-3, Temperature distributions for a rectangular fin in rotation [13].

Watel et. al. [14] analyses the effect of fin cooling experimentally using infrared thermography. The study explores how the rotational speed and fin spacing affect the heat exchanged in a finned tube. The experimental testing on the finned tube is carried out at rotational speeds between 50 to 3200rpm. The results from the experimental testing found that a reduction in the fin spacing resulted in a decrease in the Nusselt number, due to the boundary layers interacting and the resulting reduction in velocity between the fins. Confidence in the results is gained from their similarity to other studies, giving the results validation.

Xie et. al. [15] experimentally studied a rotating and a stationary heat pipe in a condenser to investigate how the temperature in the pipe changes due to the rotation. By measuring the temperature at five points along the shaft using infrared thermocouples, it was possible to determine that when using the rotating shaft the temperature difference between the condenser and the shaft was reduced to almost zero, opposed to the stationary shaft whose temperature was much higher. The analysis was carried out experimentally only, in order to refine and improve their design the use of Computational Fluid Dynamics CFD would be very advantageous to provide results at a faster rate. Mori et. al. [16] presents a CFD analysis of heat transfer on rotating blades. The boundary conditions represented real world characteristics that the geometry would be experience in practice. The results were verified experimentally using infrared thermography to study the temperature distribution. The method developed from the work can be used in other rotating machinery examples where accessing the object to gain readings is problematic.

Gai et. al. [17] explores a method of cooling a shaft of a traction motor by flowing water through a hole in the centre of the shaft. The heat transfer coefficient is estimated from CFD analysis and the results from two turbulence models compared. They draw on the conclusion that the rotational speed of the shaft can significantly increase the heat transfer through the

shaft. In a study by Mahesh et. al. [18] analysis is carried out on the flow and heat transfer analysis of variable diameter circular pillar disc brake rotor using CFD and experimental testing. Taking different diameters and configurations of car disc brakes the report looks at how effective the different designs are at dissipating heat.

One area of study for consideration when carrying out analysis of a design at elevated temperatures, are how the mechanical properties of that material are affected from being subjected to those temperatures. Heidarpour et. al. [19] looked at how the mechanical properties of very high strength steel compared at elevated temperatures. The yield strength, ultimate and 0.5, 1.5 and 2.0% strain compared with known values from literature. This was carried out experimentally with the results obtained not matching predictions made by the Australian and American standards used for comparison. Reasoning is given for this as the process used in the manufacture of the test pieces but equations are proposed for high strength steels that can be used to predict future outcomes successfully.

Sultan [20] developed a model for predicting one dimensional heat transfer through non-insulated unloaded steel-stud gypsum board wall for the National Fire Laboratory. The paper assesses the predictions made compared to the measurements taken at various locations on the wall assembly. The model developed is only able to predict conservative measurements in comparison to the experimental data. In a similar study Belhocine et. al. [21] analysed the thermomechanical behaviour of brake disc pads during the braking phase of operation using Ansys 11. The purpose of the analysis is to determine an optimal method of keeping the temperature as low as possible when in operation. The finned section of brake disc used to provide ventilation, was shown to provide good resistance to temperature. This was compared to a none ventilated disc. Moreover, three types of cast iron were simulated to assess their thermal behaviour. The results found the temperature and stress fields increased together during the braking phase. The results determined the most suitable cast iron to manufacture the discs from, this was FG 15. Cracks had occurred when the pads are in operation leading fractures, the results for stress back agree with this and other results from previous literature. The study did not validate the results experimentally, which would be required to take the research further.

Megherelu et. al. [22] carried out a numerical study of the cooling in the shaft of a gas turbine. The study explored the effects of conduction and convection on the turbine blades and how the heat is transferred to the shaft. To provide a cooling effect on the shaft to prevent damage to the turbines components, a secondary air flow path is introduced. A number of geometrical configurations and materials were analysed to study the secondary air path, to try and prevent too great heat transfer. The results found that a reduction in the thermal conductivity coefficient and increasing the inlet pressure had a significant effect on the peak temperatures. Changing the rotational speed of the turbine had a greater effect on the overall temperature distribution. From the study a most efficient configuration of the factors mentioned was found. Furthermore, additional research could be carried out to optimise the materials used for the manufacture of the turbine. To further improve the heat transfer.

Chai et. al. [23] investigates the temperature field of a high power motor using CFD. A method is presented for creating an accurate model to calculate the thermal conductivity in the model, with the results verified experimentally. The main method of cooling is an air gap, the optimum length of this gap was studied and determined. During the analysis of the air gap, if the gap length became too great the effect on motor cooling showed a significant reduction. The results provide a good reference for design of this gap.

2.4. Mechanical Design Analysis

Engineering design forms a key part of the product development process. It is where the products characteristics are defined enabling it to carry out its required task successfully. Pahl et. al. [24] divide engineering design into four categories, Planning and clarification of the task, Conceptual design, Design embodiment and Detail design. The initial stage of Planning and clarification is carried out to determine all the known information of the task at hand to establish the problem to solve and any constraints to achieve this. The Conceptual design stage is used to create ideas that can be used to solve the problems that arose during the Planning and clarification stage. The most promising ideas are progressed through the remaining engineering design process. Design embodiment looks at developing the initial ideas created, into solutions that can be applied into working design. This leads onto Detail design which takes the design created and prepares it for manufacture.

Design for manufacture (DFM) and Design for manufacture and assembly (DFMA) are processes and methods that develop a product to reduce the overall cost or improve reliability, without compromising functionality. These processes and methods would be utilised throughout the engineering design procedure. For successful implementation a collaboration between the design and manufacturing teams must be reached. Venkatachalam et. al. [25] carried out a knowledge based approach to design for manufacturability. This developed a rule-based system that has the ability to be used for; process selection decisions based upon parameters set by design and production to achieve a cost-effective manufacture and to estimate costs of manufacturing from the processes identified. The processes they considered are casting and forging techniques for the primary and the secondary processes such as milling and drilling. From these processes they are able to estimate costs in addition to the manual assembly tasks, to give an overall cost. Figure 2-4 details the DFM approach used in the study, the chart shows how the types of manufacturing processes lead to manufacturing the proposed design in a cost effective manner.

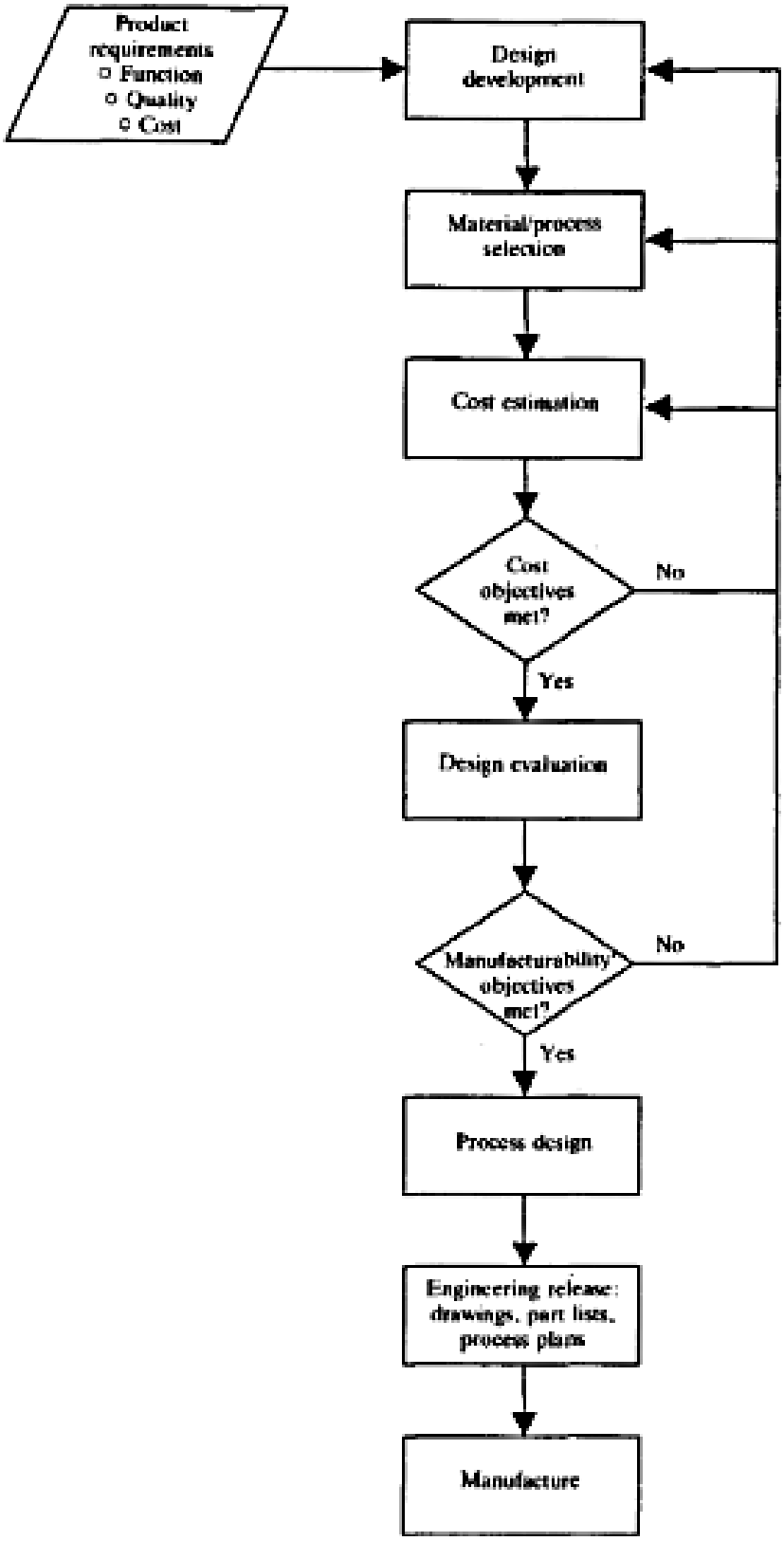

Figure 2-4. Design for Manufacture approach [25]

In a separate study from Venkatachalam et. al. [26] titled Automating design for manufacturability through expert systems approaches. The design phase of developing a product accounts for an estimated 70-80% of the product cost, with the remaining 20-30% decided during the actual production. It is therefore crucial that the issues with product design are addressed within the design phase to maximise profitability.

The design for manufacture principles can be applied to a wide range of products that require the process to be undertaken. A study by Weiss et. al. [27] used DFMA principles to redesign a product used for shredding fruit. They incorporated customer feedback into their design, allowing for potential oversights to be captured and addressed before final manufacture. This user feedback enabled higher user satisfaction and resulted in a product with: a reduced number of parts, easier to maintain and build. The result of the DFMA carried out led to a reduction of 42% in the cost of the product.

A study by Kerbrat et. al. [28] explored a number of machined products from within the automotive industry. To test their methodology of evaluating the machined products current manufacturability and comparing to using an additive manufacturing process, such as selective laser sintering or laser deposition. Initially the analysis carried out determines the difficulties that arise when manufacturing each part, an example in figure 2-5 depicts how the different geometry can vary in difficulty to manufacture. The hybrid modular design methodology presented focuses on the difficult areas to manufacture allowing the designers to decide on a one piece or modular hybrid design.

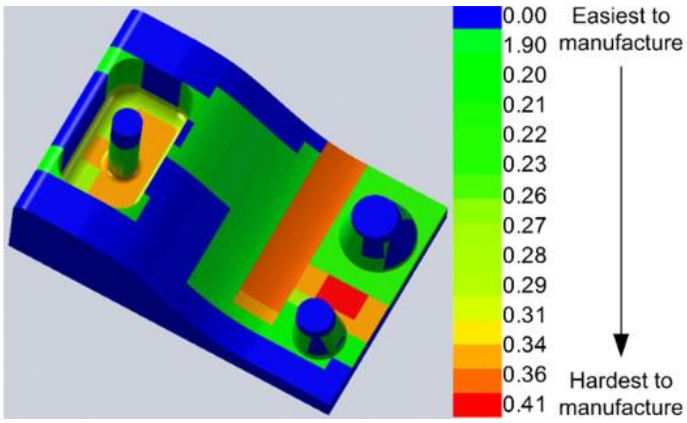

Figure 2-5. Complex areas of a part to manufacture [28]

Ong et. al. [29] uses the DFM principles and applies them to the machining of rotational parts to develop a fuzzy set AHP-based tool. The algorithm formulated gives designers a greater understanding of the machining required for the features within their design. The Manufacturability Indices (MIs) developed can be utilised for the three main components when machining a part: the support index, the clamping index and the feature index. The introduction of an analytic hierarchy process (AHP) enables the assigning of factors with relation to their importance within the function they are providing. The use of fuzzy set representation and reasoning is utilised to select the support method and type of operation to generate MIs. This use of MIs instead of measuring cost or time improves the efficiency of the system by removing factors affected by economics.

G.Boothroyd [30] discusses two examples of how design for assembly can achieve cost savings by improving the products design. One example is a small sheet metal assembly that is manufactured in large numbers, the assembly costs form a large percentage of the total build cost. The design for assembly analysis showed that large cost savings can be made as a result of the new hub created. Another example discussed is larger assembly made up of solid machined parts manufactured in small quantities. The main point for discussion regards the relatively few number of parts that used for the assembly, making the overall assembly cost not appear noteworthy. The point is made however that through product simplification from the resulting DFA methods and ideas applied that significant savings can be made. Figure 2-6 depicts the savings made with regard to the overall cost of the product, through the use of DFA methods.

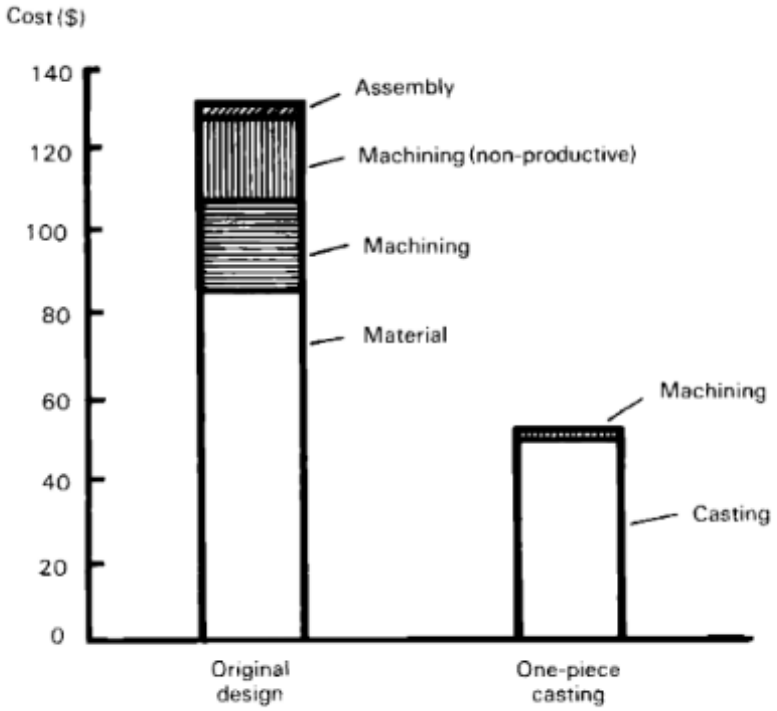

Figure 2-6. Changing a complex part to a One-piece casting can reduce the overall cost of a product, by reducing the manufacturing processes [30]

Ashley [31] explored ways in which Douglas Commercial Aircraft reduce costs by using DFMA principles and techniques. They discovered that the costs for, assembly, fabrication, quality assurance, inventory levels, tracking and purchasing are all governed by the number of parts in company products. The adoption of DFMA techniques highlighted to designers how the company's existing parts can be simplified. One study carried out simplified the aircraft door assembly, a product known to be difficult and time consuming to manufacture and install. This was achieved by reducing the number of parts in the assembly by 36%, leading to a 34% reduction in the number of assembly procedures. The team at Douglas Commercial Aircraft applied the DFMA principles to a number of other company products, including the waste pipe and harness assembly shown in figure 2-7. By utilising the DFMA principles the number of

parts was reduced from 15 to 3 and the resulting assembly operations cut from 210 to 8. The original assembly took 46 minutes to fully assemble, the new hub reduced this figure to 3 minutes. The original product design cost the company $64.01 the resulting cost of the new hub, $4.74.

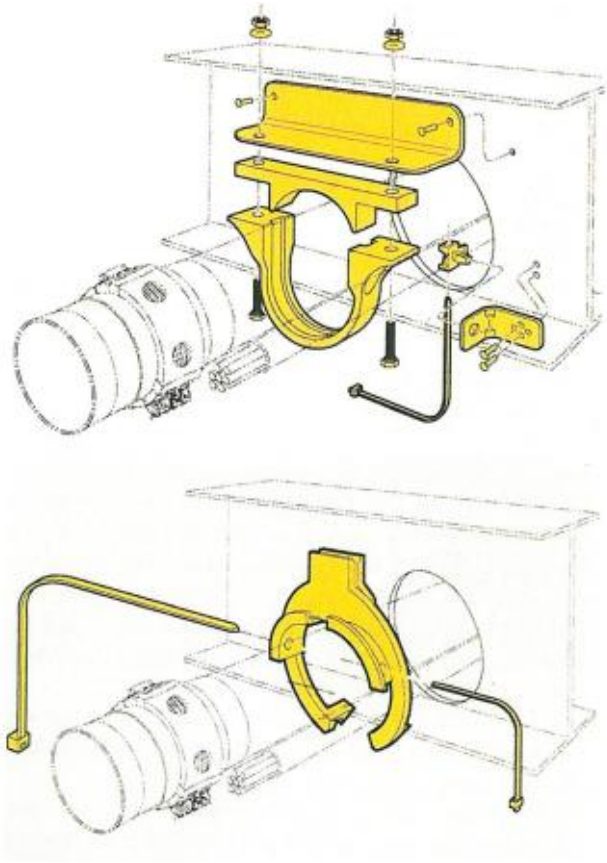

Figure 2-7. Comparison between the number of parts used in the original waste pipe and harness and the design created using DFMA principles [31]

Gerhardt et. al. [32] reviews successful DFMA in the portable compressor division at Ingersoll-Rand. One of the company products selected to be redesigned was a control and instrument panel assembly. The original design comprised of 36 parts and 24 fasteners. This required 45 assembly operations and an assembly time of 8.5 minutes. Table 2-2 presents these values and the gains made from the DFMA process. The reductions in the number of parts, fasteners, assembly operations and overall assembly time, is achieved through the simplification of the product. Figure 2-8 depicts how the previous design of the instrument and control panels were separate entities. The new hub, also shown in figure 2-8 combines the two panels together, creating significant savings with respect to the number of parts used.

Table 2-2 Comparison of the control and instrument panel assembly at Ingersoll-Rand following DFMA.

	Original Design	DFMA Revision	Percentage Gain
Number of Parts	36	24	33%
Number of Fasteners	24	15	38%
Assembly Operations	45	30	33%
Assembly Time (Minutes)	8.5	6.1	28%

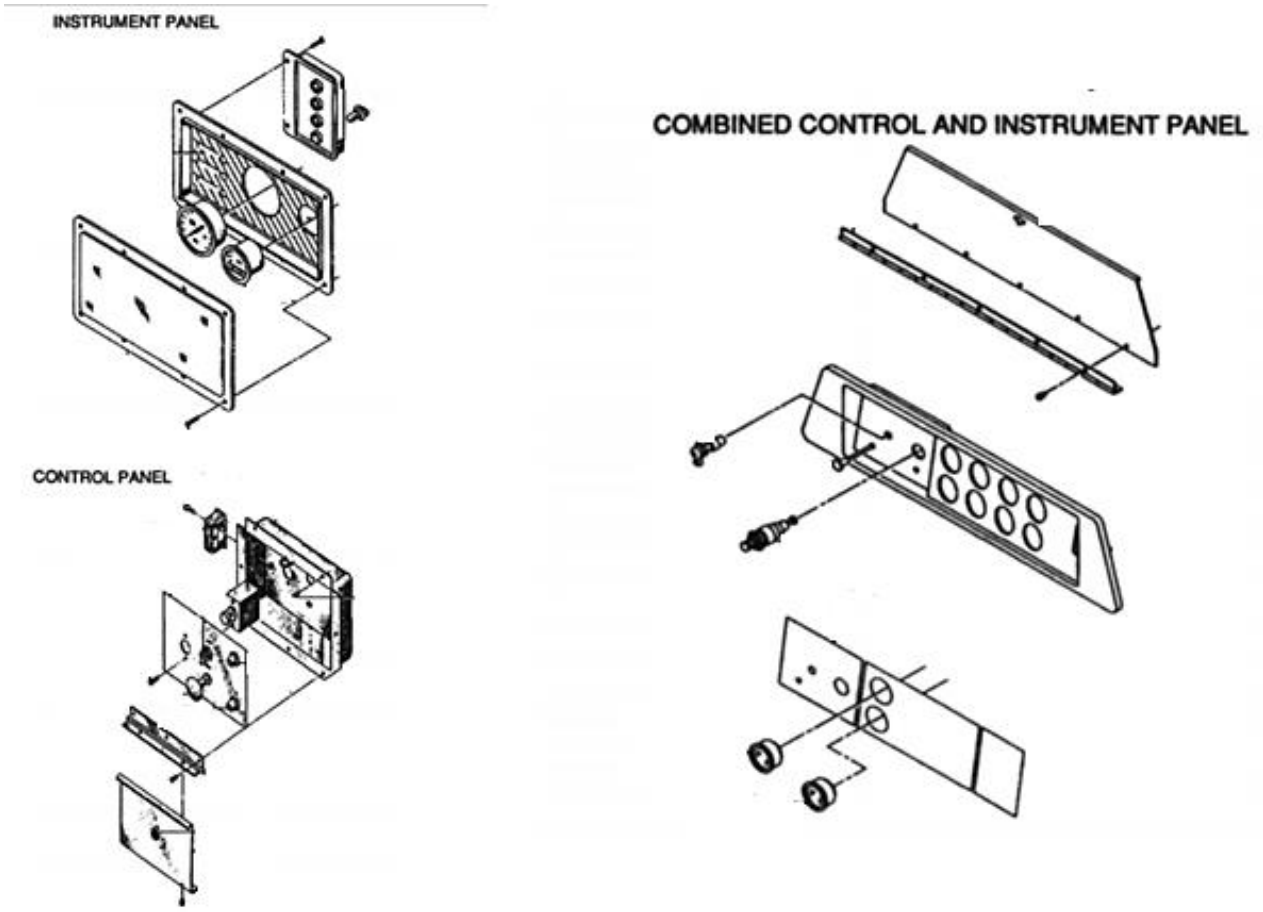

Figure 2-8. Reduction in the number of parts used by combining the instrument and control panels [33].

2.5. Summary of Literature Review

Based on the literature review for the structural, thermal and mechanical design analysis, it can be summarised that there is a substantial knowledge within these areas. The areas of using FEA to determine the stresses and displacement on rotating apparatus provided resources, proved to provide a number of resources. This research can be used as a starting point to carry out the required FEA on the baseline hub model. Substantial knowledge is available within the field

of using apparatus to dissipate heat away from rotating shafts. The majority of examples found use fins in various arrangements and have calculations that are able to support their findings. Potential areas lacking in knowledge are the direct application of heat dissipation products for use in fan environments. Studies into using design for manufacture and design of manufacture assembly, are plentiful enough to again provide a starting point for the research. With the methods from the research being able to be applied directly to the present study. All three areas provide an excellent starting point that will allow the development of a novel hub design.

2.6. Scope of Research

A large body of research has been carried out experimentally, making certain aspects within models difficult to monitor. Moreover, experimentation of new hubs such as those created using techniques like DFM and DFMA, have to be manufactured before testing. With the availability of modern computational methods and tools, it is possible to study the heat transfer of prototyped rotating components in greater detail.

Based on the review of published literature, important areas of research have been found regarding the heat transfer in rotating systems. The first two main areas of this study will explore the stresses and thermal properties of the baseline high temperature hub design. The third key area of research for this study is the effect operating speed has on the high temperature fan hub. This will consider the stresses generated and the heat transfer characteristics during these speeds. The fourth and fifth key areas of research for this study is to carry out a design for manufacture study of the high temperature fan hub. This is to develop a new hub that will be easier and more cost effective to manufacture.

2.7. Research Objectives

1. To carry out stress analysis of a baseline high temperature fan hub design

2. To carry out thermal analysis of a baseline high temperature hub design

3. To investigate the effects of the operating speed of a high temperature fan hub on its structural and thermal characteristics

4. To carry out a design for manufacture study for high temperature fan hubs and develop an innovative hub design

5. To establish the design superiority of the new hub design compared to the baseline design

To complete the research objectives stated, this study will utilise computational analysis tools to explore the stress, displacement, natural frequencies and the thermal properties of the baseline model. The next chapter presents the techniques used for this numerical modelling.

CHAPTER 3 EXPERIMENTAL AND NUMERICAL MODELLING OF HIGH TEMPERATURE FAN HUB

The research objectives identified in the previous chapter of this study require the use of CFD, FEA and experimental techniques to determine the heat transfer through the hub model. To achieve this the correct boundary conditions and solver settings are detailed and discussed within this chapter. The use of these techniques allows for the development of a model that meets the design and manufacturing requirements.

3.1. Experimental Modelling

The diagram shows the main components of the rig. Located within the main housing is a heater that heats the air inside the housing to the required temperature, up to 400°C. In addition to the heater located inside the casing, sits a small impeller. The design of the impeller is very basic and used solely to circulate air internally within the casing, to maintain and evenly distribute heated air. The impeller is connected to a drive shaft that provides the rotational movement using the hub. A section of the hub remains within the casing but a section, along with the shaft is external to the casing. To prevent hot air escaping a seal is used. The hub is connected to a cooling disc, which as already discussed draws heat away from the shaft through its use of fins, the shaft then passes through a dummy bearing unit.

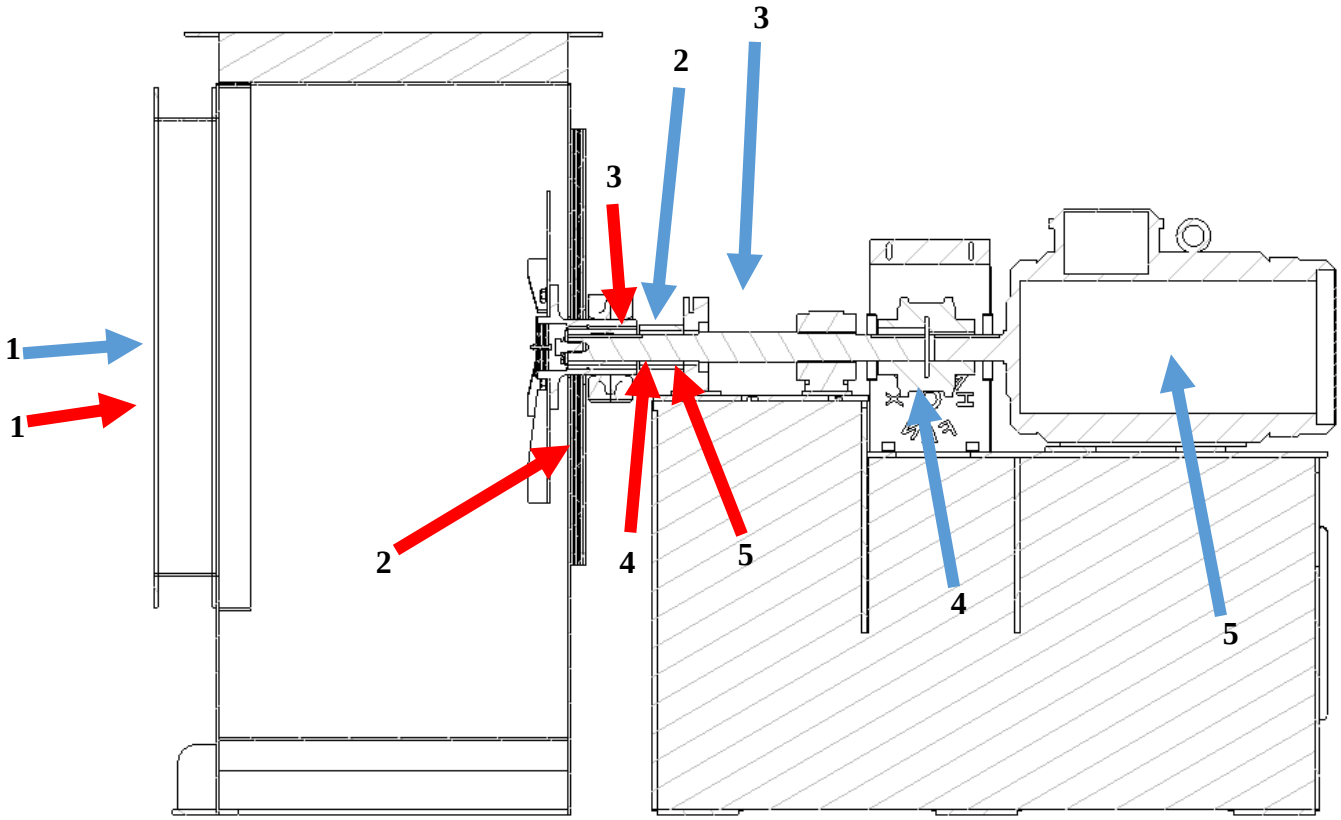

Figure 3-1. Test rig used to validate CFD results depicting locations of components used and the locations of the temperature readings taken (blue arrows) and locations of temperature readings (red arrows).

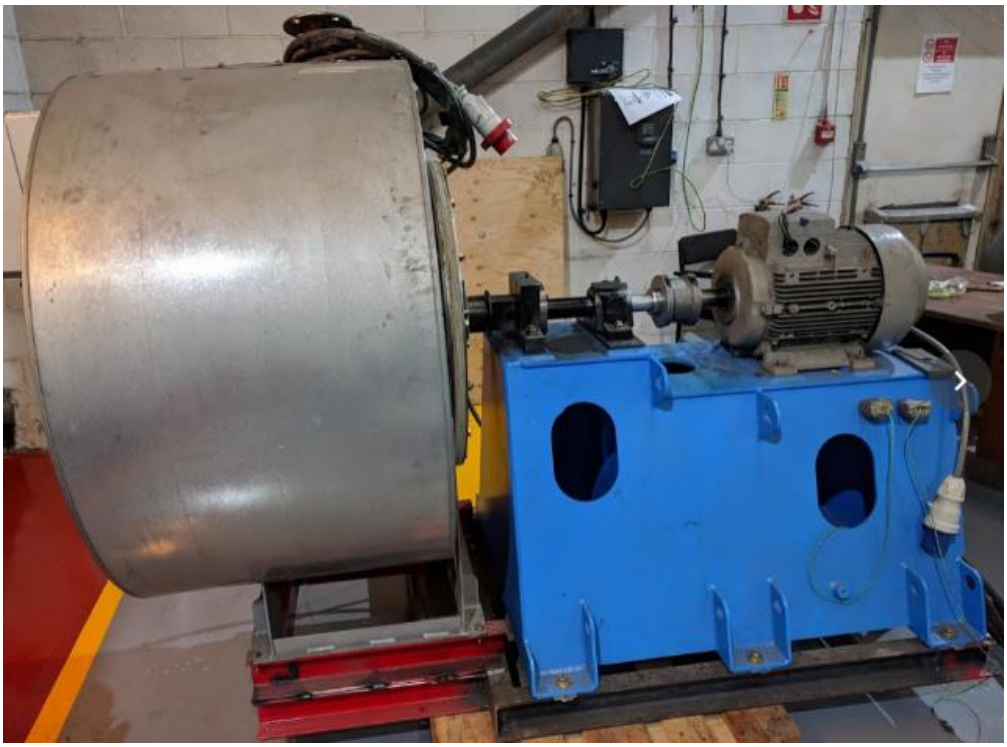

Figure 3-2 Test rig used for experimental analysis

To prevent damage to the motor a dummy bearing unit allows for the temperature of the shaft to be taken at the point where the motor's bearings would sit for a directly driven fan. To find the temperature of the shaft at this point the use of a temperature probe is required. This provided a dilemma, using a standard probe for this measurement the shaft would have to be stationary. This created the possibility in the reduction in the accuracy of the results from the shaft being able to cool down whilst the shaft stopped rotating. This was also apparent from the literature review as the studies conducted by Zainullin et. al. [12], Watel et al. [14] and Xie et. al. [15] all took measurements while the shaft was rotating. To solve this a IR thermometer was used to record the results. The components selected for the experimentation are can be seen below.

Temperature Meter (1)	Measures the temperature inside casing using a K type thermocouple. The readings are taken to 1 decimal place, to an accuracy of +/- (0.05% + 0.3°C). The measurement range is -200°C to +1372°C.	

IR Thermometer (2)	Measures shaft temperature at the location where the motor bearing would sit. Readings taken to 1 decimal place., to an accuracy of +/- 1.5%. The measurement range is -30°C to +500°C.

Motor (5)	22kW Motor used to provide the rotation to the system. The speed can be adjusted using a variable speed drive to achieve the required rotational speeds.

Coupling (4)	Connects the motor shaft to the impeller shaft.

Bearings (3)	Two bearing housings are used for the experimentation. The housing on the right is a standard plummer block housing. The bearing housing on the left was machined especially for the experimental

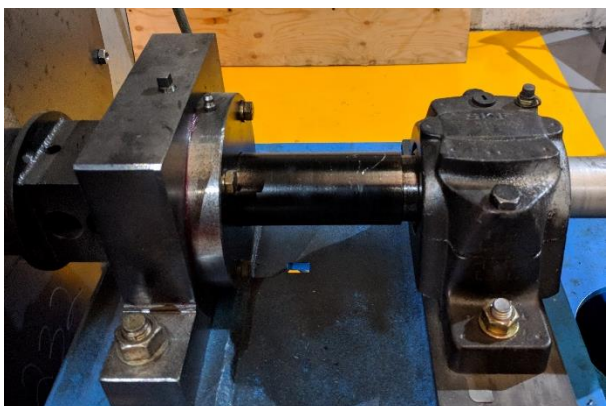

	analysis as it allows temperature readings to be taken where a motor bearing would sit.
Heater and Control Panel (1)	The heater used to heat the inside of the casing is set using this control unit. The temperature is set to the nearest 1°C.

3.1.1 Experimental procedure

The initial step in the procedure is to make sure the test area is free from obstruction and any potential hazards are removed. Power is fed to the motor from the mains and the rotational speed is set using the Variable Speed Drive (VSD). The temperature in the fan case is set to 300°C using the control panel. It takes approximately 15 minutes to reach the required temperature. Monitoring of the internal case temperature is carried out using the temperature meter. Once up to temperature, the measurements can be taken at the various locations to assess the temperature throughout the rig. The scope of work is to take temperature readings at the various locations throughout the rig. The locations of the readings taken are depicted in figure 3-1. Readings are taken at 15-minute intervals until the temperature levels remain constant. This process is repeated for testing of the other rotational speeds.

3.2. Stress analysis

To calculate the stresses and displacement due to the loading from the operational rotating speeds a Finite Element Analysis (FEA) is carried out. FEA uses the geometry presented and builds a number of smaller interconnected sub regions called elements [33]. From the 1950s onwards, advances have been made to use FEA to solve complex engineering problems throughout a range of disciplines and industries. There are three main methods used for the derivation of finite element equations [34]. The direct method used for structural analysis problems, variational method consisting of energy methods and principle of virtual work and the weighted residual method. The direct method is simple and subsequently limited to the calculation of problems using one-dimensional elements. The variational method and weighted residual methods are easier to use for two and three dimensional elements for analysis of more complex geometry. All elements of an FEA are linked through interfaces, nodes, boundaries

and surfaces. The material designation of the geometry is required to determine the behaviour of any given node, with respect to its stress and strain properties [35]. The geometry of the model was created in inventor and the FEA simulations carried out using the inventor FEA package seen in figure 1-7.

3.2.1 Meshing

For the simulations a mesh is applied to the mode. This mesh uses 2nd order tetrahedral elements, with four physical points and ten nodes per element. The overall number of elements used was 500,000, this allows the simulations to be accurate without compromising on computational time.

Figure 3-3 Mesh used for FEA

3.2.2 Solver settings

The material for the model was set to mild steel for the hub. A pin constraint was utilised constraining the rotation of the model to be axial only. The rotational speeds are applied to the hub using a body load. This applies the relevant centrifugal forces to the hub for the different rotational speeds. The simulation is run and the results are plotted for, von mises stress, first principle stress and displacement. Furthermore, a modal analysis is carried out to determine the natural frequencies of the model. Knowing the natural frequencies of the model is important to understand if there is the possibility of excitation from the frequencies caused by rotation.

3.3. Computational Fluid Dynamics

Computational Fluid Dynamics (CFD) is the analysis of fluid flow and heat transfer in a system. The applications for the potential simulations are vast, which is the reason why the method is used throughout a large number of industries. One of the main benefits to using CFD is its ability to reduce the time in research and development of a product or system, as the

number of simulations that can be carried out compared to physical experimentation in the same period can be very different. This can have large cost savings and result faster solutions to problems.

The coding within CFD is structured around solving fluid flow problems, the process for solving any problem like this looks at three elements, Pre-processor, Execution of the solver and Post-processing. The initial Pre-processing is the point at which the geometry is defined within the region that the simulation will take place. The boundaries of the model are defined including any domains. Once a complete model is defined, the mesh is generated. The software version used is Ansys 17.2.

3.3.1 Flow Domain

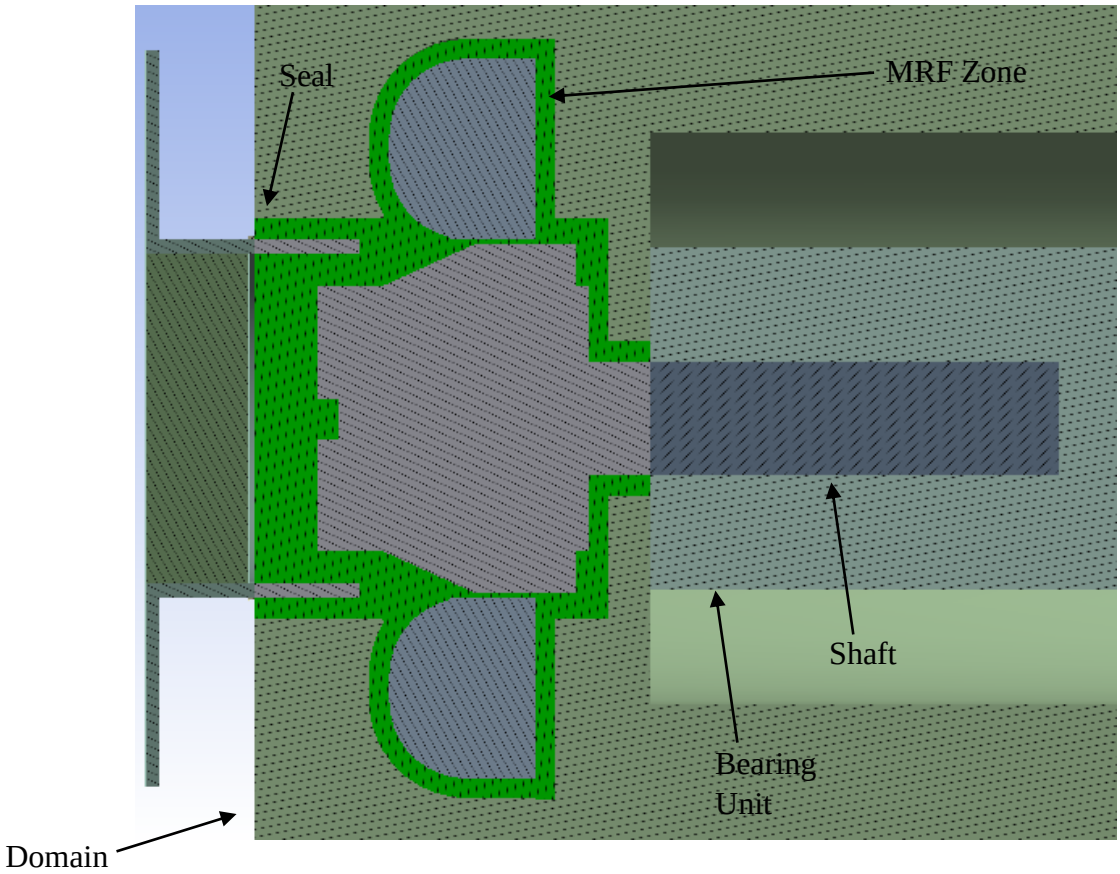

Figure 3-4. Baseline model used for simulation

For the numerical solutions, the baseline model geometry has been created using the Design Modeller in Ansys. The baseline model forms part of a system made up of, the shaft with the hub attached, a small gap to simulate the seal between the fan casing and the shaft and an area representing the bearing unit terminating the shaft, as seen in figure 3-4. The shaft has a diameter of 28mm and the point at which it reaches the bearing unit is 15mm from the hub body. When modelling the hubs the components are kept the same for both models were the overall length, diameter, materials (the hub body is carbon steel and the cooling disc aluminium) and the cooling disc position.

3.3.2 Meshing

For the simulation a hybrid mesh has been used. This means that two types of mesh have been used for the simulation. The model has utilised both hexagonal and polyhedral elements. The hexagonal elements have a low skewness and are simple to generate. Moreover, they give accurate results due to a low numerical diffusion. Polyhedral elements are used on the more complex elements to the geometry such as the curved sections. The domain consists of 3.3 million elements in total, with 1.1 million for the solids zone and 2.2 million for the fluid zone. It has been noticed that the mesh considered in the present study can be effectively used to capture the complex flow phenomena, and the associated heat transfer, with reasonable accuracy.

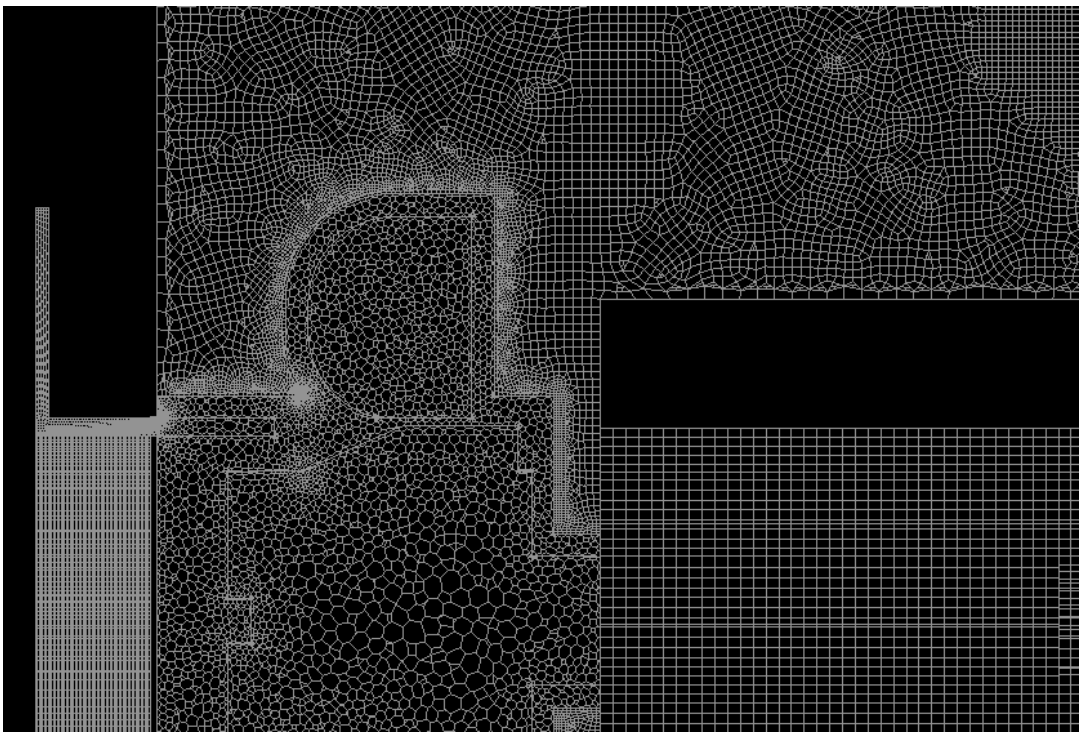

Figure 3-5. Meshing of the model

3.3.3 Boundary conditions

The temperature at the flange section of the baseline model used in the current study is set to 300°C. This temperature represents the environment the baseline model is operating within as part of a fan system. The pressure at the seal is representing the leakage that would be experienced within a fan system. The rotation of the MRF zone is simulated at four rotational speeds these speeds are the most common found within fan systems. The ambient temperature of the domain was set to 26.85°C the average temperature of factory at the time of experimental testing.

The boundary conditions for the simulation are summarised in table 1.

Table 3-1 Boundary conditions

Item	Boundary Type	Value
Flange	Temperature	300°C
Seal	Pressure (Total)	2000Pa
Cooling Disc	MRF Zone	1000, 1500, 2250 and 3000rpm
Surrounding of fluid domain	Temperature	26.85°C

The Moving Reference Frame (MRF) is a robust and efficient CFD technique to simulate rotation. For the simulation, it is assumed that the MRF region has a constant rotational speed and the boundaries of the geometry within the MRF region are surfaces of rotation. A weak interaction is assumed between the volume of the MRF and the non-rotational volume; however, it can be used effectively for this simulation. The rotational aspect is important for the simulation to replicate the operating conditions of the hub. The rotation is expected to provide a key part in the heat dissipation of the hub, therefore simulating the rotation is a requirement.

Some limitations do exist when using MRF and these should be considered for the application at hand. The interfaces from the adjacent regions must be lined in such a way that the velocity of the frame normal to the boundary is zero. Velocities both translational and rotational are assumed constant. Care should be taken when assessing the results, furthermore the experimental validation will help to put confidence in the results.

3.4. Solver settings

To accurately predict the behaviour of the fluid flow and heat transfer from the model application based solver settings are required. Ansys uses the energy transport equation [33];

$$\frac{\partial(\rho E)}{\partial t} + \nabla.\left[\vec{V}(\rho E + p)\right] = \nabla.\left[k_{eff}\nabla T - \sum_j h_j J_j + \left(\overline{\tau_{eff}}.\vec{V}\right)\right] + S_h \qquad (3.1)$$

Where E is energy per unit mass defined as;

$$E = h - \frac{p}{\rho} + \frac{V^2}{2} \qquad (3.2)$$

A number of turbulence models are available in CFD, they each have advantages and disadvantages. For this study, the k-epsilon model is chosen for the turbulence modelling. The

reason for choosing this model is the flow in the model is not overly complex and the study is not interested in separation or streamlines. The k-epsilon model is known to be robust and allows for run times to be reduced which is preferable as no benefit is gained from switching to a different model. In this study SIMPLE algorithm is used as it can help to converge the solution quicker and has good accuracy for the basic geometry used [34]. An approximation of the velocity field is gathered from solving the momentum equation. Gradients are required to obtain values at the cell faces for computing diffusion terms. Green Gauss Node based gradient is used for evaluation. This constructs of a linear function at a node from a cell, this preserves a second-order spatial accuracy. The solver uses upwind spatial discretisation, which takes the face value from the relative cells upwind. This study uses second order upwind methods for pressure, density, momentum, turbulent kinetic energy and dissipation rate. This is done to increase overall accuracy of the results.

3.5. Convergence Criteria

Achieving a converged result is the desired outcome of the numerical solutions, this gives the knowledge that the solution has reached a stage where it is stable. This is why only a solution that has reached convergence can be used to predict problems with the required accuracy. [35] The convergence criteria used by Ansys is 0.001. This means that the change in continuity values must reach the fourth decimal place for a successful convergence. In practice this default criteria may not indicate changes in the solution have completely finished. This is why it is preferred to monitor convergence instead of using the default criteria. In the present study the temperature values monitored throughout the iterative process must reach the steady state as described. The solution is considered converged once the temperature values at the monitored points become stable. A solution with stability is where the temperature values no longer experience fluctuations.

The settings and conditions detailed in this chapter are utilised to carry out the numerical simulations to analyse the stresses and thermal properties of the model. Detailed discussions on the results are presented in the following work, the next chapter explores the results from these simulations of the baseline model.

CHAPTER 4 ANALYSIS OF BASELINE MODEL

This chapter presents and discusses the results from the experimental and simulation work. A detailed qualitative and quantitative analysis of the results gathered is carried out to understand the baseline models heat dissipation characteristics. The models suitability for operation in terms of the stresses and displacement will also be analysed.

4.1. Introduction

This chapter deals with how the existing hub baseline model currently performs when in operation. The hub is tested experimentally at various operating speeds that are most commonly used within the industry that the hub is used within. The analysis within the chapter looks at the stresses the hub experiences at the different rotating speeds and high temperature. The results from the first section of the chapter are compared and analysed against results gained from CFD analysis.

The current baseline model is used successfully for high temperature applications in a range of industries. Figure 4-1 shows a section view of the hub detailing the fabricated fin arrangement.

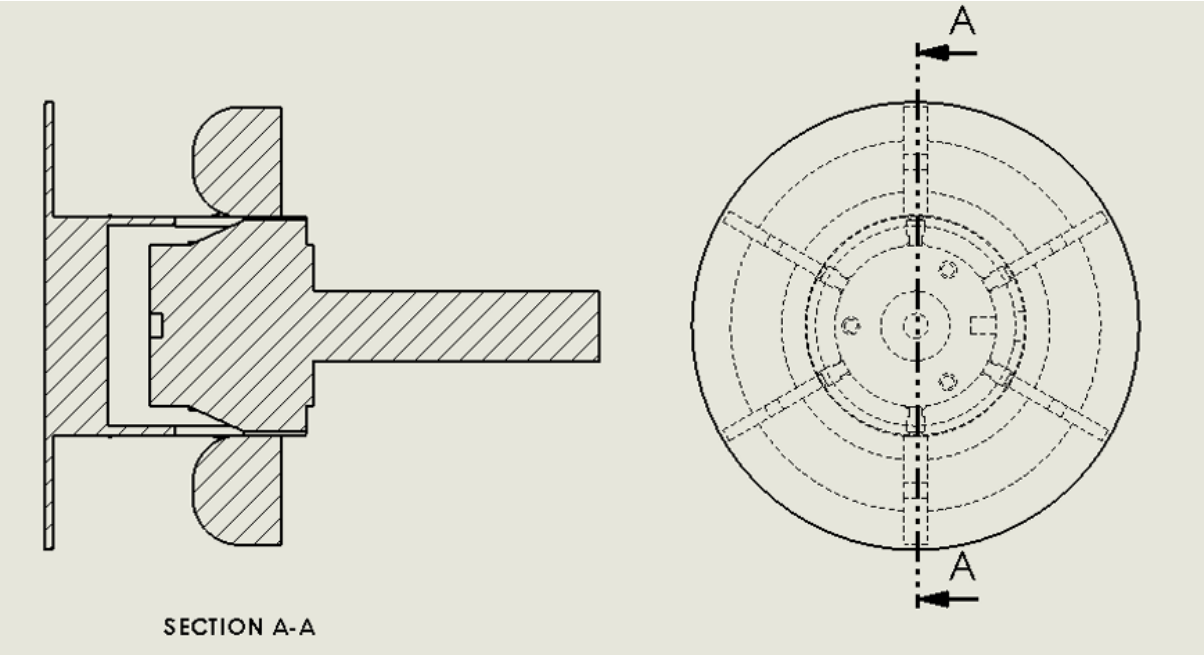

Figure 4-1. Cross section view of the baseline model

The theory of how the fins enable heat to be directed away from the hub is discussed in chapter 2. The use of fins however has created a complexity in the manufacture of the component. Figure 4-2 details the hub broken down into its constitute parts. The flange, the three retaining plates and fins are all laser cut from mild steel. The existing technology available means that these can be cut at a relative low cost [36]. All parts are cut at the same location reducing any travel time between suppliers. Laser cutting enables precision that leaves a minimal amount of work required to get the part ready for fabrication.

The hub body is machined from a section of steel, a number of processes are required to produce the body that the fins are then welded onto. The bar would first be cut to length, then the bore machined out to the correct diameter whilst considering the required tolerance and finally the correct keyway added. This part needs to be machined within a tolerance as it is this point at which the hub connects to the shaft. The connection must be secure between the shaft and the impeller to prevent the possibility of the impeller coming loose and having the potential to cause catastrophic damage.

The second machined part is the hub outer. This is manufactured differently from the hub body even though it is cylindrical in shape. To machine the part from a solid steel bar would incur a

large amount of waste material, to reduce this the part is initially cut from sheet steel and rolled into the required profile. The first cut will be to create the shape that can be rolled to the cylinder as required. The notches will also be removed at this stage.

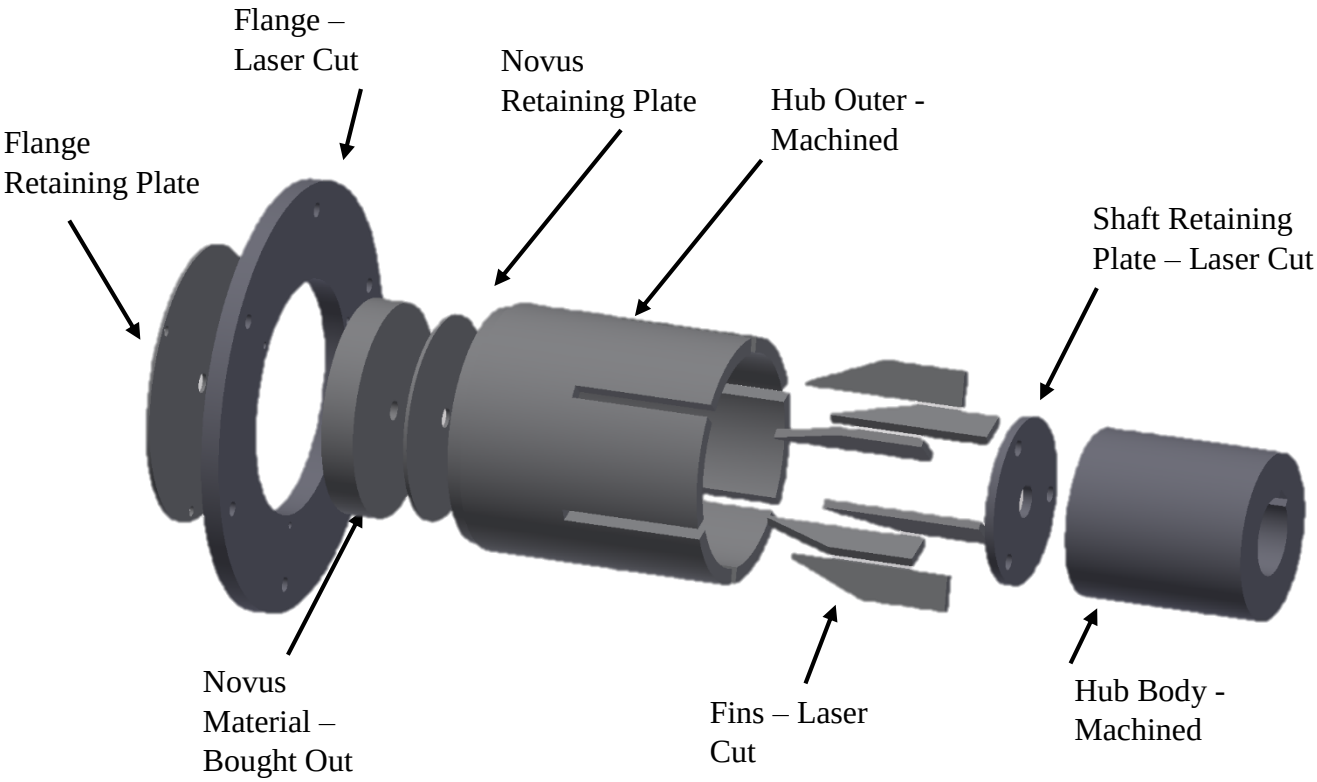

Figure 4-2. Parts that make up the baseline hub

4.2. Experimental Analysis of the Baseline Model

The experimental approach as discussed in chapter 3 has being used in the present study to analyse the heat dissipation capabilities of the baseline model. The tests were carried out at four rotating speeds of 1000, 1500, 2250 and 3000rpm. It is important that the models capabilities are known at these speeds, as this is what they are most likely to experience when in use. The internal temperature of the of the rig is set to 300°C and readings are taken at various points as shown in figure 4-3. These point locations are chosen to understand how the temperature differs throughout the rig and how the hub is affecting the heat transfer through the shaft. Point 1 is the thermocouple used to measure the temperature inside the test rig casing. Readings are taken at the other points when this value reached and stabilised at 300°C. Point 2 is located at the edge of the fan casing to measure the temperature just after the seal. Point 3 is the temperature of the hub body outer. Point 4 is located at the point where the motor bearing would be located in a directly driven fan. Point 5 is just after where the bearing of a motor

would be to see how the exposed shaft length can affect the temperature from point 4. The results obtained are presented in table 4-1.

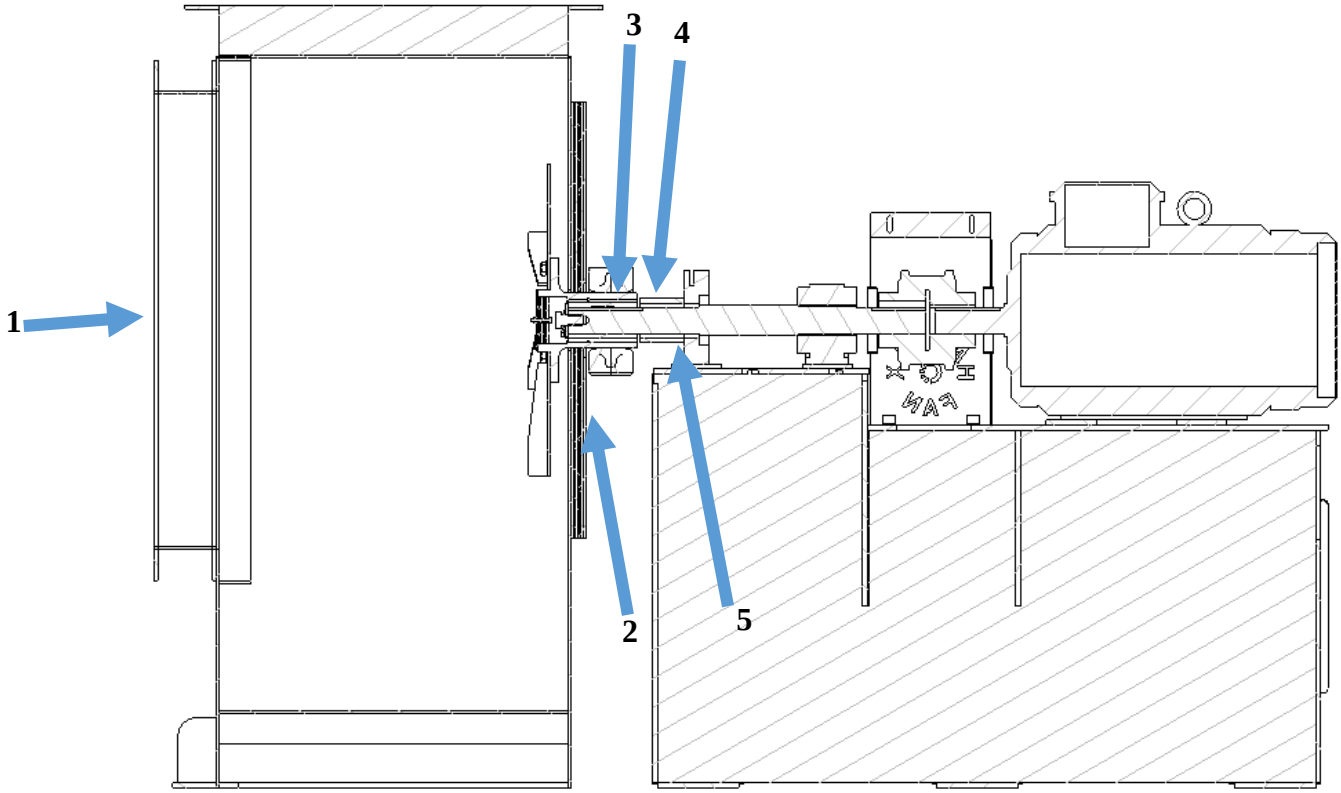

Figure 4-3. Locations of where the temperature readings are taken from

Table 4-1 Experimental results from the baseline model, rotating at 4 speeds.

Point	Temperature (°C) at 1000rpm	Temperature (°C) at 1500rpm	Temperature (°C) at 2250rpm	Temperature (°C) at 3000rpm
1	300	300	300	300
2	220	205	191	190
3	101	89	76	62
4	101	91	62	53
5	101	90	62	51

The results show a decrease in temperature for readings taken after point 1. Point 2 is located at the outside of the casing just after the seal so can give an indication of the temperature difference from within the casing and the point where the hub exits the casing. This temperature is lower than the inside of the casing however, the shaft rotational speed also has an effect. The higher the shaft rotation the lower the temperature at this point. This trend is similar for all the other points also. The reasoning for this could be due to the effect the cooling disc has on the components. As the rotational speed increases the amount of air displaced by the cooling disc

increases creating an increased cooling effect on the surrounding components. The results show a similar trend to those found by Watel et. al. [14], with respect to a reduction in heat at higher rotational speeds. The points 4 and 5 are where the motor bearing would sit on a direct drive fan. The readings at these points are important as if the measured temperature is too high the bearings can potentially fail.

4.3. Finite Element Analysis of the Baseline Model

The baseline model is proven to operate successfully within industrial applications. To understand the manufacture and material choices a stress analysis should be carried out. This analysis was carried out using Autodesk Inventor finite element analysis software. Analysis is carried out to determine the von mises stresses. This gives an indication of the overall strength of the model. The first principle stresses are analysed to determine the fatigue life of the welds used to connect the fins to the hub body. The displacement of the model when in operation is evaluated to assess the movement of the model when the forces or operation are applied. A modal analysis is carried out to determine the natural frequencies of the model. This analysis all forms part of the complete finite element analysis of the baseline model to understand how it will withstand operating conditions.

Analysis is undertaken into the effect the four rotational speeds have on the hub model with regard to the stresses it experienecess. The highest von mises stresses were found at two points, at the end of the slotted section of the hub outer and where the fin connects to the hub body as shown in figure 4-4. The values for the stresses at both points for all rotating speeds are presented in table 4-2, and depicted in figure 4-4.

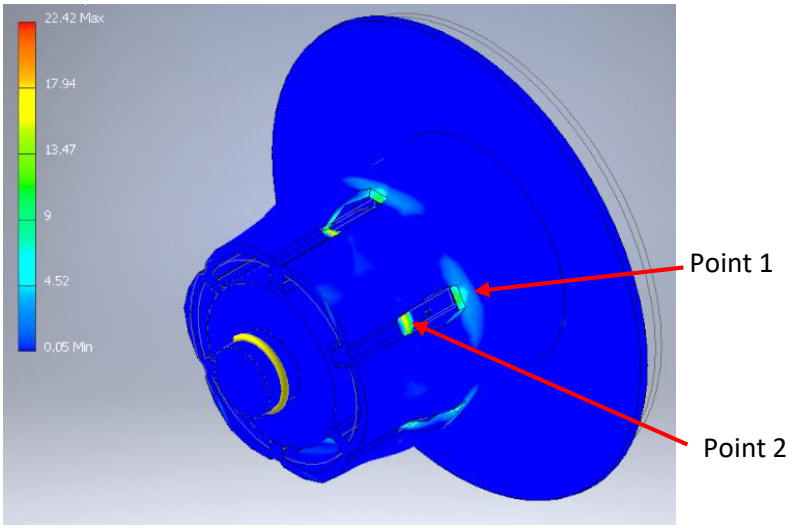

Figure 4-4. Locations of high stress on the baseline model

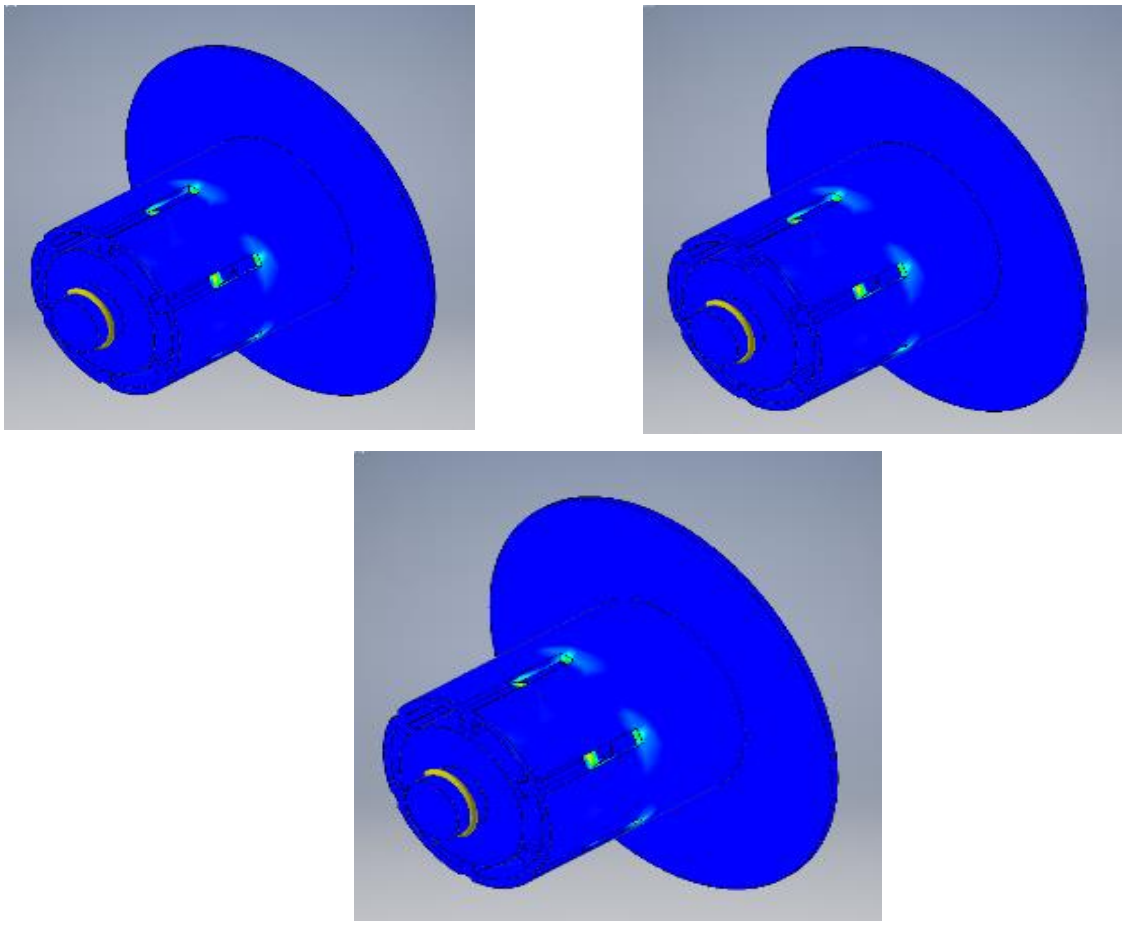

Figure 4-5. Von mises stress on baseline model rotating at 2250, 1500 and 1000rpm respectively.

According to BS5500 [37] the maximum bulk stress should not exceed yield and localised bulk stress should not exceed 1.5 times yield. Moreover, BS5500 states that the maximum surface stress should not exceed 1.5 times yield and localised surface stress should not exceed 3 times yield. For mild steel at 300°C yield is 229MPa therefore localised bulk and surface stress is acceptable up to 344MPa. The values at points 1 and 2 are substantially below this value.

The location of the stresses at point 2 occurs in the weld region where the fin connects to the hub body. These welds are in accordance with BS7608 [38], class F2 welds. Class F2 welds are fillet welds and are the welds used to attached the fins to the hub body. This means that the stress within these regions can be 3 times the yield strength of the material. The highest value of 22.42MPa at point 2, rotating at 3000rpm is substantially below the three times yield of 688MPa. This is true for all three rotating speeds. This analysis of the von mises stresses does not highlight any areas of significant stress that would lead to failure.

Table 4-2, Von mises stresses due to four rotational speeds on baseline model

Rotating Speed (rpm)	Stress at Point 1 (MPa)	Stress at Point 2 (MPa)
1000	1.68	2.49
1500	3.77	5.60
2250	8.48	12.61
3000	15.08	22.42

Analysis of the first principle stresses is carried out to assess the fatigue life of the welds. Start/stop fatigue life can be assessed from the first principle stresses on the welded fins. Figure 4-6 depicts the first principle stresses at the rotating speeds of 3000, 2250, 1500 and 1000rpm. The high stress points from the first principle analysis are located in similar areas to those of the von mises analysis this can be seen in figure 4-4. Moreover, the values for the stresses are very similar to those from the von mises stresses. Table 4-3 presents the results from the first principle analysis at point 2. The same scale is used to present all the contours in figure 4-6 this allows a clear depiction of how the stresses change with rotational speed. The lowest value for stress occurs at 1000rpm, giving a value of 2.19MPa. At 1500rpm the stress value increases by 55.67%. The stress increases by 55.50% from 1500rpm to 2250rpm. The increase in stress from 2250rpm to 3000rpm is 43.77%. The increases in stress between each rotational speed show the effect the increased centrifugal forces have on the hub. The difference between the stress value at the lowest and highest rotational speed is 88.91%. The stress values are well below the failure point however, this is a point for consideration. If the design speed of a rotating piece of equipment is set at a low running speed, an appreciation is required as to the impact of increasing the rotational speed can have on the stresses. The highest value of 19.74MPa at 3000rpm is 22% different from the von mises value. As stated this value is well below the failure point.

Table 4-3, First principle stresses found at two points on the baseline model at different rotating speeds.

Rotating Speed (rpm)	Stress at Point 2 (MPa)
1000	2.19
1500	4.94
2250	11.10
3000	19.74

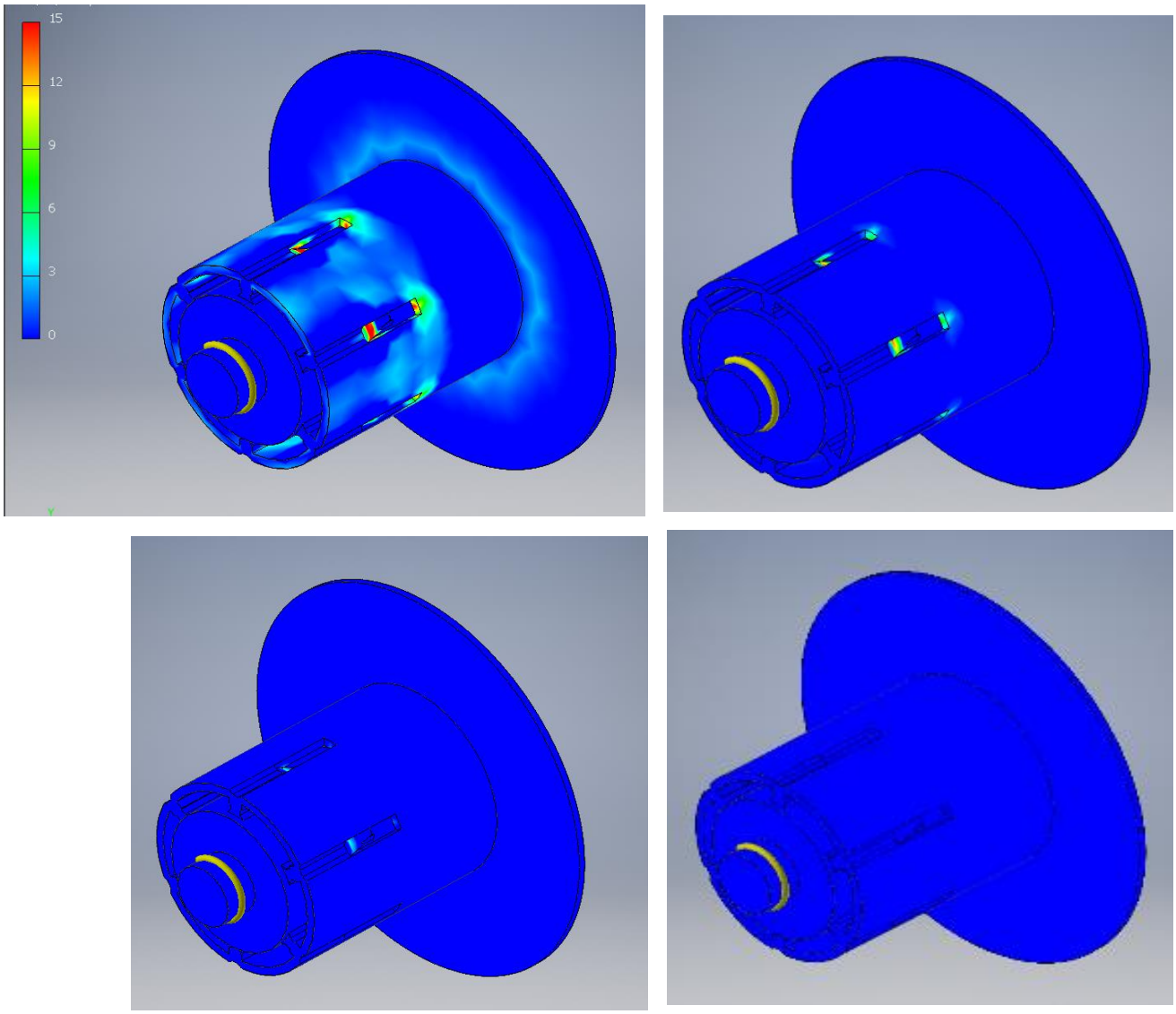

Figure 4-6. First principle stresses on the baseline model rotating at 3000, 2250, 1500 and 1000rpm.

An investigation into the displacement of the model determines if the stress applied will cause the model to deform. The expectation is that a model will experience some displacement. Should this deformation be too great the model will move whilst in operation and cause problems for the fan system. The hub is located at the centre of impeller used within a fan system, any movement within the hub will cause the impeller to move also. If the impeller movement is significant enough it will collide with the fan casing, having the potential to cause catastrophic damage. The impeller is usually set a minimum of 10mm from the casing. The results for the simulations run at 3000, 2250, 1500 and 1000rpm are depicted in figure 4-7. The maximum displacements at each rotating speed are presented in table 4-4. The scaling in the figures is presented so the displacement from each rotational speed can be clearly viewed. The general trend of the displacement is an elongation of the flange section and at the centre of the hub outer. The displacement at the centre of the hub outer is caused by the notch sections. As

found by the stress analysis this is a weak point in the model and the displacement in this area confirms this. The flange extends out from the hub body experiencing an increased displacement at the edge. This is due to the centrifugal forces affecting the flange due to its relative position from the hub body. At 1000rpm the maximum displacement of the flange is 0.00047mm at 1500rpm the displacement increases by 57.27%. At 2250rpm the displacement increases by 54.17% from 1500rpm. The largest displacement of 0.0042mm occurs at the rotational speed of 3000rpm a 42.86% increase in the displacement at 2250rpm. Like the values for stress the displacement increases with rotational speed. The difference in the displacement between the lowest rotational speed and highest is 88.81%. This increase is within 1% of the increase in the values for stress between the highest and lowest rotational speed, providing a clear correlation between the two. The highest value for displacement is not significant and does not cause any cause for concern.

Table 4-4 Maximum displacement on the baseline model at the four rotating speeds.

Rotating Speed (rpm)	Max Displacement (mm)
1000	0.00047
1500	0.0011
2250	0.0024
3000	0.0042

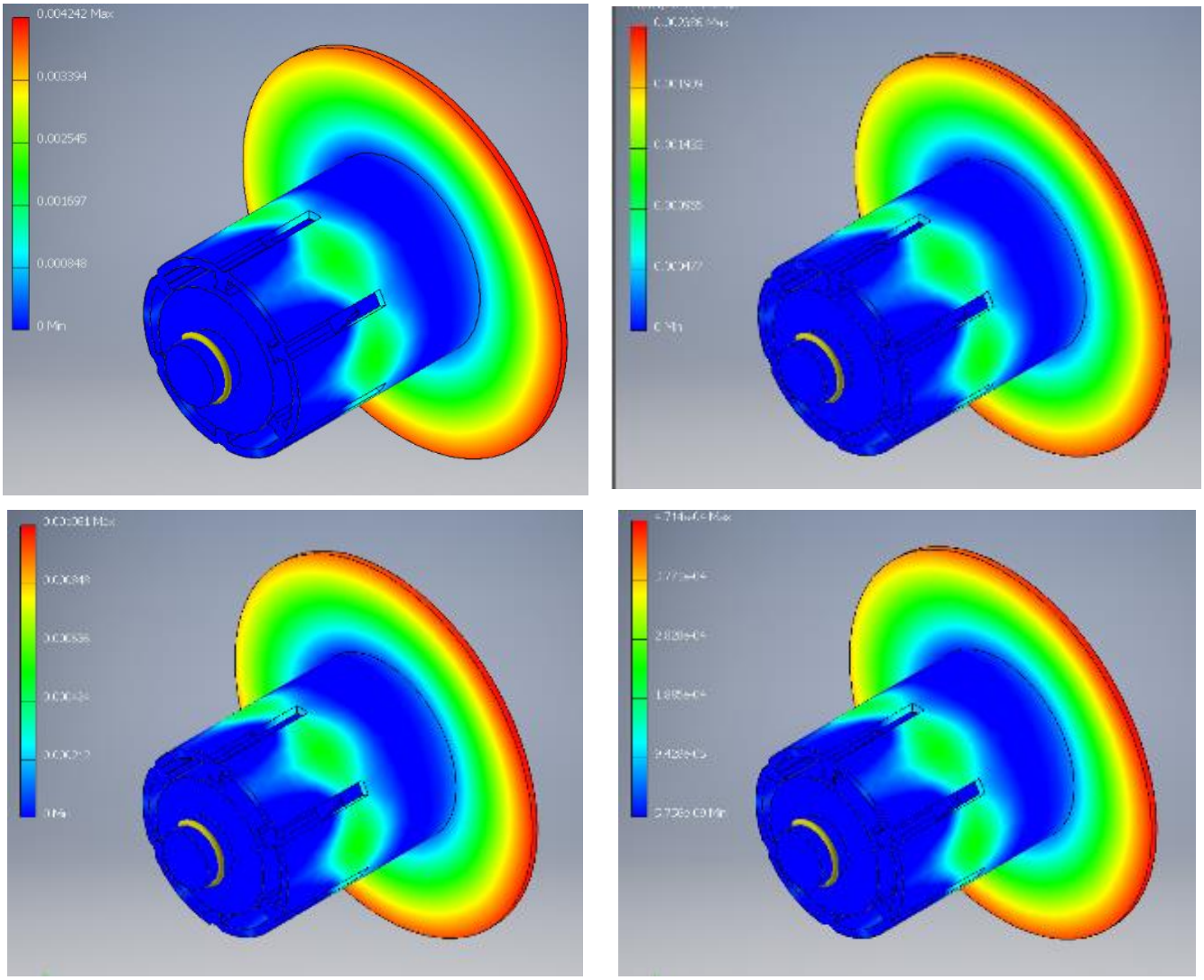

Figure 4-7. Displacement of the baseline model rotating at 3000, 2250, 1500 and 1000rpm.

4.3.1 Modal Analysis

Modal analysis is used to validate the design through assessment of the natural frequencies when in operation. Natural frequencies are the frequencies at which vibration occurs in an object when exited by a force. This is important for fan equipment because the air drawn through the fan can create vibrations. This analysis finds the natural frequencies at eight modal shapes, mode 1 is depicted in figure 4-8. At these frequencies, the structure is most susceptible to forces that can lead to failure. The operating frequency depends on the rotating speed table 4-5 gives the operating frequencies for the rotating speeds simulated. Table 4-5 presents the results for the natural frequencies from the eight modes. The lowest natural frequency of the modes is 595.94Hz this value is 545.94Hz higher than the highest operating frequency of 50Hz. Tis finds the baseline model suitable for operation at the required running speeds.

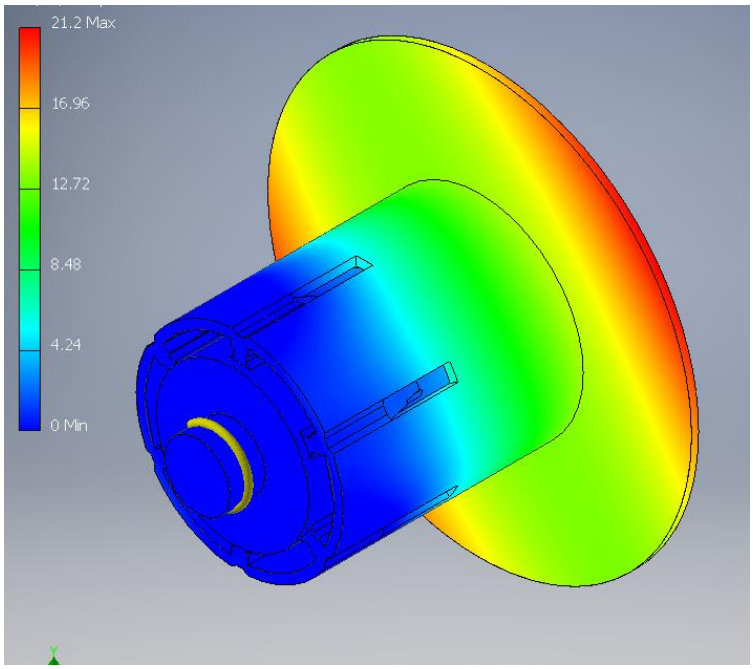

Figure 4-8. Mode 1 of the modal analysis of the baseline model.

Table 4-5 Operating frequencies of the four rotating speeds

Rotating Speed (rpm)	Operating Frequency (Hz)
1000	16.7
1500	25.0
2250	37.5
3000	50.0

Table 4-6 Results from modal analysis

Mode	Natural Frequency (Hz)
1	595.93
2	599.83
3	845.16
4	905.81
5	917.06
6	955.90
7	988.12
8	1243.08

4.3.5 Finite Element Analysis Summary.

No high level stress that could lead to potential failure were found from the simulations on the baseline model. The analysis of the von mises stress indicated two higher stressed areas. The stresses within both these areas are significantly lower than the maximum allowable stress of 229MPa on the model. The displacement and first principle stress were found to be insignificant. The modal analysis did not show any modes that were close to the operating frequencies. From the simulations it is clear the baseline model is suitable for operation at 300°C for the three operational speeds tested.

4.4. Thermal Analysis of the Baseline Model

The baseline model operates successfully within high temperature environments to dissipate heat from the motor shaft to which it is attached. By carrying out a thermal analysis of the model an understanding will be gained of the hubs effectivity at reducing heat transfer. Figure 4-9 depicts the temperature contours of the baseline model and shows the effect the rotation has on the surrounding ambient air. The rotation of the model causes the temperature in the trailing edge of the cooling disc to be as high as 108°C. The temperature at the centre of the hub is 23.94% higher than at the edge of the cooling disc. The reason for this are the fins on the hub body and the fins of the cooling disc. The fins are dissipating the heat from the central section of the hub. The finned and other sections of the model are analysed in the following section.

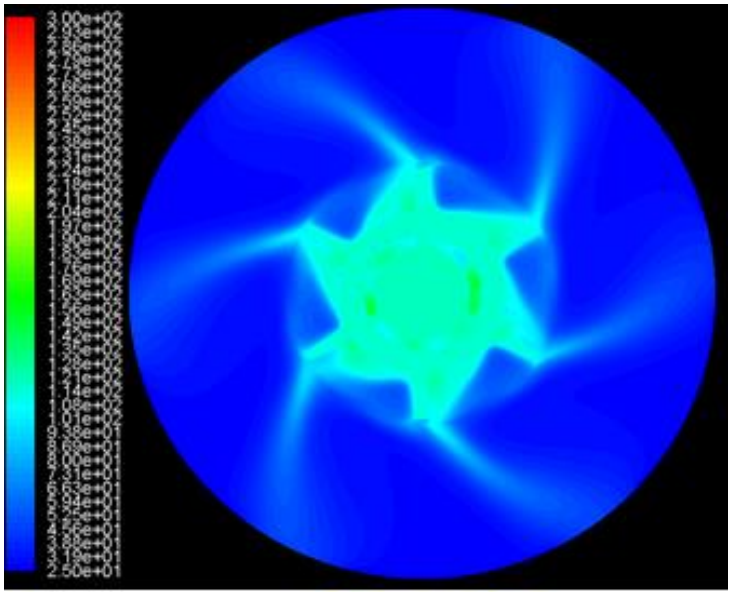

Figure 4-9. Temperature distribution with surrounding domain

Figure 4-10 depicts a cross section of the baseline hub model rotating at 1500rpm with the temperature set at 300°C at the flange section. The high temperature regions can be seen on the flange section of the hub. The temperature distribution shows how the temperature differs throughout the model. The general trend depicts the temperature decreasing through the model from left to right. The higher temperature contour regions are depicted in red, with the cooler ambient air represented as blue contours. This is an expected trend as the further you are from a heat source the cooler you would expect the model to be, based upon the laws of heat transfer. The contours give a visualisation of how the hub geometry affects the heat transfer in the model. The section of the hub that resides with the impeller within the fan casing is depicted in red on the contours in figure 4-10. The seal section is where the hub exits the fan casing and enters the ambient air the leakage of the seal can be seen in the contours in figure 4-10. This leakage is important as the seals used on the fans are not 100% efficient so some leakage occurs. This is important as the leaked hot air passes out of the casing and interacts with the outer edge of the hub and the cooling disc causing a heating effect, as seen in figure 4-10.

Figure 4-10 depicts six points where temperature readings were taken from the simulation of the baseline model. The location of these points was determined based upon the key areas of interest within the model. Point 1 is the area located within the fan casing, where there is a process temperature of 300°C. Point 2 is located just after the seal leakage section to show the

temperature of the gas passing through the seal section and onto the hub located outside of the fan casing. Point 3 is located at the centre of the hub. Point 4 is the location of where a motor bearing would sit should this value be too large bearing failure will occur. Point 5 is located at the point where the cooling disc connects to the hub. Point 6 is the outer edge of the cooling disc. The results for all four rotating speeds are presented in table 4-7.

The rotational speed has a significant impact on the results for the points plotted in figure 4-10, apart from point 1 which shows a 0% difference between the points. This is due to it being taken at the location where the temperature is set on the flange of the hub. At 1000rpm the temperature at point 2 where the seal leakage section is located is 191°C. In comparison the temperature at this point at 1500rpm is 4.19% lower, 7.85% lower at 2250rpm and 9.95% lower at 3000rpm. At point 3 the temperature at 1000rpm is 121°C, for 1500rpm, 2250rpm and 3000rpm, the temperatures are 1.62%, 27.27% and 38.02% lower respectively. The average temperature differences from 1000rpm for the four rotational speeds are, 1.99%, 22.80% and 30.61% respectively. What is clear from the results is that as the rotational speed increases the temperature values the points on the hub decrease. This could be from a number of reasons, the cooling disc acts as a small fan and is able to displace air to provide a cooling effect this would only be emphasised at higher speeds.

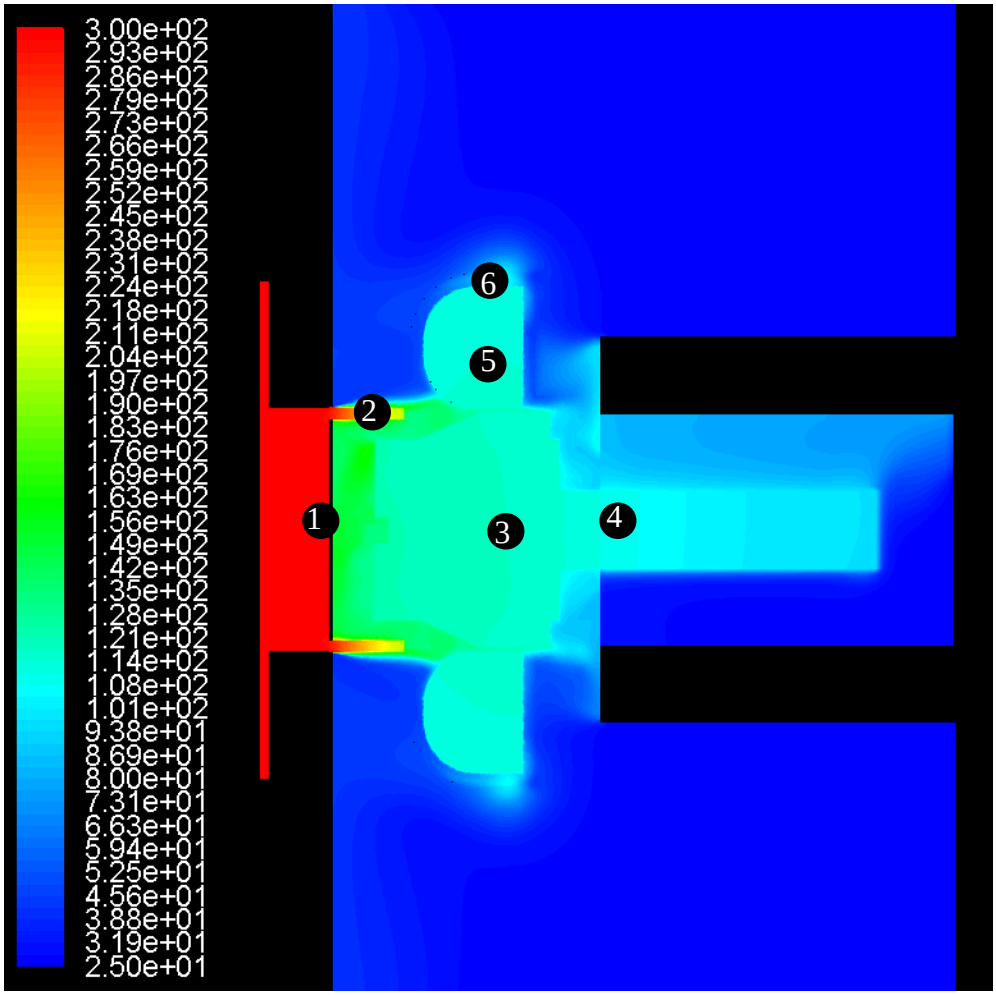

Figure 4-10. Temperature distribution through cross section of the baseline model

Table 4-7 Temperature values taken at six points on the model

Point	Temperature Value (°C) at 1000rpm	Temperature Value (°C) at 1500rpm	Temperature Value (°C) at 2250rpm	Temperature Value (°C) at 3000rpm
1	300	300	300	300
2	191	183	176	172
3	121	119	88	75
4	121	119	86	71
5	103	101	67	56
6	119	116	74	61

To gain a greater understanding of how the temperature changes within the model, two lines have been drawn through the model as shown in figure 4-11. This will give a better understanding of the temperature distribution through the model. Line 1 is located along the hub outer beginning after the seal section of the hub. It passes through the cooling disc before terminating at the end of the hub. Figure 4-12 and 4-13 show the temperature variations through this section. Figure 4-12 details the linear reduction in temperature along Line 1, until a point where the temperature on the graph becomes almost constant. The point at which the levelling off occurs on line 1 is where the cooling disc is located. The levelling off occurs at 118°C and only decreases by 5°C for the remainder of line 1.

Line 2 begins at the centre of the hub and runs the length of the hub, remaining in the centre of the shaft until the point where the motor bearing sits. Figure 4-13 shows the temperature distribution from line 2 in the baseline model. In comparison to the plot from Line 1 there is a visible difference in the overall shape of the lines. Line 2 shows a much steadier gradient whereas the temperature in line 1 decreased rapidly in a liner trend before levelling out. Line 2 begins at 122°C and by the time it reaches the cooling disc (position 0m on the graph) the temperature has only decreased to 118°C. After this point Line 2 follows the same gradient until position -0.02m, where Line2 exits the hub but remains in the shaft. The temperature drops to 111°C by the end of Line 2 a reduction of 6%. The reasoning for this decrease in temperature is the shaft section being exposed to the ambient section of the simulation causing an increased cooling effect.

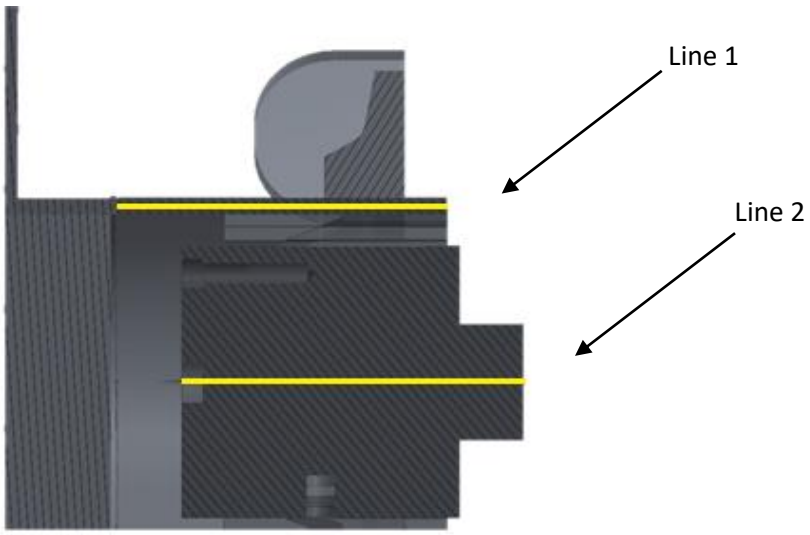

Figure 4-11. Lines used to investigate the temperature distribution through the model

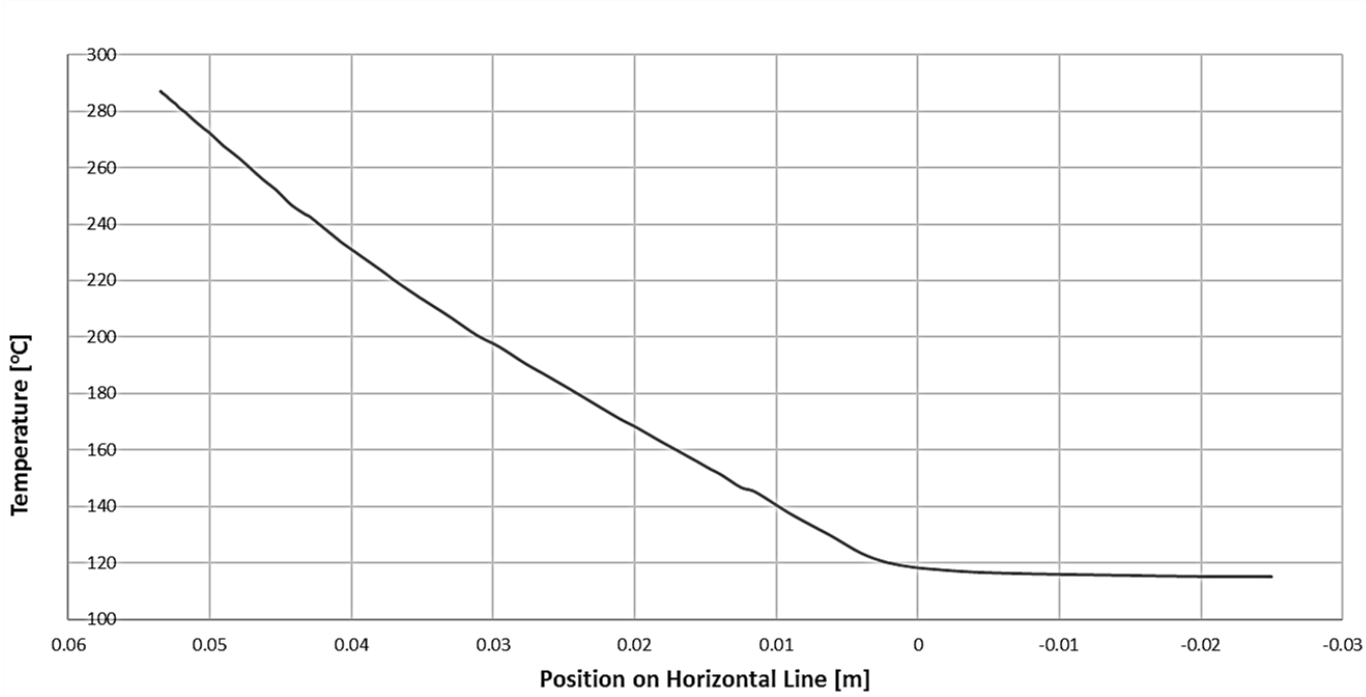

Figure 4-12 Temperature distribution through line one

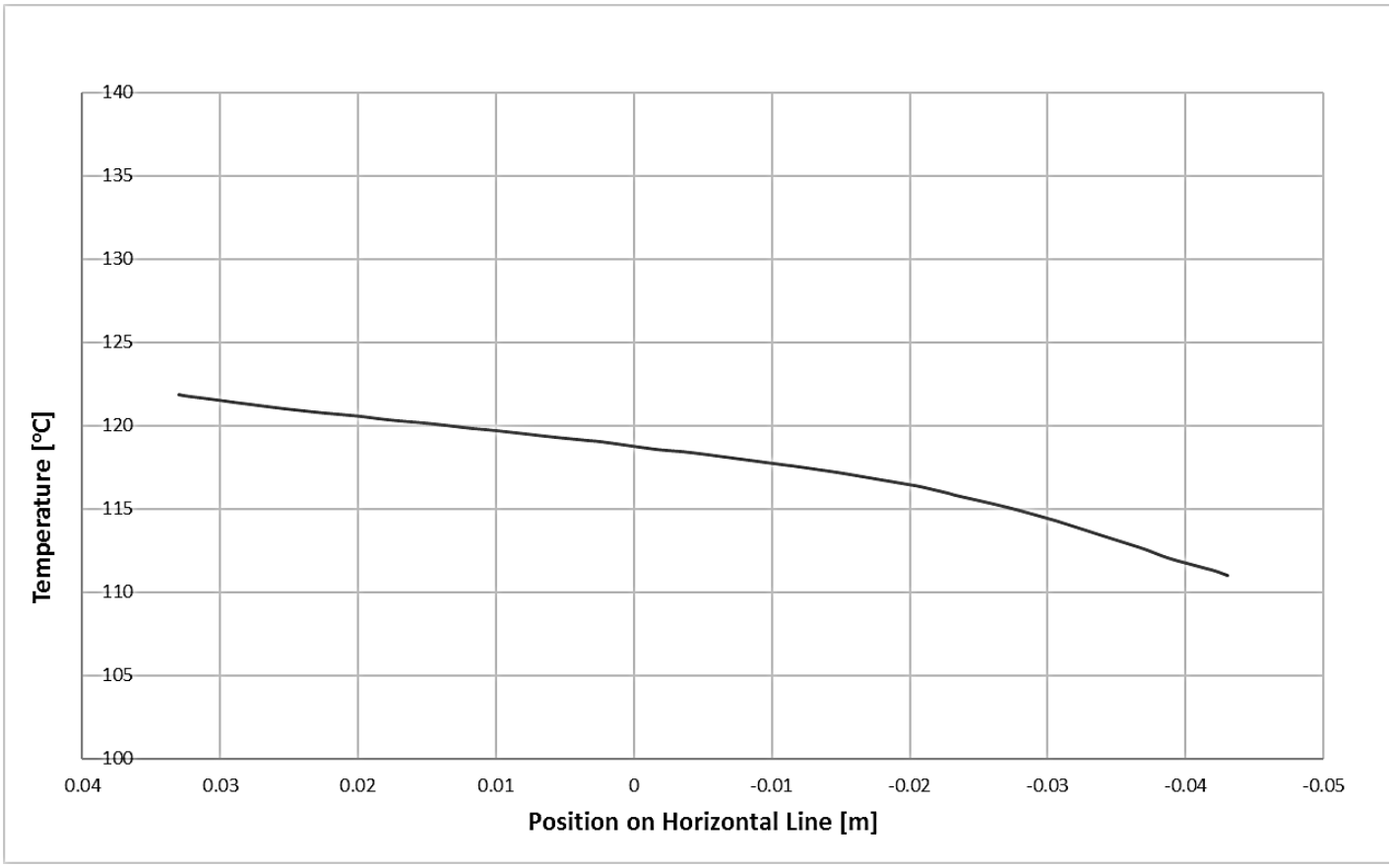

Figure 4-13 temperature distribution from line 2 in the baseline model.

The heat transfer coefficient is important as it allows visualisation of the effectivity of heat transfer through the various sections of the model. The variations of heat transfer coefficient in the baseline model have been depicted in figure 4-14. The model can be split into six areas, shown in the figure 4-14. These areas can then be compared to determine how different operational speeds affect the values for heat transfer coefficient. The contour plots use the same scale to show the difference in heat transfer in the models. The model operating at 3000rpm has very distinct areas showing the high and low values for the heat transfer coefficient. The dark blue areas on the cooling disc fins give a value of -197 at point 4, this is due to the rotational direction of the hub. The lower values are on the back of the fins due to the rotational direction of the hub. This effect is similar for 2250rpm rotational speed with a value of -182 at point 4 giving a 7.61% decrease. At 1500rpm the value is -22 an 88.83% difference and at 1000rpm the value is 18 a difference of 109.14% from the coefficient at 3000rpm. This highlights how the rotational speed allows greater heat transfer in the model.

At point 6, located on the on shaft where the motor bearing would sit, the heat transfer value for the four rotational speeds is identical. This shows the higher effect the rotational speed has on the main hub body over the bare shaft section. The highest value for heat transfer coefficient is located at point 3. This is where the cooling disc attaches to the hub body, at 3000rpm the value is 201. At the other three rotational speeds this value decreases by 33.33%, 76.62% and

84.58% respectively. Again the rotational speed is found to be a significant factor in how the heat transfer coefficient is affected.

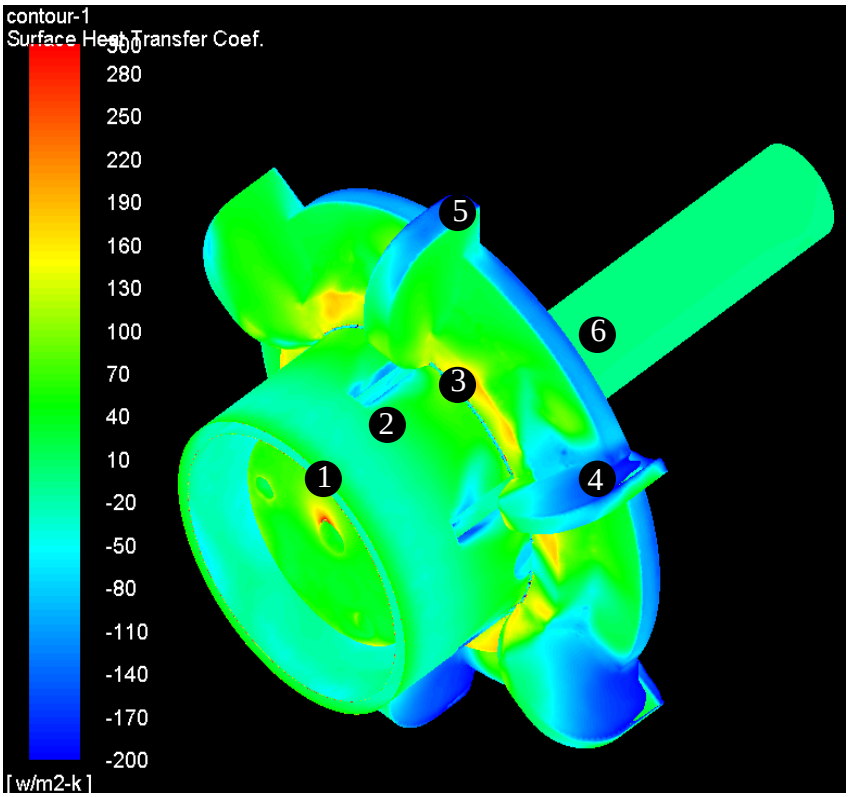

(a)

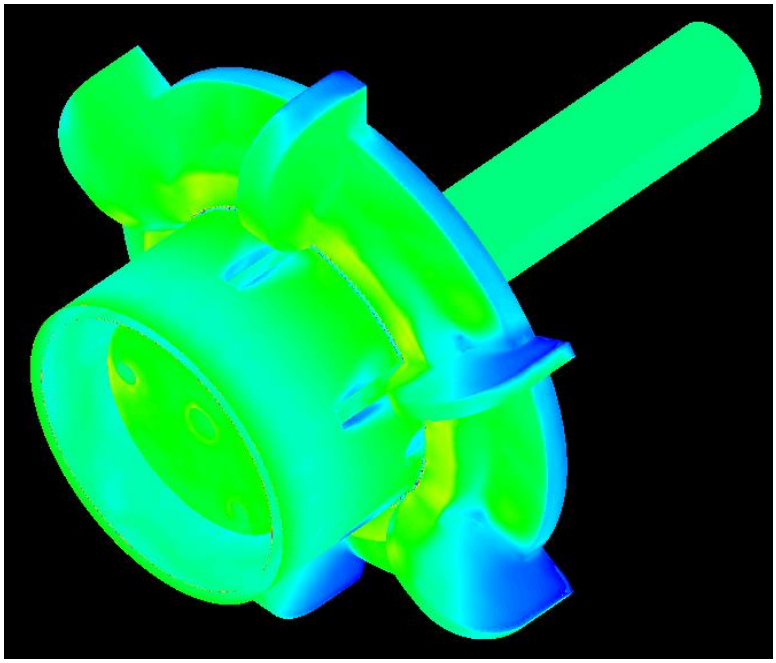

(b)

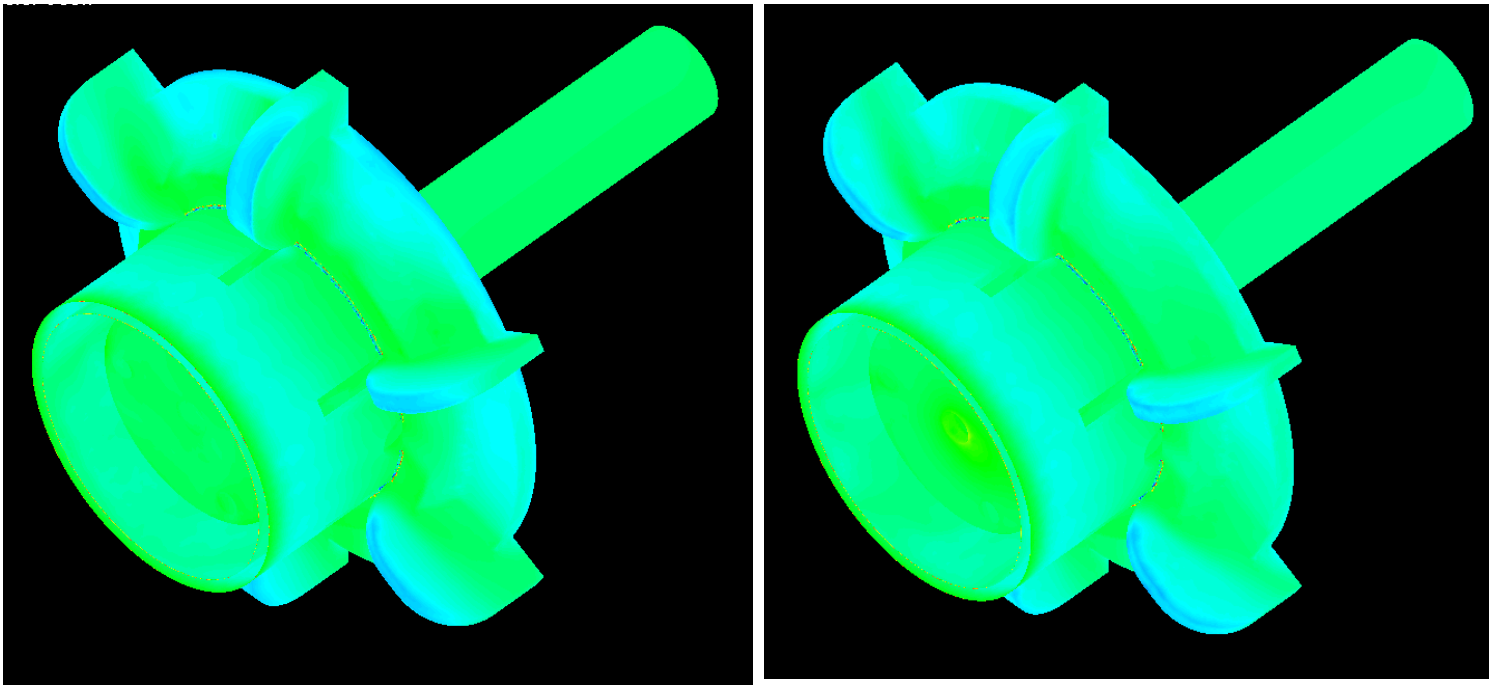

(c) (d)

Figure 4-14. Heat transfer coefficient plots of the baseline model for the four simulated speeds (a) 3000, (b) 2250, (c) 1500 and (d) 1000rpm.

4.5. Validation of Experimental Results

Validation of the simulated results is important to determine the accuracy. The temperature at point 1 is 300°C in both sets of results. This is not surprising as this is the input temperature and the only value that can be controlled for both sets of results. Figure 4-15 depicts the results from the experimental and CFD analysis for all four rotational speeds. Unsurprisingly after point 1 for all rotational speeds, the initial temperature of 300°C decreases. Point 2 is located at the seal region of the model where the baseline model exits the casing. At this point at the four running speeds the differences between the CFD and experimental results are, 1.36% increase, 5.09% decrease, 6.37% decrease and 3.55% decrease respectively. These values show confidence in the results due to the low fluctuations in results. At point 3, located at the centre of the hub body the difference between the experimental and CFD values decreases by, 16.53%, 25.21%, 13.64% and 17.33% respectively. In comparison to the values taken at point 2 there is a significantly larger difference to the results. This could be due to method of recording the measurements. The IR thermometer is aimed at the same location for each set of readings. The geometry of the hub could affect the readings. This is due to point 3 being in-line with the slots in the hub outer for the fins to sit in. This has the potential to affect the results as the slot would break the IR beam as it rotates. Point 4 located at the point where the motor bearing would sit on a directly driven fan found the differences between the experimental and CFD results to be lower by, 15.12%, 21.55%, 15.07% and 13.11% respectively.

The general trend in the results show the experimental values to be lower than the CFD values at the same points apart from point 1. The average difference between the values is 4.09%, 18.18%, and 16.21% for point 2,3 and 4 respectively. As discussed the placement of some points used to take the temperature readings, could be a contributing factor for the difference in the results.

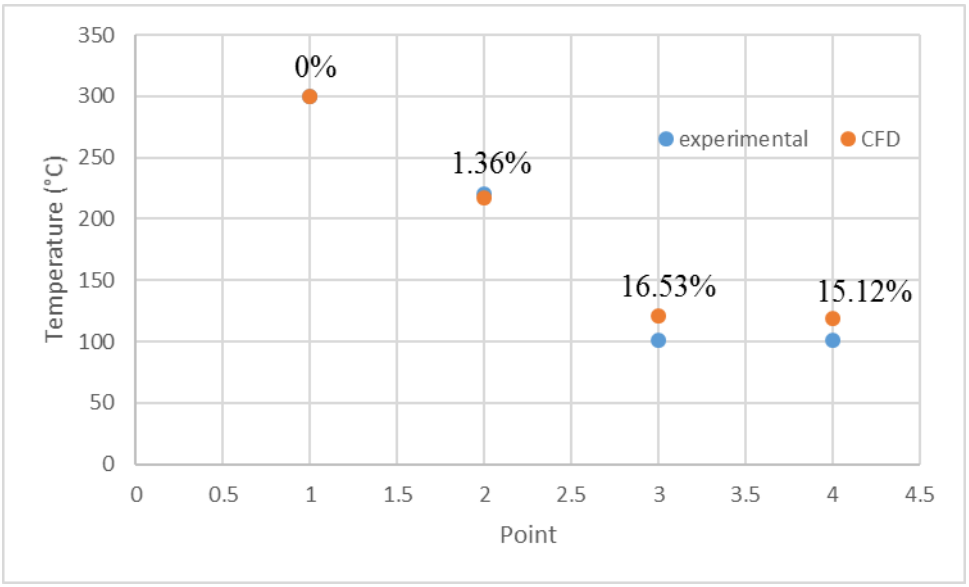

(a)

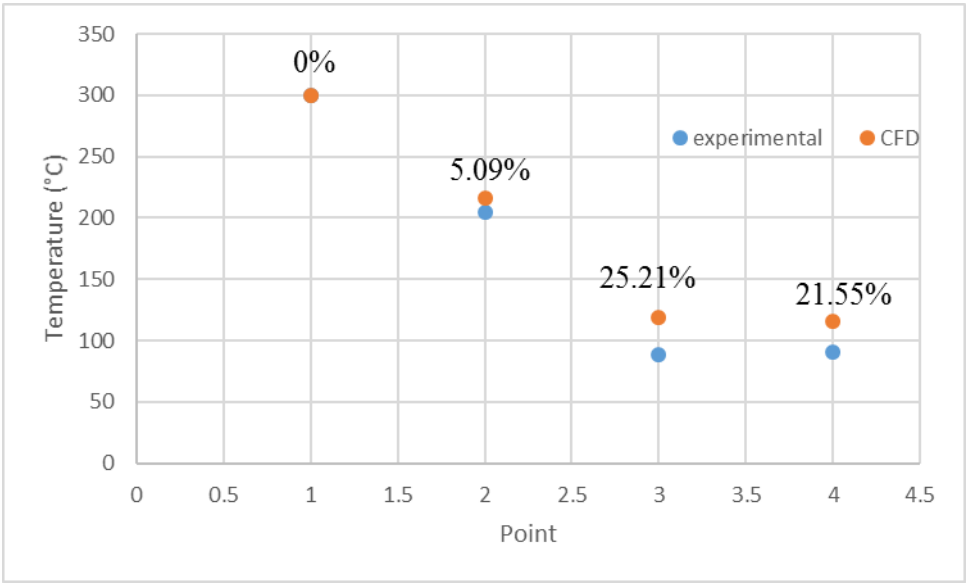

(b)

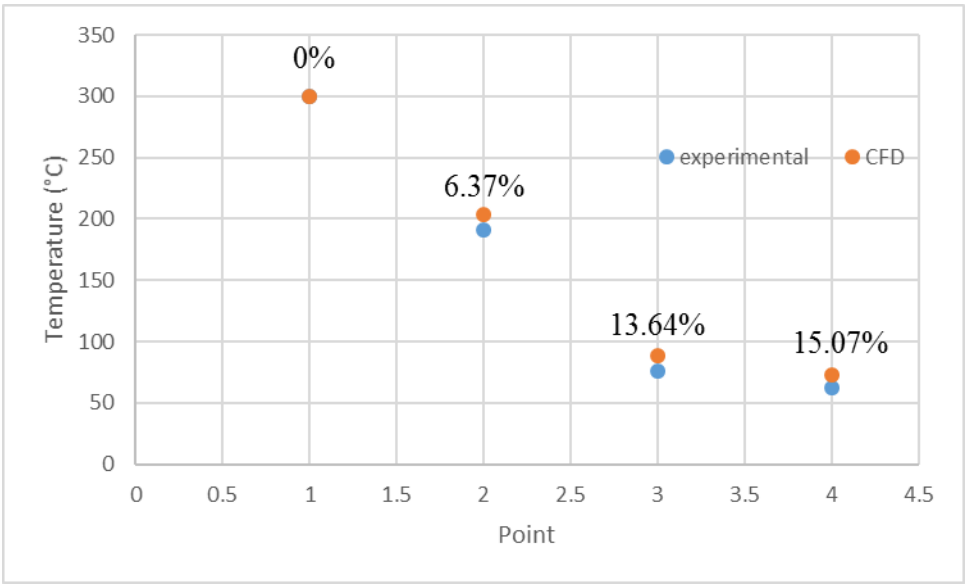

(c)

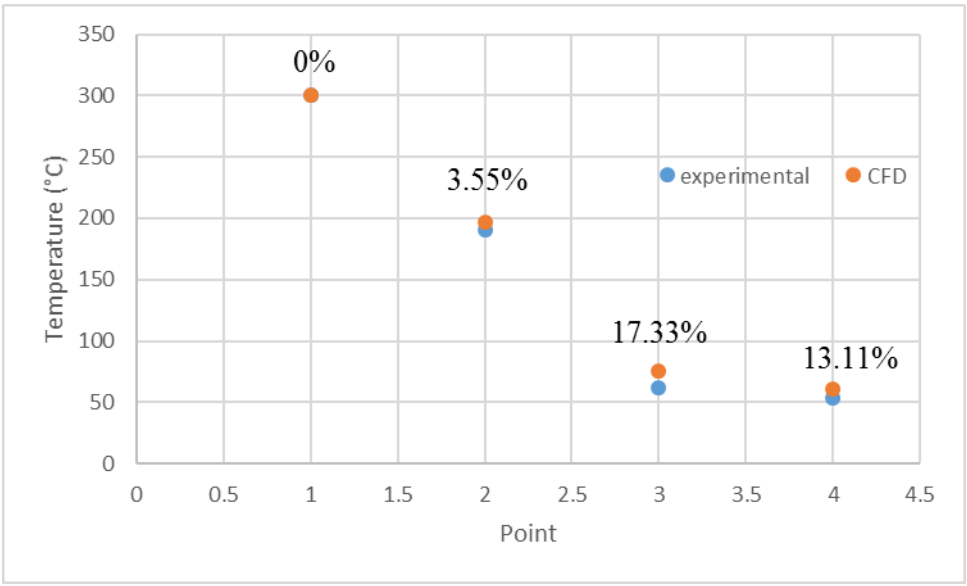

(d)

Figure 4-15. Experimental to numerical comparison. (a) 1000rpm, (b) 1500rpm, (c) 2250rpm and (d) 3000rpm

4.6 Summary

After analysing the baseline model with respect to how many parts it is made up of, how long it takes in assembly and any travel time required between the manufacturing processes. It is concluded that the model is difficult and time consuming to manufacture. The baseline model is known to operate successfully at its design temperature. A stress analysis was conducted to determine the stresses the model experiences under its normal operation. The stress analysis did not find high levels of stress or displacement. Moreover, the natural frequencies of the

model were determined though a modal analysis. The natural frequencies of the model were not found to be close to those of the running speed.

The purpose of the baseline model is to dissipate heat away from the drive shaft to reduce the heat transfer in the shaft. The model is known to be effective at this, preventing damage to bearings on fan units operating at elevated temperatures. To determine the heat dissipation properties of the model a thermal analysis was conducted. This explored the temperature at various points on the hub body and shaft. The resulting temperatures coincided with the knowledge of the baseline models successful operation, as the temperature that the motor bearing must remain below is 120°C [41]. A level of confidence was gained in the results as they were validated experimentally using a purpose built test rig.

The following chapter looks at the results from this chapter in addition to the literature review and uses them to develop a novel hub model.

CHAPTER 5 DEVELOPMENT OF NEW HUB DESIGN

The main issue with the baseline model is the time it takes to manufacture. This is due to the large number of parts and processes required. To try and reduce this a Design For Manufacture and Assembly DFMA analysis has been carried out. As shown in the previous chapter the new hub will be required to dissipate heat to the extent that at the point where the motor bearing sits the temperature in the shaft is below 120°C.

5.1. Concept Design

Having discussed the large number of parts that make up the baseline model in chapter 4, the complexity of the process including all the manufacturing processes are highlighted in figure 5-1. Once the drawings for the model are issued the next stage is to laser cut the fins and get the outer and inner bodies machined. Once all the parts are located together the next stage is the fabrication stage. The first task is to tack weld the fins onto the hub body once these are located correctly a seam weld will be completed securing these in place. The hub outer is welded to the flange, before the fins are located in the hub outer slots and welded in place. In addition to the manufacturing processes that have to take place, the flow chart also depicts the amount of travel involved in moving the components to the various stages of the process. What this means is that with every additional process and the travel times associated the cost of the part increases.

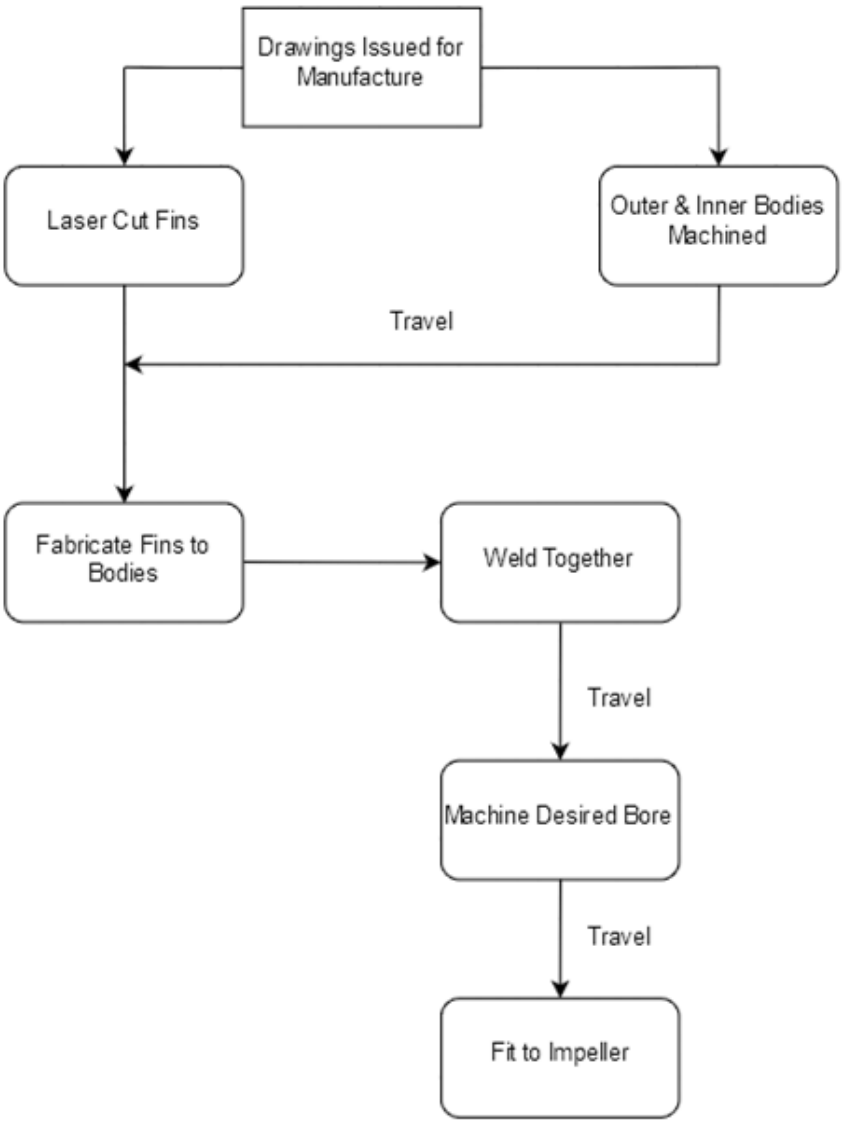

Figure 5-1 flow chart detailing the fabrication process of the baseline model

5.1.1 Assembly Analysis of the Baseline Model

Design for Manufacture and Assembly (DFMA) explores ways in which efficiencies can be made within the manufacturing and assembly processes. Boothroyd et. al. [7] recommends a method of determining whether the current product is overcomplicated by carry out a design for assembly (DFA) analysis. This involves looking at the components that make up the assembled product and making assessments based upon a certain criteria. The first criteria relates to the products movement:

- Does the part move relative to the other parts already assembled?
- Is the movement essential for operation?
- Does the part have to be separate to provide movement?

If all the answers to the questions relating to movement are 'Yes' then the part is deemed as an essential part to the assembly as a whole.

The second criteria determines if the current material selection is suitable:

- Is the material of the part different to those it is in connection with or is it isolated completely?
- Is the part currently manufactured from a different material, or used in isolation essential for its operation?
- Is the part separate as to fulfil the isolation or different material need?

Third criteria relates to whether the parts are adjustable or replaceable:

- Is the part separate to allow for adjustability or replacement?
- Is this adjustability and how easy is the part to replace?

Applying these principles and criteria to the hub during its assembly, enables the opportunity for components that are not necessarily required for the product to begin a redesign:

- Hub Body: This is the first part that work begins on therefore in relation to the other components nothing can come before it, making it a necessary part. The only aspect that is completely necessary is the ability to create a secure connection to the drive shaft this is a possible area of redesign.
- Flange Retaining Plate: The purpose of the retaining plate is to ensure that the Novus material remains located as required. It is a bolted connection, which in theory could be replaced by an integral fastening arrangement. The plate must remain separate, therefore is a required part.
- Flange: Connects the hub to the impeller through a bolted connection, theoretically this could be an integral fastening arrangement and possibly designed so that it is combined with the outer hub body.
- Novus: This is used to provide heat insulating properties which contributes to the overall effectiveness of the model with regard to dissipating heat from the shaft. It is used in isolation. In theory if something else could achieve the same characteristics for the same value then it could be replaced.
- Novus Retaining Plate: The purpose of the retaining plate is to ensure that the Novus material remains located as required. It is a bolted connection, which in theory could be replaced by an integral fastening arrangement. This plate is isolated but there is the possibility of integration with the hub body especially as the flange retaining plate is also used. The part is theoretically not required.

- Hub Outer: This connects to the fins and the flange to bring the model together. If a creation of a design that allows for integration between the hub body, fins and flange then the part would not be required.
- Fins: These are welded to the hub body to help draw heat from the shaft. Their design forms a very crucial part in what the model is trying to achieve. For these to be deemed unnecessary an alternative design for the model would need to be produced.
- Shaft Retaining Plate: This retaining plate helps to hold the hub on the drive shaft. It is a bolted connection, meaning theoretically an integral fastening arrangement could be used this would be quite difficult on a shaft. Making this a critical part.

Table 5-1 breaks down the parts from the discussion above. Only the parts that make up the theoretical part count are included. Details of how long it takes to assemble each aspect of the part are included with the quantities. From this the assembly cost is calculated based on a labour rate of £30 an hour. This cost can be used to estimate a total cost for the prodiuct.

Table 5-1 Results of the assembly analysis

	No.	Theoretical Part Count	Assembly Time (s)	Assembly Cost (£)*
Flange Retaining Plate	1	1	150	1.25
Flange	1	0	300	2.5
Novus	1	0	100	0.83333
Novus Retaining Plate	1	0	150	1.25
Hub Outer	1	1	1200	10
Fins	6	6	1200	10
Shaft Retaining Plate	1	1	200	1.66667
Hub Body	1	1	300	2.5
Totals	13	10	3600	30

(*Labour at £30 an hour rate)

5.1.2 Cost Analysis of the Baseline Model

The time taken to manufacture the baseline model equates to a cost of £30 however there are additional costs to be considered. As the assembly analysis only accounts for the time working to assemble the model. The flow chart in figure 5-1 depicts how travel costs form a contributing factor to the overall cost. There are three individual instances during the products manufacture that require travel for a different process to be carried out. The other costs are related to the manufacture of the parts initially such as the laser cut fins and the machined central section. There is a cost for the actual work and the material required.

In total including the travel, material, assembly and manufacture of parts the cost of the baseline model is around £390.

5.1.3 New Product Development

The new hub needs to be manufactured in as few stages as possible thus reducing the number of processes and the time spend travelling between suppliers, each carrying out a separate task on the product. The first question to be asked is what material is suitable of the new hub? To

determine this a method of process elimination is used to determine the appropriate manufacturing methods. From this the most preferable are selected. Figure 5-2 presents an elimination process and the possible manufacturing techniques. Wilson et. al. [42] applied a similar technique. The processes for consideration are as follows.

5.1.3.1 Solidification Processes

Sand Casting – a widely used casting process that uses moulds made from sand to form complex parts that can be made from a range of metal alloys. The use of sand enables expansion in the process which helps to form the more complex shapes. To remove the parts however the moulds must be destroyed which means that the production rate for parts using this method is quite slow. The initial step is to create the mould. This step must be repeated for each casting. Sand is packed into two halves of a mould with the pattern being covered. Once removed the pattern leaves a cavity. Once the mould is complete the inner surface is lubricated to assist in the removal of the casting. The two halves are then clamped together. The molten metal is then poured into the mould and left to cool. If the cooling process is rushed and the metal cools too rapidly then defects in the casting can occur. To remove the casting, the mould must be broken down completely. The surface of the casting may require additional work to remove the outer layer left.

Investment Casting – uses a wax pattern that is covered in a ceramic material which hardens and the internal shape formed is that which is required. The reason for using the wax is that it can be easily melted from the mould and reused. Complex geometry can be created effectively and several patterns can be used in a single casting, this is done using a 'tree' in that the patterns are set off from a main trunk-like structure. The ceramic coating is created by dropping the pattern into a 'slurry' that is made up of fine silica and other binding media, the desired thickness of the coating is created by dipping the pattern repeatedly. Once the mould has hardened it is heated to remove the wax, leaving the cavity inside. The mould is then heated again this time to a much higher temperature to increase its strength. The molten metal is poured into the mould whilst it is still hot. The reasoning for this is that any thin and detailed sections can be created with a greater tolerance as the mould and molten metal will shrink as one whilst cooling. The process is time consuming and to remove the casting the mould must be destroyed which adds cost to the process overall.

Die Casting – Compared to Investment casting and Sand casting, the moulds for die casting can be reused, thus giving large savings in time and cost for the pars produced, however the initial investment in setting up the process is considerable. The process is like that of sand casting, in that the moulds are in two halves which are then clamped together, the difference being that the halves of the moulds can be reused. Once clamped together molten metal is then injected at high pressures into the mould, the high pressure is used to hold the metal in the mould during the solidification process. Once cooled the mould is opened and the casting removed. The only remaining process is to clean up the casting. The die casting process can become a very efficient method for producing parts as it can be an automated process, however this obviously increases the cost.

Injection Moulding – This method is used for high volume production; the initial setup costs are high but the price per part is very low. The process is used to produce parts made from thermoplastics, the raw material used comes in the form of plastic pellets. These are fed into the machine through a hopper. Once in the machine a reciprocating screw moves the pellets

through a heated barrel section to melt the polymer. Once melted the polymer is injected into split moulds at a high pressure. Once set the moulds open and the new part is removed.

Structural Foam Moulding – this process is identical to injection moulding apart from the fact that a 'foaming agent' is added to the molten polymer which is then delivered to the mould at a lower pressure. This agent is added as a gas and is done so to reduce the density of and therefore the overall weight of the finished product. Strength is also added using this method, which in addition to the lower pressure used means that large and complex parts can be manufactured in a single cycle and at a lower cost.

Blow Moulding – This is a very common process used within industry to produce a variety of different shaped products. The process is similar to injection moulding in that the polymer is fed into the system through a hopper and then heated in a barrel type section before going onto the mould. The difference is that instead of filling the mould completely with the polymer to create a solid, air is forced at the molten polymer as it reaches the mould, sending the material to the sides of the mould in a thin layer, used to create items such as plastic bottles. Extrusion blow moulding is very similar to the injection method except the molten polymer is forced into a cylindrical pipe section initially, before the mould closes around it sealing the polymer off. The mould then moves to a separate air hose that extrudes the cylinder into the edges of the mould. The main difference between the two is that extrusion moulding is cheaper as it is a much simpler process but it is slower.

Rotational Moulding – Is used to create hollow parts however, the main difference from the methods already discussed is the powdered raw material used and the fact that no pressure is involved. This reduces the cost of the moulds. As they do not have to withstand the high pressures, which makes the process cost effective for small batches of parts. The powder is placed into the mould directly and closed up. The mould then begins to rotate in two axis planes. The mould is heated as it rotates which melts the polymer and builds layers of material up on the faces of the mould, the material is cooled and the part removed from the mould.

5.1.3.2 Bulk Deformation Processes

Impact Extrusion – Is a very simple process in which a die is forced onto a piece of material, usually soft metals such as aluminium, at a very high pressure. The piece of material is placed into a mould and the die strikes this material at such a force that it forces the material into the desired shape. Due to the high forces that are applied the tooling must be designed to within stand the stress that it will be subjected to. The most common use of this process is in the manufacture of hollow metal tubing that has one end closed or partially closed.

Cold Heading – Uses metal to form a large range of shapes through forcing the metal at high speed and pressures into moulds. The fact that the metal is worked on whilst cold increases the hardness and strength of the part. Parts are manufactured using the same die with little to no waste making the process very efficient and cost effective.

Closed Die Forging – Takes a piece of metal heated to a very high temperature allowing moulding to a desired shape to take place. The heated piece of metal sits in the bottom half of a mould. The top half is pressed onto the bottom half and the material experiences plastic deformation filling the cavity. The process can produce small to very large parts with high tolerances.

Powder Metal Processing – Uses a powder of metal alloys combined with other elements in a mould with very high precision and often do not require any further post processing work. This precision comes from the power material being compacted in the mould with no possible gaps or cavities able to occur. This mould is then subjected to high temperatures in a furnace bonding the powder together to form a solid to the shape to the mould. The process is able to produce complex parts consistently that have good hardness and wear resistance to close tolerances.

Hot Extrusion – A widely used method to produce parts with a constant cross sectional area. Metals are heated to a temperature that prevents any hardening to take place whilst the work is taking place. The process is similar to that of impact extrusion in that a large force causes the material to form through a mould. The type of product produced is mainly bar and tube section, due to the high pressure required and the heating element the main disadvantage to the process are the high set-up and running casts.

Rotary Swaging – A method of shaping tubing profiles into a desired geometry. The material is forced into the swaging unit and dies are pushed onto it, the general effect is a reduction in the diameter of the tubing. Complexity tapers sections are possible adding to the complexity of the processes capabilities.

5.1.3.2 Material Removable Processes

Machining (From Stock) - Machining covers a large range of techniques and processes used to remove material from a work piece. The most common processes involve some form of either, turning, drilling and milling. The process of turning is work carried out on lathes. Drilling is the production of circular holes using a drill bit and milling uses rotating tooling to remove material from a stock piece. Milling is more of an involved process where the table moves in addition to the tooling. This creates a very diverse process that can produce complex profiles and shapes.

Electrochemical Machining (ECM) – Uses a similar method to milling to create complex shapes however the main difference is the processes ability to work on materials with a high hardness level. A high current is passed through the work part and using conductive cutting fluid the result is a cutting tool that does not wear down, as it never actually touches that part. This makes the process more complex than traditional milling which vastly increase the production costs of a part.

Electrical Discharge Machining (EDM) – Again a similar process to milling but instead of a rotating tool removing the material, very fast discharges of electrical current are used.

Figure 5-2 details different methods used to manufacture parts. The general shape attributes defined initially are the most common elements that make up a part. The purpose of figure 5-2 is to eliminate the processes that are unsuitable to manufacture new hub design from. It achieves this by eliminating the shape attributes that do not form part of the new hub design. This is denoted by the dark grey box the light grey box shows the processes that could be used but are not done as frequently. This leaves the white boxes that are possibilities for the material selection and the process of manufacture for the new hub design.

From the analysis of the manufacturing techniques, the methods to manufacture the new hub are either:

- Casting (using different types)
- Casting parts and welding together
- Machining

Shape attributes

1. Depressions Yes
2. Uniform Wall Yes
3. Uniform Cross-section No
4. Axis of Rotation Yes
5. Regular Cross-section No
6. Captured Cavity Yes
7. Enclosed Cavity No
8. No Draft Yes

Key

Normal Practice

Less Common

Not Applicable

Solidification Processes													
	Cast Iron	Carbon Steel`	Alloy Steel	Stainless Steel	Aluminium and Alloys	Copper and Alloys	Zinc and Alloys	Magnesium and Alloys	Titanium and Alloys	Nickel and Alloys	Refractory Metals	Thermoplastics	Thermosets
Sand Casting													
Investment Casting													
Die Casting													
Injection Moulding													
Structural Foam Moulding													
Blow Moulding (ext.)													
Blow Moulding (inj.)													
Rotational Moulding													

(a)

Bulk Deformation Processes													
	Cast Iron	Carbon Steel`	Alloy Steel	Stainless Steel	Aluminium and Alloys	Copper and Alloys	Zinc and Alloys	Magnesium and Alloys	Titanium and Alloys	Nickel and Alloys	Refractory Metals	Thermoplastics	Thermosets
Impact Extrusion													
Cold Heading													
Closed Die Forging													
Powder Metal Processing													
Hot Extrusion													
Rotary Swaging													

(b)

Material Removable Processes													
	Cast Iron	Carbon Steel`	Alloy Steel	Stainless Steel	Aluminium and Alloys	Copper and Alloys	Zinc and Alloys	Magnesium and Alloys	Titanium and Alloys	Nickel and Alloys	Refractory Metals	Thermoplastics	Thermosets
Machining (from stock)													
ECM													
EDM													

(c)

Figure 5-2 Selection of appropriate materials for manufacture of the new hub design, (a) – Solidification Processes (b) – Bulk Deformation Processes (c) – Material Removable Processes

To improve on the current method of manufacturing, using a combination of machined and laser cut parts, a reduction in time taken carrying out different processes could lead to a cost saving. Machining the current design as a single component would eliminate the laser cut parts and any additional fabrication processes, however due to the design complexities of the

baseline model this is not achievable. To create a design like this the baseline model would need to be redesigned.

5.1.4. Concept Design Creation

One way in which the overall cost of the model can be reduced is by eliminating the amount of travel compared to the baseline model. To achieve this the new model must be manufactured as much as possible in a single location, thus eliminating any processes that require further work after the initial process is complete. The most effective way of accomplishing this is to machine the model as a solid part. For the new hub, a solid casting is utilised, incorporating the flange and hub outer profile of the baseline model. The theory behind the effectiveness of the baseline model is down to the fin arrangement and the cavity within the model, as this reduces the area of material the heat can transfer through. The machining of the casting will remove the same amount of material that the cavities in the baseline model created.

As the casting process only achieves a rough overall shape, the first machining process is to remove the excess material from the casting process to the required outer profiles. The second stage is to begin removing the internal material. To achieve the required amount of material removal, holes are drilled into the hub body. Eight holes are drilled axially the full length of the hub body this can be seen in figure 5-3. In addition to this a further eight holes are drilled vertically into the hub body. These connect up with the first set of holes drilled. By machining the hub in this way the overall cost is reduced significantly by 31%. This is due to a reduction in transport costs, as the only transport is from the place where the machining takes place. The elimination of welding and laser cut parts reduces the direct costs and negates further work in fabricating the parts to the hub body.

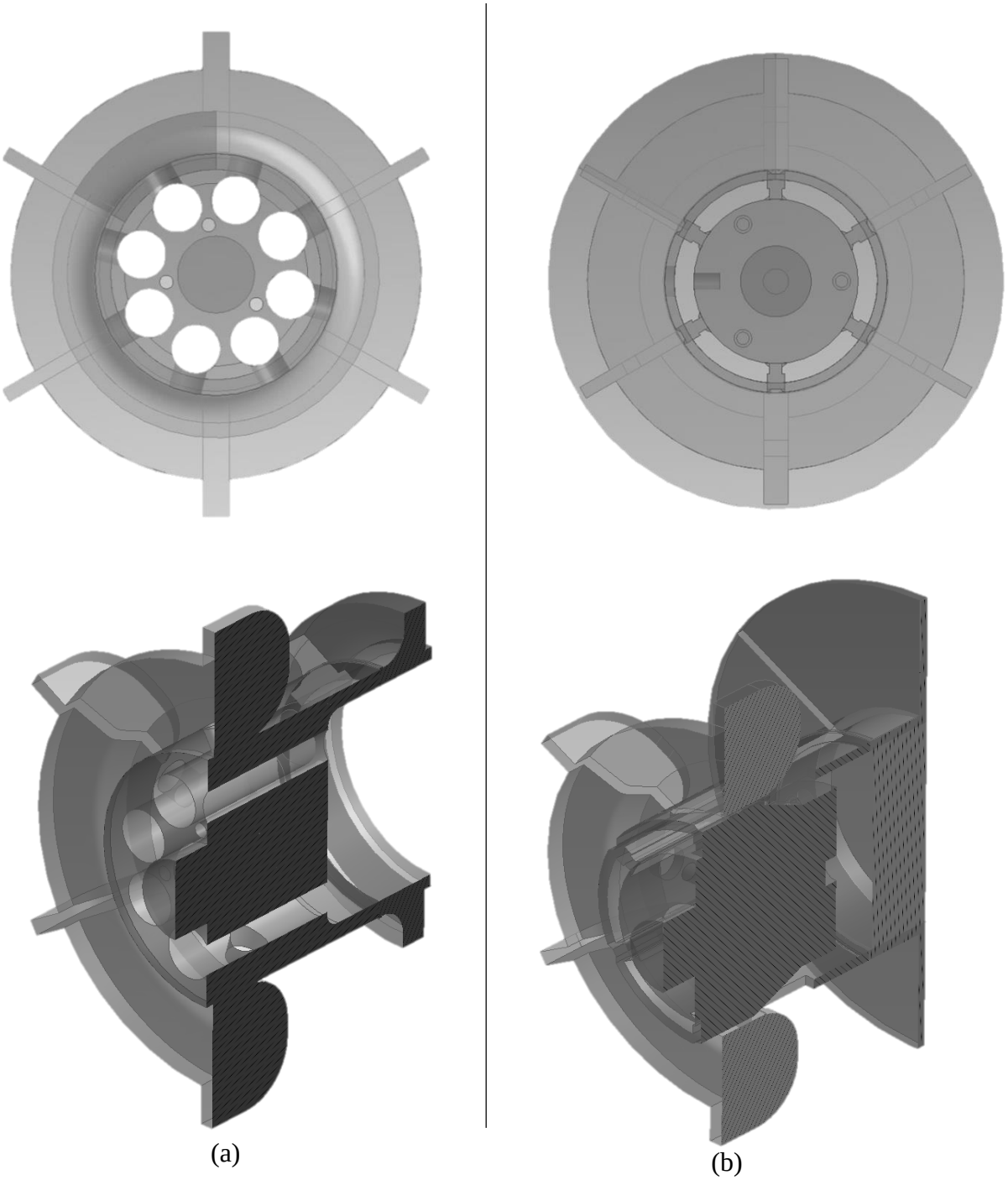

(a) (b)

Figure 5-3 Geometry comparison of the new hub (a) and the baseline model (b)

5.2. Experimental Comparison

Table 5-2 presents the experimental results of the new hub at the same five points as previously tested on the baseline model. It can be seen that like the previous results the temperature after point 1 begins to decrease. An initial comparison of the results finds that like the baseline model the value at point 1 remains the same regardless of the rotational speed. Initially the values for the temperature appear to be higher for the new hub. To compare the results from the experimental analysis for both hubs directly they are plotted graphically in figure 5-4. Like the

baseline design results the rotational speed has a significant effect on the results of the new hub. With the temperature at the points decreasing as the rotational speed increases.

As discussed point 1 shows a 0% difference as this is the input temperature set using the control panel on the test rig. Point 2 shows on average the temperature on baseline model to be 3.15% lower. This is the point located at the seal section of the model the main difference lies within the centre of the hub. The location of the seal on the baseline model is just behind where the fins are welded on. This leaves a space between the hub body and the hub outer giving a slight reduction in the temperature. Moreover, the wall thickness of the baseline is defined by the hub outer section. This gives a thinner profile to the outer edge than the new design. This would cause an increase in temperature due to the increase in material.

The temperature values at point 3 on the new hub are on average 29.19% higher than the baseline model values at the same point. This shows how the different designs can have a significant impact on the results. Point 3 is located at the centre of the hub body this gives a good understanding of the effectivity of how the different designs dissipate heat. On the baseline model point 3 is located directly under the centre of the fin sections. This allows the fins to dissipate heat to reduce the temperature by 59.56% on average from point 2. In comparison the new hub reduces the temperature by 42.52% from the same point. Point 4 is the location of the motor bearing in a direct drive fan. The temperature at point 4 is on average 33.62% higher on the new hub over the baseline model. This gives an understanding of how effective both designs are.

Table 5-2 Experimental results of new hub

Point	Temperature (°C) at 1000rpm	Temperature (°C) at 1500rpm	Temperature (°C) at 2250rpm	Temperature (°C) at 3000rpm
1	300	300	300	300
2	214	210	202	194
3	151	148	92	84
4	157	143	88	79
5	154	138	83	75

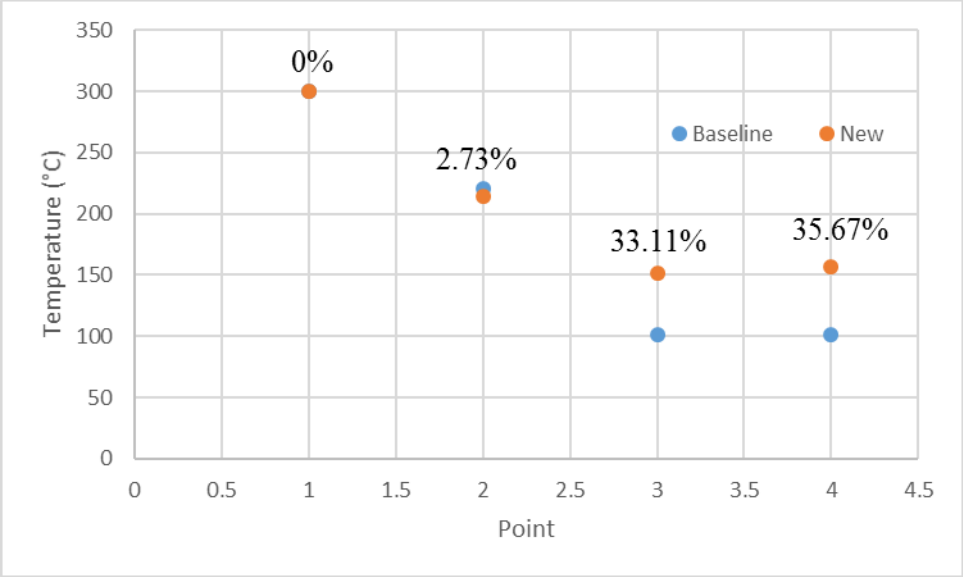

(a)

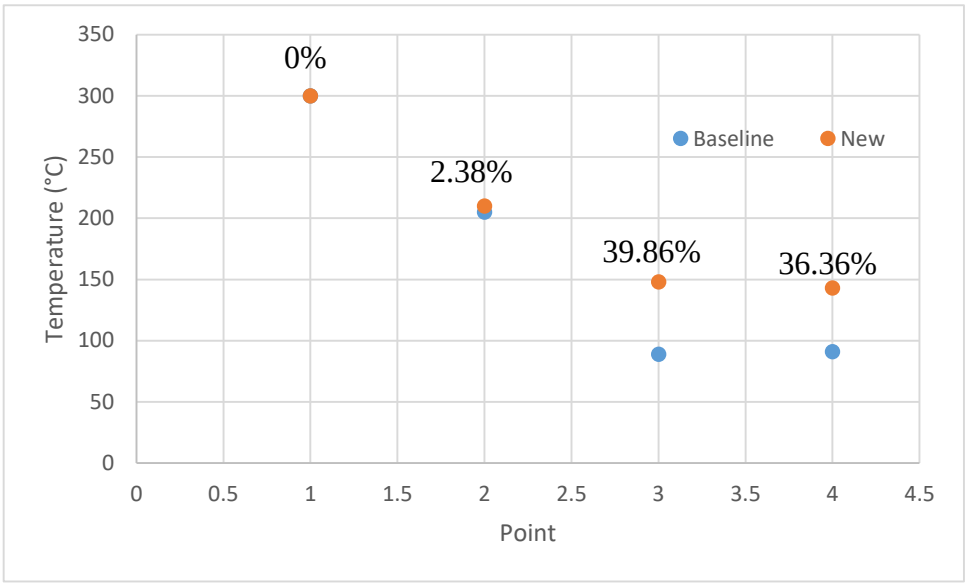
350
300
250
200
150
100
50
0
Temperature (°C)
0
0.5
1
1.5
2
2.5
3
3.5
4
4.5
Point
Baseline
New
0%
2.38%
39.86%
36.36%

(b)

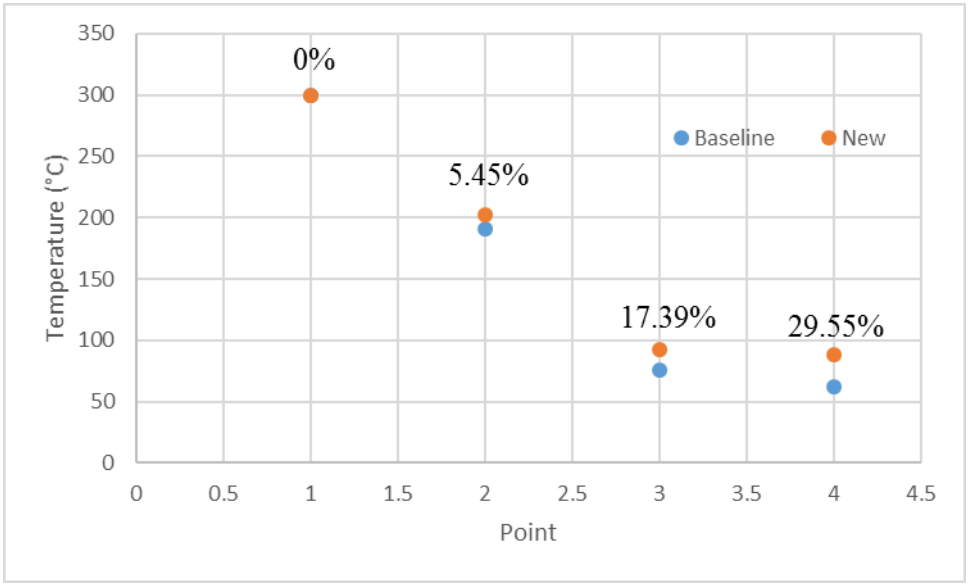
350
300
250
200
150
100
50
0
Temperature (°C)
0
0.5
1
1.5
2
2.5
3
3.5
4
4.5
Point
Baseline
New
0%
5.45%
17.39%
29.55%

(c)

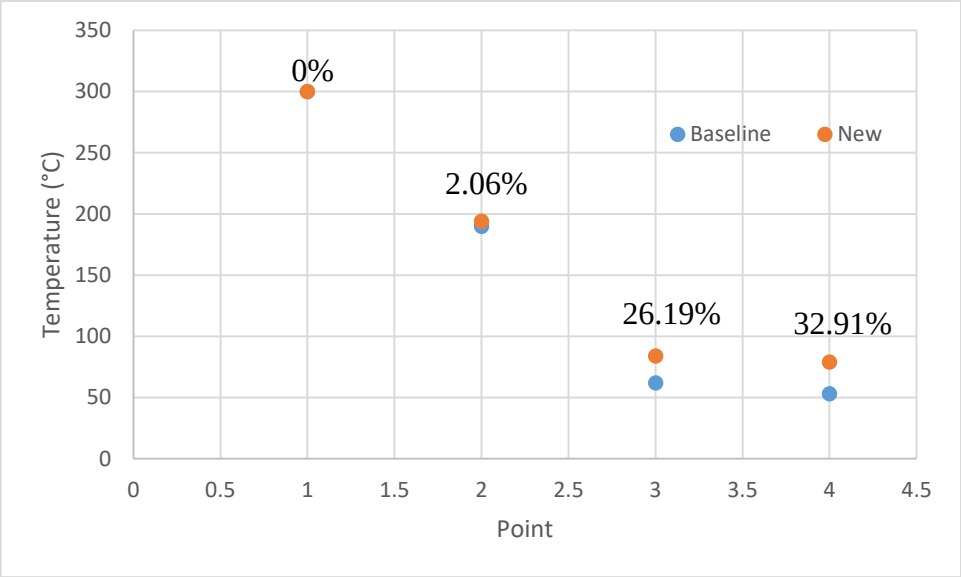

(d)

Figure 5-4 Percentage difference between experimental results. (a) 1000rpm, (b) 1500rpm, (c) 2250rpm and (d) 3000rpm

5.3. Stress Analysis Comparison

Table 5-3 presents the von mises stresses at two points on the new hub these points are depicted in figure 5-5. The high stress points are in different locations to those on the baseline model. The baseline models stresses were caused by the notches on the hub outer for the fins to be welded to. As the new hub does not have these notches this stress is eliminated. The highest stress value on the new hub is caused by the spigot section on the back of the flange, located at point 2 in figure 5-5. The highest value for the stress at this point is 7.25MPa at a rotational speed of 3000rpm. A reduction of 67.66% compared to the baseline models highest value for stress. This trend is similar for both the points at all the rotational speeds. The stress contours for all the rotational speeds are presented in figure 5-5 on the same scale. This gives an understanding of how the new hub has reduced the levels of stress through its design. The highest stress value on the baseline model at 1000rpm is 2.49MPa 67.47% higher than the new hub. At 1500rpm and 2250rpm the stress on the baseline model is 5.60MPa and 12.61MPa 67.68% and 68.04% higher than the new hub at the same rotational speeds. This gives an average of 67.71% higher stress on the baseline model.

Table 5-3 Von mises stress on new desgin

Rotating Speed (rpm)	Stress at Point 1 (MPa)	Stress at Point 2 (MPa)
1000	0.72	0.81
1500	1.55	1.81
2250	3.86	4.03
3000	6.58	7.25

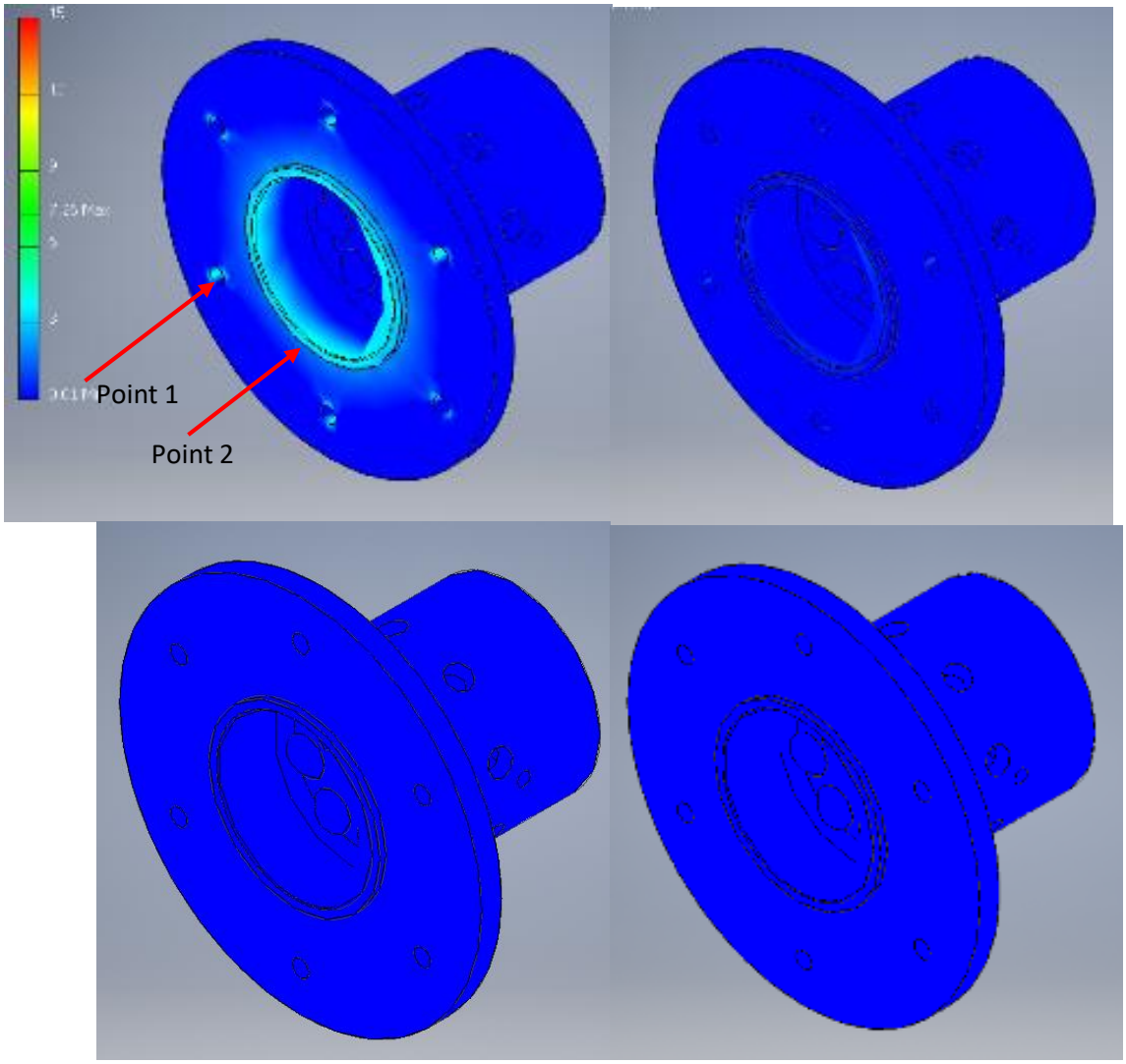

Figure 5-5 Von mises stresses on new hub at 3000, 2250, 155 and 1000rpm respectively from left to right.

Analysis of the first principle stresses on the baseline model are used to assess the welds on the fin sections. As the new hub does not include any welded sections the reason for investigating first principle stresses is to investigate any other locations found to be stressed from the loading conditions. Figure 5-6 depicts the results from the first principle analysis, finding very similar contour profiles for each rotational speed. All the contours are presented on different scales to depict the maximum stress for each running speed. The highly stressed areas of the new hub are all located on the same side of the flange shown in figure 5-6. One of the reasons for this is spigot section, required for attached the hub to the impeller. The spigot is thinner than the rest of the flange making it a weaker point. Secondly, the large green ring section on all the plots is caused by the centrifugal forces acting on the hub body against the flange section. Finally, the highest stressed point is located where the bolts connect to the flange to connect the hub to the impeller, this is labelled as point 3 in figure 5-6. Table 5-4 presents the high stress values for the four rotational speeds at point 3 in figure 5-6. The highest value for stress is found to be 8.17MPa at 3000rpm. This value for the first principle stress is 58.61% lower than the

highest value for the first principle stress on the baseline model. This is reduction in stress compared to the baseline model is also true for the slower rotational speeds. The stresses are 58.45%, 58.70% and 58.56% higher on the baseline model for the running speeds, 1000rpm, 1500rpm and 2250rpm respectively. The average increase in stress on the baseline model is 58.58%. The reasoning for this is similar to the increase in the von mises stresses caused by eliminating the welded sections of the design.

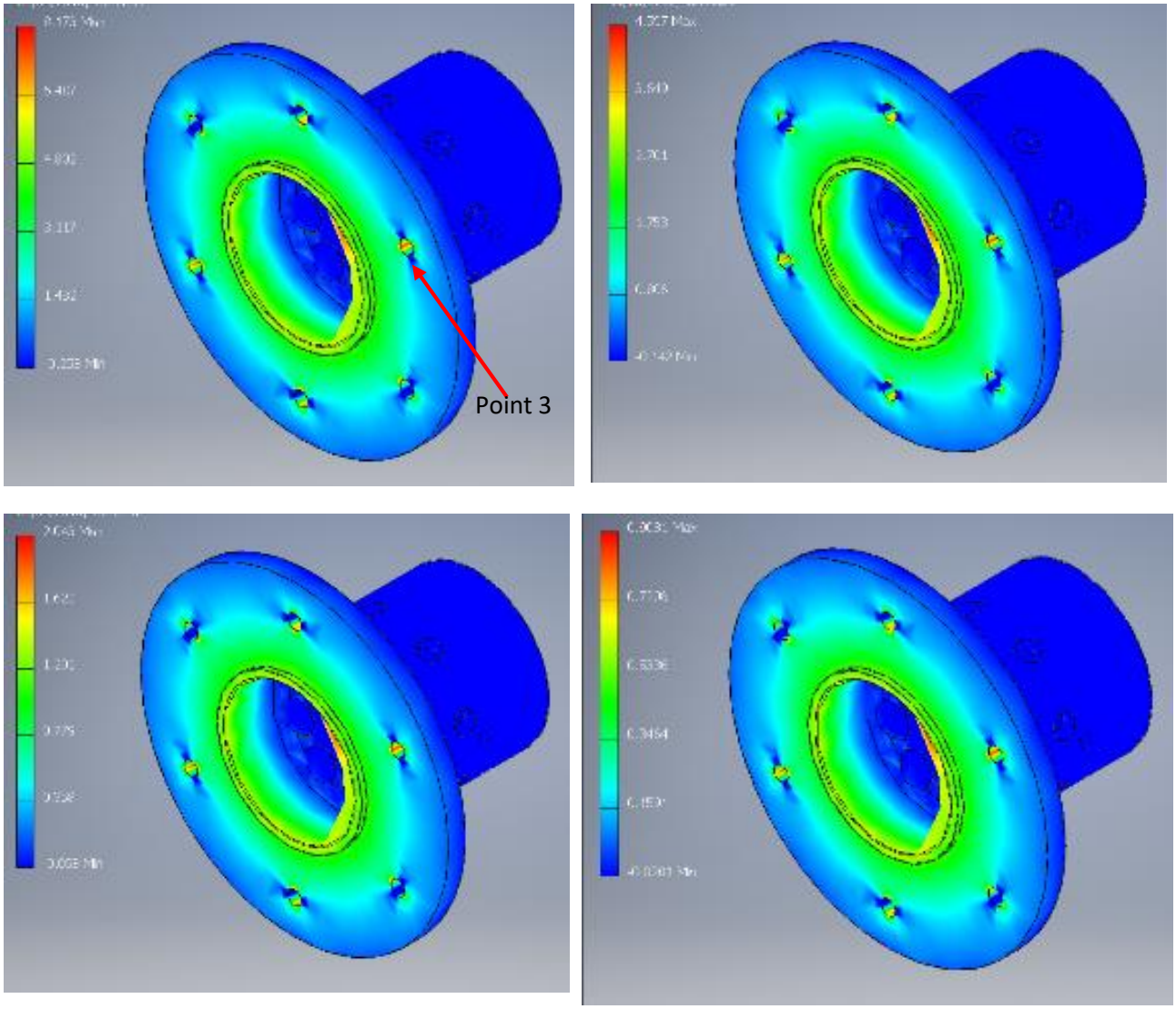

Figure 5-6 First principle stresses on the new model rotating at 3000, 2250, 1500 and 1000rpm

Table 5-4 First principle stresses on new hub

Rotating Speed (rpm)	Stress at Point 3 (MPa)
1000	0.91
1500	2.04
2250	4.60
3000	8.17

The deformation of the new hub is presented in figure 5-7. The scaling is presented so the displacement at each rotational speed can be clearly viewed. The general trend of the displacement shows an elongation of the flange section causing the largest displacement to be at the outer diameter of the of the flange. This is the only area of displacement on the new hub. On the baseline model displacement occurred on the hub body. By removing the welded sections there is no deformation on the hub body of the new hub. The von mises and first principle stress analysis of the new hub found the highly stressed areas to be on the flange section. The contours in figure 5-7 show displacement in the same areas. As the flange extends out from the hub body the centrifugal forces experienced are greater hence the increased stresses and displacement.

The largest displacements at each rotational speed are presented in table 5-5. The displacement increases with rotational speed, this is similar to the baseline model. The difference in the displacement between the lowest rotational speed and the highest is 88.5%. This is within 1% of the difference taken on the baseline model between the highest and lowest rotational speeds. Showing how the effect of rotational speed affects the centrifugal forces in a linearly. At 1000rpm the maximum displacement on the flange is 0.00023mm compared to the baseline model this is a 5.11% reduction. At 1500rpm and 2250rpm the reduction in displacement to the baseline model is 53.64% and 54.17% respectively. The largest displacement of 0.0020mm on the new hub occurs at 3000rpm this is 52.38% lower than the largest displacement on the baseline hub at the same operating speed. The results find the displacement on new hub to be on average 52.81%. This is probably due to the solid one-piece construction of the new hub. This solid design stiffens up the model by eliminating the welded sections that can cause some degree of flexing in the model. The displacement on both models caused by the rotational speeds is substantially low and not a concern.

Table 5-5 Maximum displacement on the baseline model at the four rotating speeds.

Rotating Speed (rpm)	Max Displacement (mm)
1000	0.00023
1500	0.00051
2250	0.0011
3000	0.0020

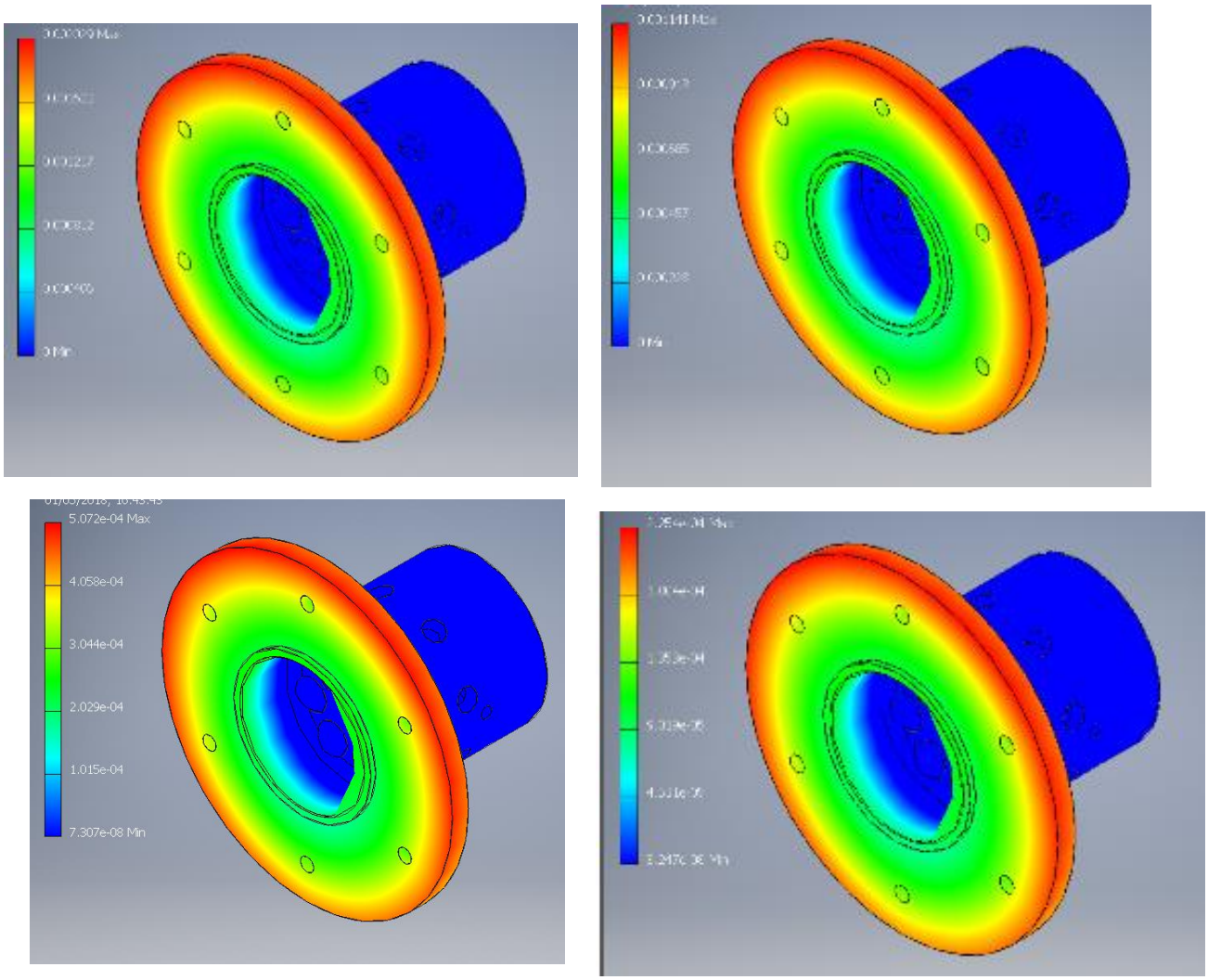

Figure 5-7. Displacement of the new model rotating at 3000, 2250, 1500 and 1000rpm.

5.3.1 Modal Analysis Comparison

The modal analysis of the baseline model calculated the closest natural frequency to be 192% higher than the highest operating frequency. The results for the new hub are presented in table 5-6. The highest operating frequency is 50Hz the lowest natural frequency is found at mode 1 depicted in figure 5-8 is 715.99Hz. 665.99Hz higher than the operating frequency. This is an increase of 16.77% in comparison to the natural frequencies calculated for the baseline model. The natural frequencies of the other seven modes are all higher than the corresponding modes of the baseline model. The average increase in the natural frequencies over the eight modes is 48.09%. Like the reduced stress and displacement values the increase in the natural frequencies of all eight modes is most likely due to the solid one-pieces construction of the new hub.

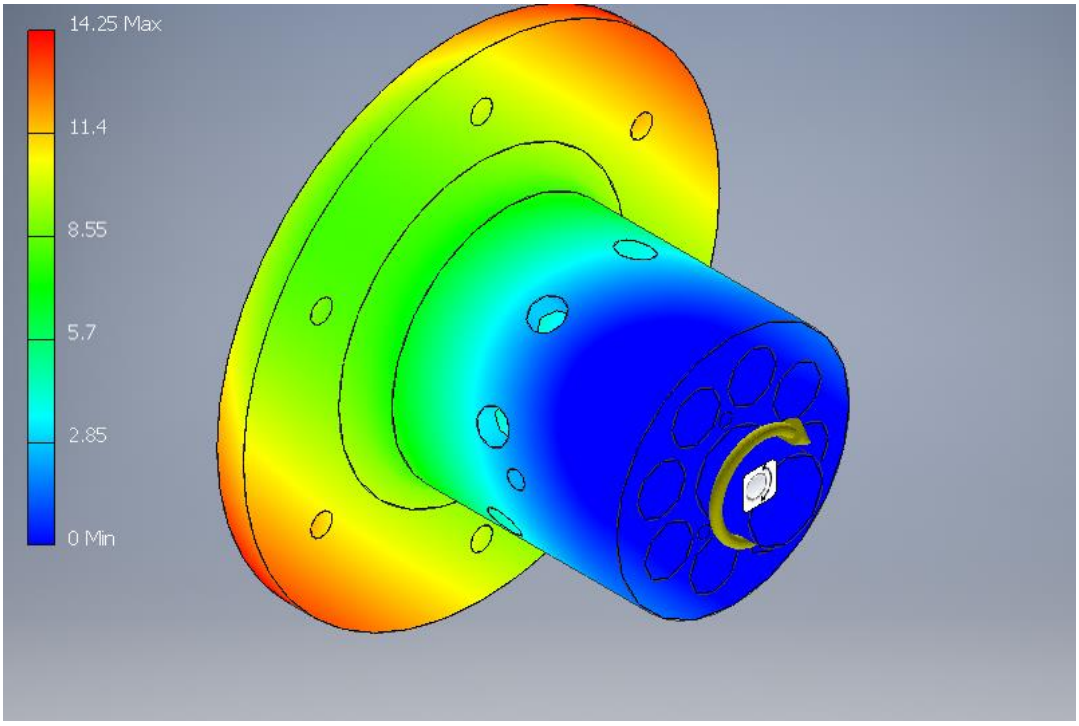

Figure 5-8. Mode 1 of the modal analysis of the new model.

Table 5-6 Results from modal analysis

Mode	Natural Frequency (Hz)
1	715.99
2	720.26
3	1036.20
4	2802.18
5	2918.65
6	2927.84
7	3149.85
8	3152.09

5.3.2 Finite Element Analysis Comparison Summary

Like the baseline model no high of stresses were calculated from the simulations that could lead to potential failure. The elimination of the welded sections on the new model reduced the von mises and 1st principle stresses. This provides a greater safety factor to the new model design. The displacement on the new model was found to be very small. The reasoning for these reduced values is the solid one-body construction of the new hub. The weak point of the baseline model lies within the welded regions. By eliminating the need for any welding to take place the stress raising elements to the model are reduced. Moreover, the welded fin sections would reduce the rigidity of the model, thus explaining why the new fully machined design had a reduced level of displacement under operational loading. The modal analysis showed an increase in the natural frequencies of the model. This again is from the elimination of the welded sections.

5.4. Thermal Analysis Comparison

The same CFD analysis on the new hub has being carried out. Figure 5-9 depicts a cross sectional view through the cooling discs showing the temperature distributions. An initial observation of the distributions finds a higher overall temperature of the new hub in comparison to the baseline model. The explanation for this is the overall design of the new model. The fin sections of the baseline model are clearly depicted and the overall temperature from the centre of the model to the edge of the cooling disc reduces by 23.94% compared to the 2.68% in the new hub. Through the removal of material by machining holes the new hub has presented a design manufactured from different methods to be applied to prevent high temperatures travelling through the shaft. Even if the temperature reduction is not as significant.

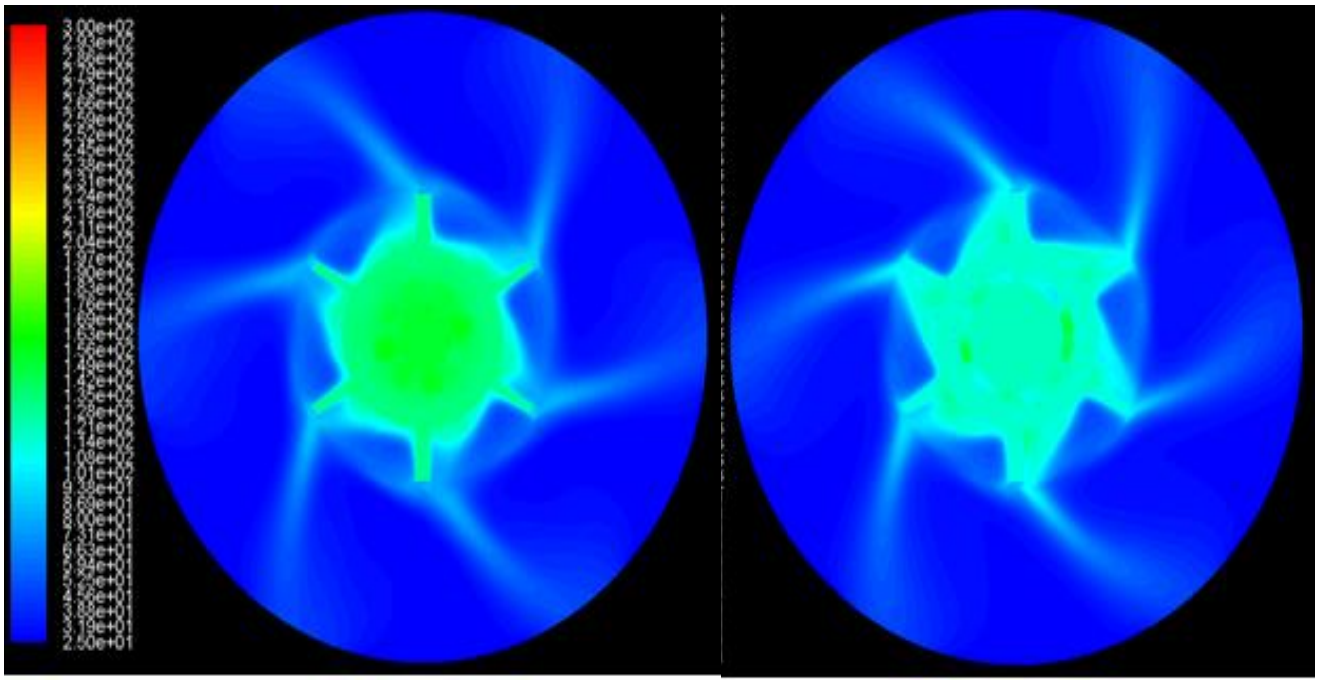

(a) (b)

Figure 5-9 Temperature distribution in the vicinity of the cooling discs on the new hub (a) and baseline model (b)

The cross section depicted in figure 5-10 presents the new hub and the baseline model together for comparison of the temperature contours at a rotational speed of 1500rpm with the temperature set at 300°C at the flange section. The same six points have been plotted as figure 4-10, allowing for a direct comparison of the results. The temperature distributions through both models present how the temperature changes through both hubs. Both models show a general trend depicting the temperature decreasing from left to right. This is expected based on the laws of heat transfer. The visualisation of the contours highlights the differences in the geometries. After the flange section on both models the seal section with the leakage can be identified. The wall thickness at this point on the two models is visibly thicker on the new hub. The results for the new hub presented in table 5-7 calculate the temperature of point 2 to be 226°C, 224°C, 200°C and 190°C at 1000rpm, 1500rpm, 2250rpm and 3000rpm respectively. In comparison to the same point on the baseline model the temperatures are lower by 15.49%, 18.30%, 12% and 9.47%. This gives an average difference of 13.82% at point 2 between the models. This difference is due to the wall thickness which is 2mm thicker on the new model. This explains the increase in temperature based on the heat transfer equations.

From the temperature contours on the hub body where point 3 is located a visible difference can be seen in the overall temperature. The calculated values at point 3 for the new hub are 165°C, 163°C, 107°C and 98°C at the four rotational speeds respectively. The baseline model temperatures at the same point are lower by 26.67%, 26.99%, 17.76% and 23.47% with an average difference of 23.72%. The location of point 3 at the centre of the hub gives a good indication to the effectiveness of the heat dissipation methods used. Point 4 is located after the hub body on the shaft meaning that no further heat dissipation techniques or methods can be utilised to reduce the overall temperature. At point 4 the new hub temperatures are 162°C, 156°C, 105°C and 90°C respectively for the four running speeds. The baseline model results are lower by 25.31%, 23.72%, 18.10% and 21.11%. Giving an average difference of 22.06%.

Excluding point 1 the general trend finds the baseline model to have lower temperature values at the remaining five points. Overall the average percentage difference between the models at the operating speeds 1000rpm, 1500rpm 2250rpm and 3000rpm, are found to be 20.75%, 20.77%, 19.70% and 20.75% respectively. This gives an overall average difference of 20.49% between the baseline model and the new model. The reason for this is a culmination of factors. The wall thickness of the new hub is 2mm thicker than the baseline model the difference is noted by point 2. The use of the finned design shows it effectiveness at point 3 and by point 4 the overall difference in the models is found to be 20.49%.

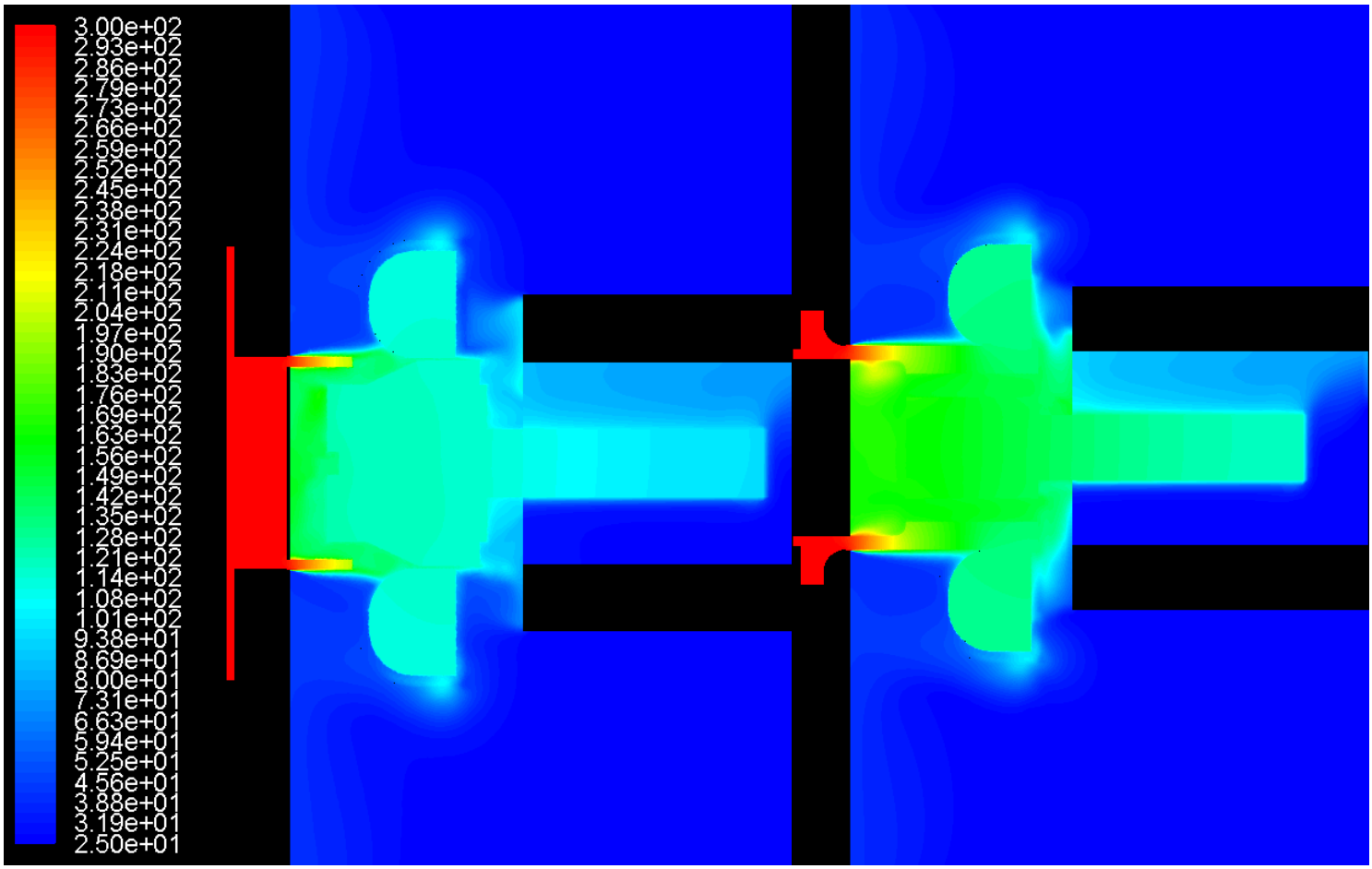

(a) (b)

Figure 5–10 Cross sectional view of baseline model (a) and new hub (b)

Table 5-7 Temperature values taken at six points on the model

Point	Temperature Value (°C) at 1000rpm	Temperature Value (°C) at 1500rpm	Temperature Value (°C) at 2250rpm	Temperature Value (°C) at 3000rpm
1	300	300	300	300
2	226	224	200	190
3	165	163	107	98
4	162	156	105	90
5	158	153	112	93
6	153	148	106	88

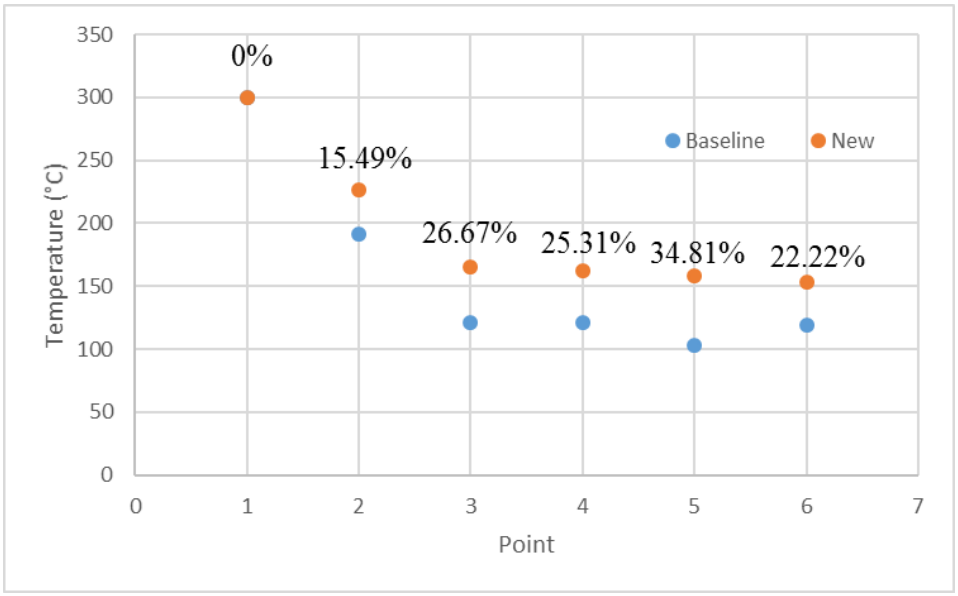

(a)

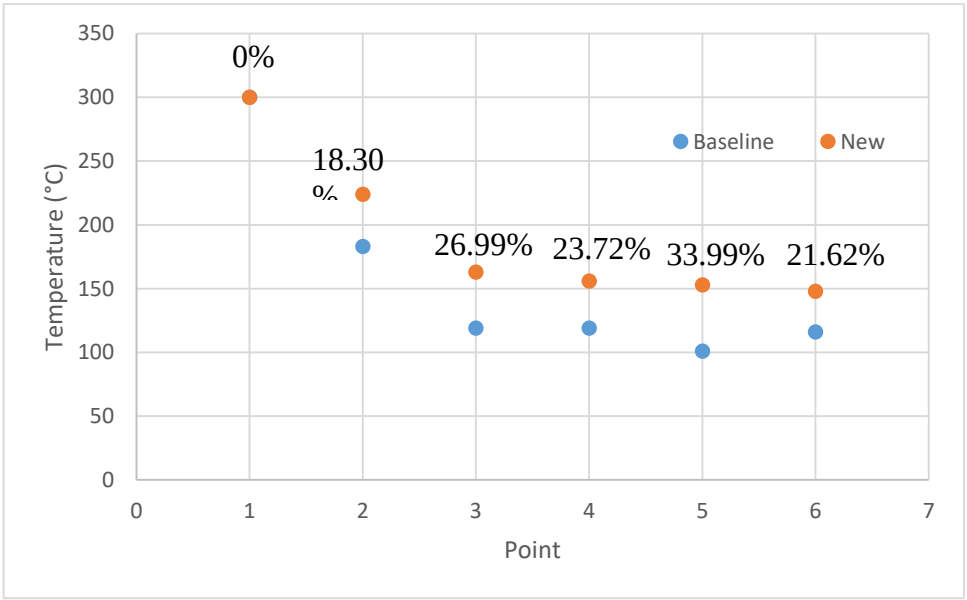

(b)

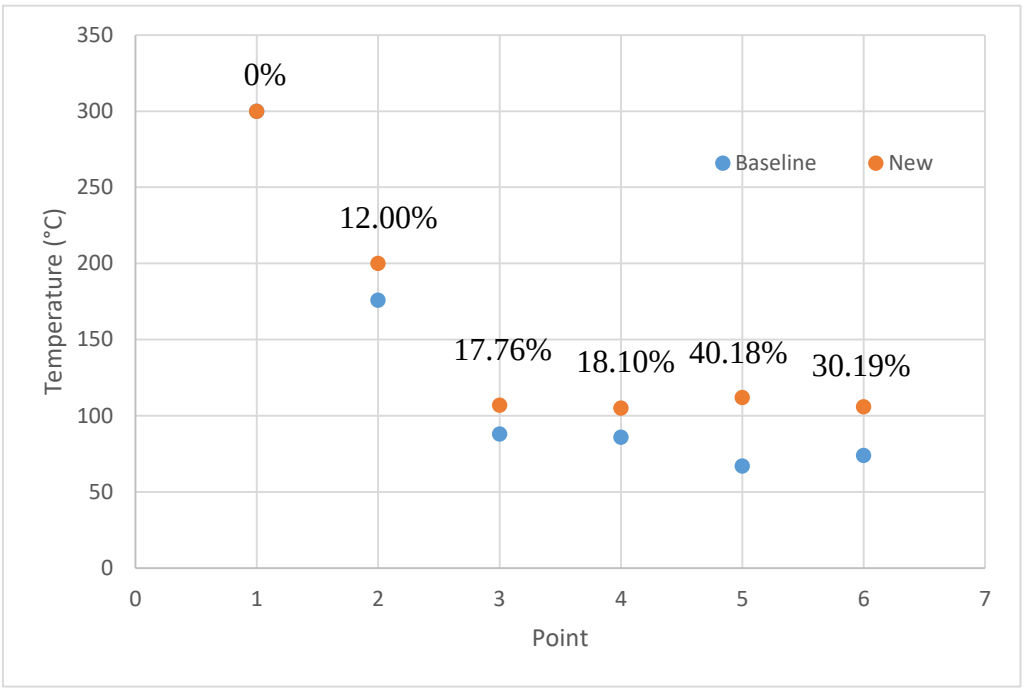

(c)

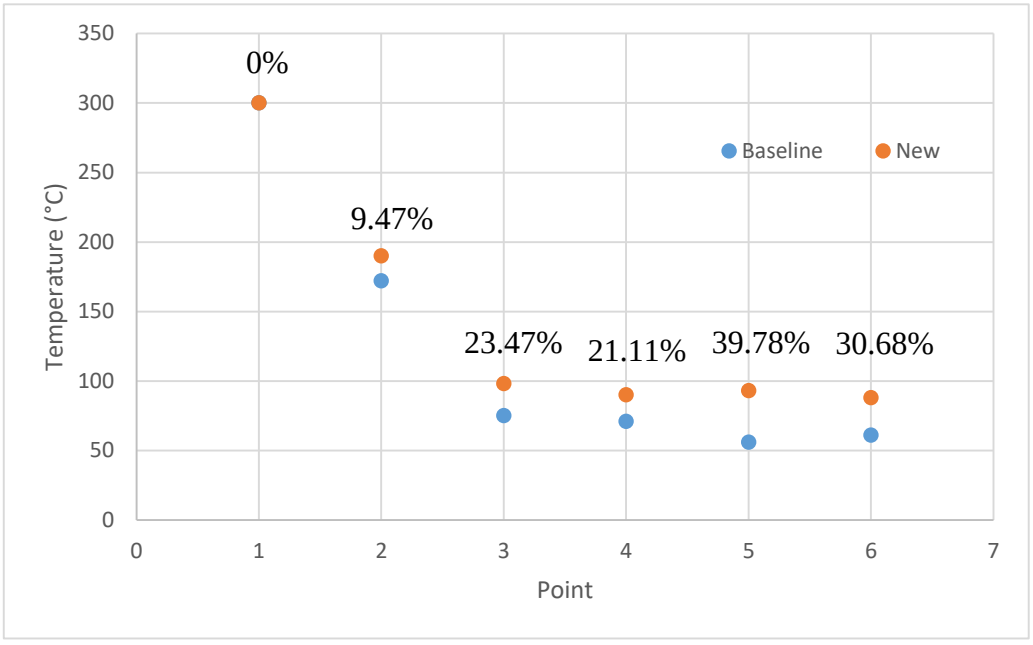

(d)

Figure 5-11 Comparison of CFD results. (a) 1000rpm, (b) 1500rpm, (c) 2250rpm and (d) 3000rpm

Figure 5-12 and 5-13 depict the results of the two lines in figure 4-11, used to investigate the temperature distributions through both models at 1500rpm. The lines follow a similar trend After the seal section the temperature decreases in a linear trend to a point. At which the temperature gradient of the new hub decreases compared to the baseline model. The two vertical bars on the graph in figure 5-12 show this region, the gradient for the baseline model within these lines is 2816.6 and 1659.4 for the new hub. The reason for this lies again in the geometry, if a comparison is made between the models in figure 5-10 it can be seen that there is a noticeable increase in the material area at the centre of the hub. Once the baseline model reaches around 120°C and the new model 140°C, the temperatures begin to stabilise on the graph. This point within both models is where the cooling disc ends, which suggests that for the cooling disc to be at its most effective it should be located as close to the end of the hub as possible.

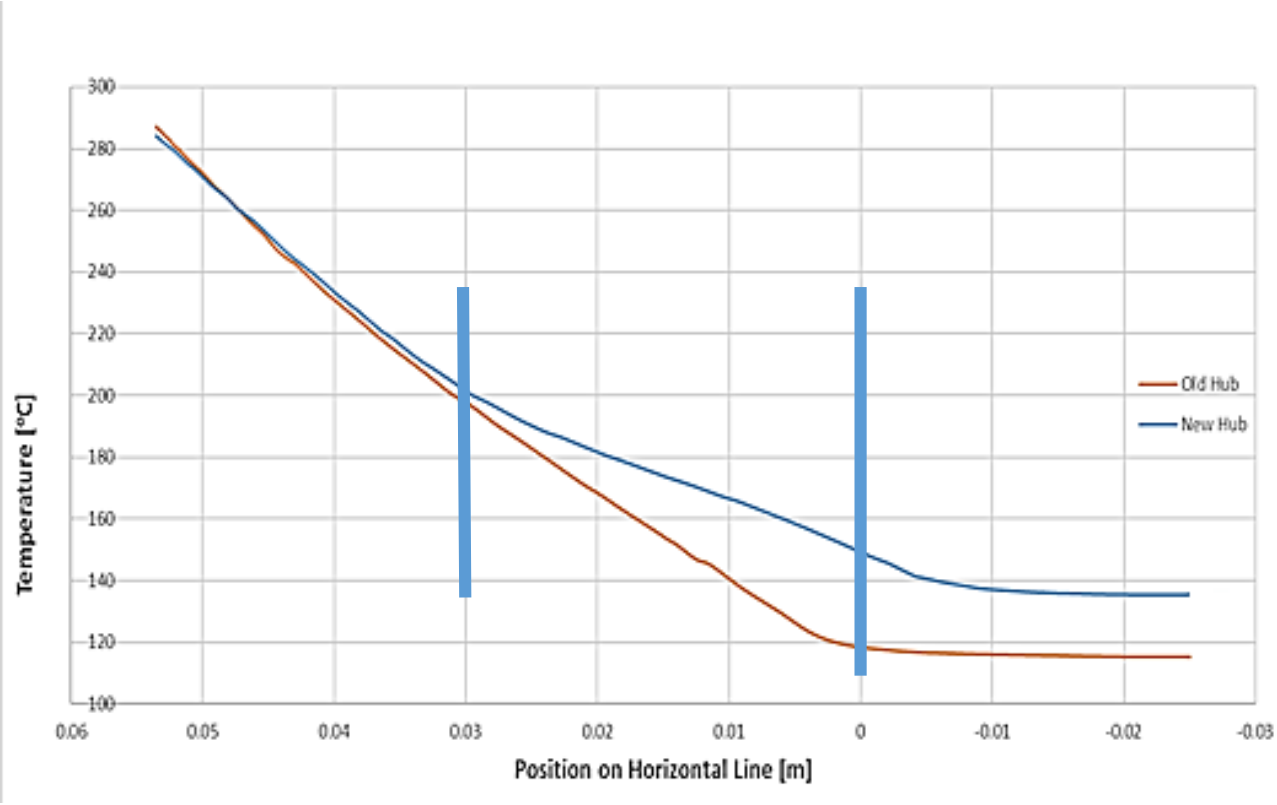

Figure 5-12 Temperature distribution from line 1 on both models

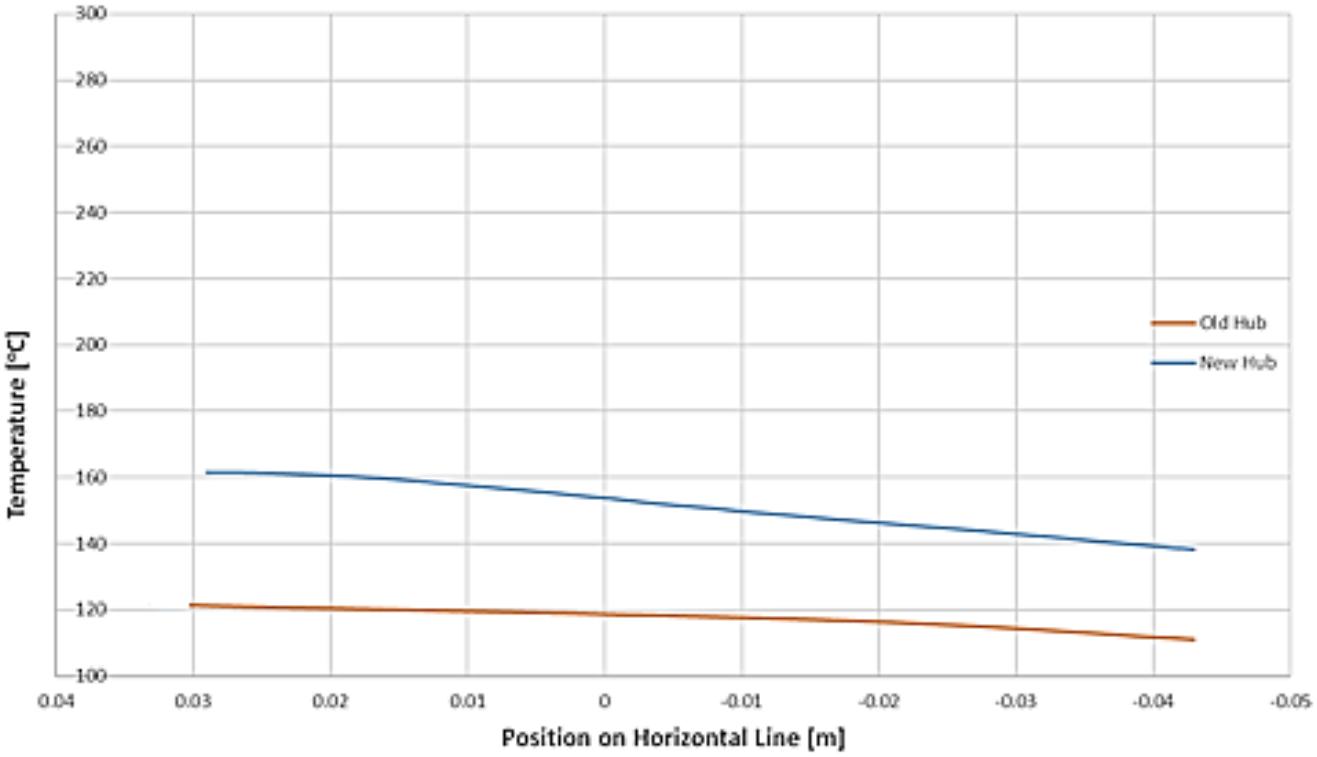

Figure 5-13 temperature distribution from line 2 on both models.

The same six areas in figure 4-14 have been monitored to gain an understanding of the heat transfer coefficient in the new hub. The dark blue areas are again prominent on the back of the cooling disc fins due to the rotation, giving a coefficient at point 4 that is within 1% of the value on the baseline model. At point 6 where the motor bearing sits, the value is identical at the four rotational speeds. This was calculated on the baseline model and found to be within 1% of the baseline model. This is unsurprising as the shaft dimensions are identical for both models. 201 is the highest value on the baseline model occurs at point 3 at 3000rpm where the cooling disc connects to the hub body. The highest value on the new hub occurs at the same location however the value is 143, 28.86% lower. The importance of this point and its value, enables an understanding in how the difference in geometry affects the overall temperature of the model. This is due to the effect the fins and the reduced wall thickness have on the baseline model, compared to the new hub. Point 3 is significant as it is located to highlight the differences in the models.

Point 2 on the baseline model is located before the fin sections giving a value of 84 at 3000rpm. At the same point on the new hub the value is 101 an increase of 16.83%. The difference between the models is that at this point on the new hub the point is located above the hole sections being used to provide the reduction in heat transfer. On the baseline model the finned sections utilised to carry out the same task are not in use at point two, which would suggest why the heat transfer coefficient is lower at this point.

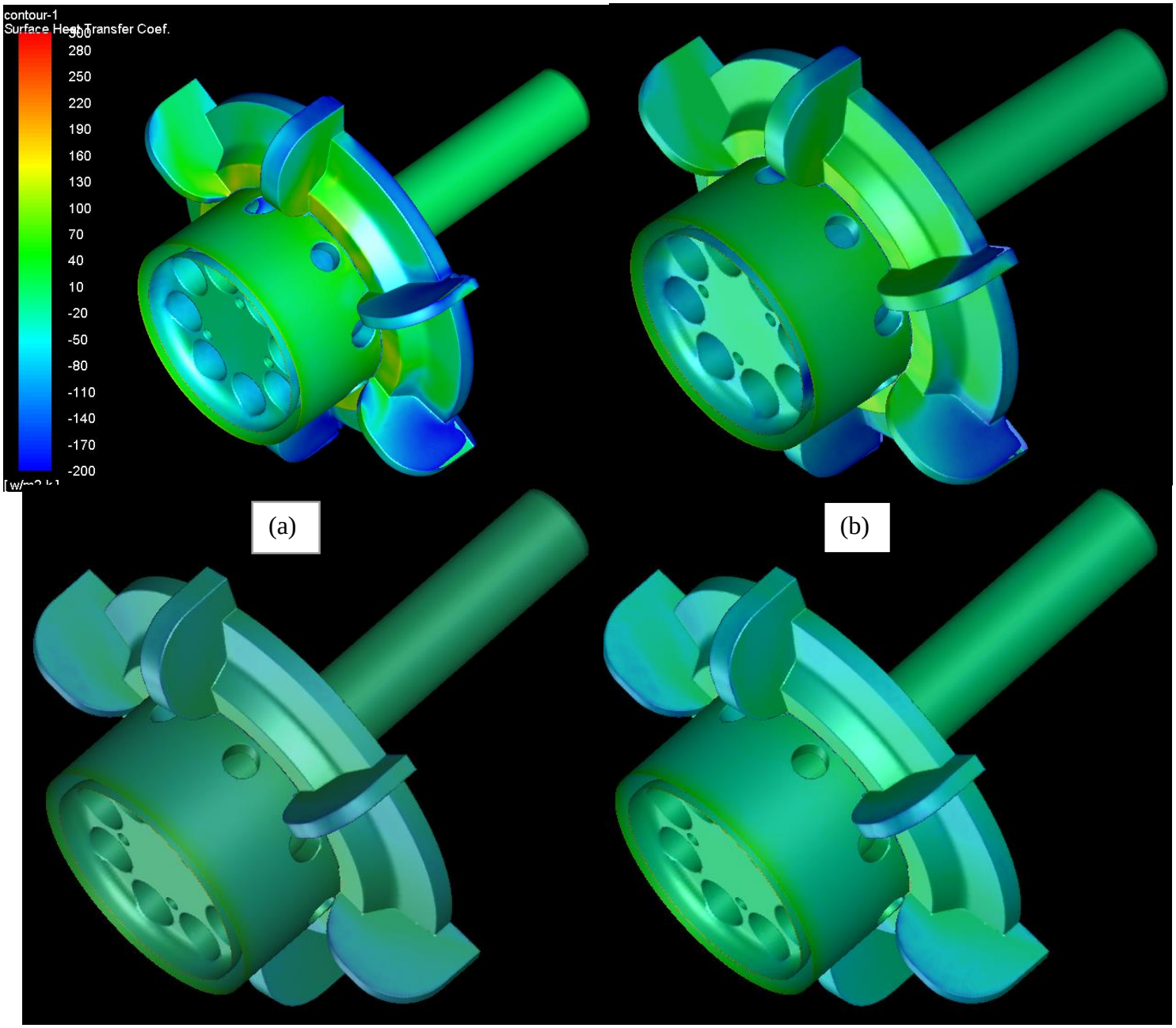

Figure 5-14 Heat transfer coefficient plots of the new hub for (a) 3000rpm (b) 2250rpm (c) 1500rpm and (d) 1000rpm

5.5. Summary

From the experimental and CFD analysis of both the baseline model and the new hub it is clear that the baseline model is more effective at dissipating heat. At the point 4 located on the shaft where the motor bearing would be located on a direct drive fan the temperature is 22.06% lower on the baseline model on average. This new hub model can be used however for heat dissipation but only at rotational speeds of 2250rpm and above. With regard to the stress analysis carried out the one-piece construction of the new hub reduced the overall stresses, displacement and increased the natural frequencies of the model.

Chapter 6 Conclusions

From the results for stress, displacement, natural frequencies and the thermal analysis obtained in the previous chapters, this chapter presents the conclusions drawn from this work. The achievements are summarised with respect to the reach search aims set out at the start of the study.

8.1. Research Problem Synopsis

The baseline model presented is known to be difficult and time-consuming to manufacture. It is however proven to be successful at dissipating heat from the shaft of a high temperature fan. A new hub is required than can be developed to improve on the complex manufacturing issues whilst retaining the heat dissipation properties The literature review found numerous studies that were able to provide gaps in the existing knowledge. This included research on high temperature rotating machinery and the techniques used to prevent the bearings from overheating. A number of examples were found that showed how the use of a Design For Manufacture DFM and Design For Manufacture Assembly DFMA study can be utilised to simplify a part through its design. A limited number of examples provided information on the use of apparatus for high temperature fan units with gaps identified within the knowledge. A summary of the primary aims of the thesis has been provided in the following works, with the achievements and contributions.

8.2. Research Aims and Major Achievements

From the literature review the main aims of the thesis are:

Research Aim #1: To investigate the structural and thermal characterises of a high temperature fan hub

Achievement #1: This study provides an investigation into the stresses on the baseline model caused by the operational rotational speeds it performs under. This include the von mises stress to find the yield of the model and the first principle stresses on the models welding regions. Similarly, the displacement of the model has been investigated under the same loading to assess what deformation of the model occurs. To investigate the natural frequencies of the model a modal analysis has been carried out and the resulting mode shapes analysed. To assess the thermal characteristics of the hub a numerical simulation has been carried out that looks at the temperatures and heat transfer coefficient within the model at various points for the different operating speeds. This data has then been validated experimentally using a purpose built test rig.

Achievement #2: Using the research from the literature review into ways of simplifying designs using design for manufacture and design for manufacture assembly a study was conducted. This study looked into the current manufacturing method to assess the processes being undertaken. Taking this and other aspect such as travel time into consideration a cost was calculated for the baseline hub design. Using this information a new hub of hub has been created based on the DFM and DFMA principles. This was carried out in addition to the structural and thermal analysis to assess the models current properties.

8.3. Thesis Conclusions

Research Objective #1: To carry out stress analysis of a baseline high temperature fan hub design

Conclusion #1: From the investigations into the von mises stress a number of points were highlighted to be causing concentrated areas of stress on the baseline hub design. Whilst these values were acceptable for operation, it was interesting to note that the baseline has these stress raising points. Possible considerations should be made before increasing the operation stresses on the design. The first principle stress analysis looked at the welded areas of the model and again found the stress values acceptable. The displacement of the model was carried out and found insignificant movement in the model from the stress applied. The modal analysis looked at 8 mode shapes and the natural frequencies of them. The lowest natural frequency value was found to be significantly higher than the highest operational frequency.

Research Objective #2: To carry out thermal analysis of a baseline high temperature hub design

Conclusion #2: From the investigations into the heat dissipating properties of the baseline high temperature hub, it was found that the fin arrangement used provides effective dissipation of heat away from the shaft. This is perhaps unsurprising due to the number of studies found during the literature review that utilised fins to reduce rotating shaft temperatures. Moreover, the use of a thin wall section helped to keep the heat transfer through the model low. These results were able to be validated experimentally.

Research Objective #3: To investigate the effects of the operating speed of a high temperature fan hub on its structural and thermal characteristics

Conclusion #3: From the investigations regarding the rotational speed, it can be concluded that the four rotational speeds, 1000, 1500, 2250 and 3000rpm affect the hub differently. The highest rotational speed 3000rpm provides the highest reduction in temperature at the point where the motor bearing sits. Consequently, the same speed is found to have the highest areas of stress.

Research Objective #4: To carry out a design for manufacture study for high temperature fan hubs and develop an innovative hub design

Conclusion #4: From the investigations into DFM and the methods gathered from the literature review, an assessment of the baseline design was conducted. This looked at reducing the number of individual parts the hub is manufactured from. To achieve this an assembly analysis was carried out. In addition to this a material analysis concluded that the new hub could be machined from a single material. With this knowledge and that of heat transfer principles a

design was created that machined the new hub design as a single part, thus eliminating any welding and fabrication processes.

Research Objective #5: To establish the design superiority of the new hub design compared to the baseline design

Conclusion #5: From the investigations into DFM and DFMA the resulting design created was found to cost 31% less than the baseline model. The machined single part design enabled the stresses and displacement to be reduced, primarily because of the elimination of the welded sections. The model performed adequately with regard to the thermal analysis however was not as effective at dissipating heat as the baseline model.

8.4 Thesis Contributions

The contributions of this study include the creation of a novel hub that can be used to dissipate heat from a rotating fan shaft. The creation of the hub was based on design for manufacture principles to make the manufacturing process more efficient.

8.5 Recommendations for Future Work

The new hub improved the cost, time and complexity to manufacture fulfilling part of the motivation for the thesis. However, the heat dissipation properties were not found to be as effective. The current design needs some modifications to achieve the heat transfer capabilities of the baseline model.

References

1- Exporting axial and centrifugal fans to Europe. (n.d.). Retrieved May 10, 2018, from https://www.cbi.eu/market-information/pipes-process-equipment/axial-centrifugal-fans/
2- Fan Application Guide - CIBSE TM42: 2006. (2006).
3- Ingham, G. (2011). *Wind Turbine Blade Analysis using the Blade Element Momentum Method.* (Master's thesis, Durham University) (pp. 1-8). Durham University.
4- Kelly, P. A. (2008, April 18). 4.4 Rotating Discs. Retrieved May 8, 2018, from http://homepages.engineering.auckland.ac.nz/~pkel015/SolidMechanicsBooks/Part_II/04_ElasticityPolar/ElasticityPolars_04_BodyForcesRotatingDiscs.pdf
5- S. M. Yahya (10 October 2010). 14. Turbines Compressors And Fans (4th Edition)
6- Bergman, T. L., & Incropera, F. P. (2011). Fundamentals of heat and mass transfer (7th ed.). Hoboken, NJ: Wiley.
7- Boothroyd, G., Dewhurst, P., and Knight, W. A. (2011). *Product design for manufacture and assembly* (3rd ed.). London;Boca Raton, Fla;: CRC.
8- Sharma, J. N., Sharma, D., & Kumar, S. (2011). Analysis of Stresses and Strains in a Rotating Homogeneous Thermoelastic Circular Disk by using Finite Element Method. *International Journal of Computer Applications (0975 – 8887), 35*(13). Retrieved May 8, 2018.
9- Wong, V. H. (2002). *Finite Element Analysis and Improvement of Impeller Blade Geometry* (Master's thesis, Griffith University). Griffith University.
10- Poirier, J. (2011). *Effective Stiffening of Thin Rotating Disks using Shape Memory Alloys* (Unpublished thesis). McGill University.
11- Rajanand, M. P. (2016). Design & Analysis of Centrifugal Pump Impeller by FEA. *International Research Journal of Engineering and Technology (IRJET), 03*(01). Retrieved May 8, 2018.
12- L. A. Zainullin, M. V. Kalganov, D. V. Kalganov, V. F. Yarchuk, (2015) Cooling the rotating shaft of a high-temperature furnace fan, Steel in Translation, 45 (9) 646-649
13- Aziz, A., & Khani, F. (2010). Analytic solutions for a rotating radial fin of rectangular and various convex parabolic profiles. Communications in Nonlinear Science and Numerical Simulation, 15(6), 1565-1574.
14- Watel, B., Harmand, S., and Desmet, B. (2000). Influence of fin spacing and rotational speed on the convective heat exchanges from a rotating finned tube. International journal of heat and fluid flow, 21(2), 221-227.
15- Xie, M., Xue, Z., Qu, W., & Li, W. (2015). Experimental investigation of heat transfer performance of rotating heat pipe. Procedia Engineering, 99, 746-751.
16- Mori, M., Novak, L., & Sekavčnik, M. (2007). Measurements on rotating blades using IR thermography. Experimental Thermal and Fluid Science, 32(2), 387-396.
17- Gai, Y., Kimiabeigi, M., Widmer, J. D., Chong, Y. C., Goss, J., SanAndres, U., & Staton, D. A. (2017). Shaft cooling and the influence on the electromagnetic performance of traction motors. Paper presented at the 1-6. doi:10.1109/IEMDC.2017.8002307
18- Mahesh, C., & Valavade, A. P. (2016). Flow and heat transfer analysis of variable diameter circular pillar disc brake rotor using CFD. Paper presented at the 146-153. doi:10.1109/ICMAE.2016.7549525

19- Heidarpour, A., Tofts, N. S., Korayem, A. H., Zhao, X., & Hutchinson, C. R. (2014). Mechanical properties of very high strength steel at elevated temperatures. *Fire Safety Journal, 64,* 27. doi:10.1016/j.firesaf.2014.01.006
20- Sultan, M. A. (1996). *A model for predicting heat transfer through noninsulated unloaded steel-stud gypsum board wall assemblies exposed to fire*. Quincy: Springer. doi:10.1007/BF01040217
21- Belhocine, A., and Bouchetara, M. (2012). Thermal analysis of a solid brake disc. *Applied Thermal Engineering, 32,* 59-67. doi:10.1016/j.applthermaleng.2011.08.029
22- Stika, L. A, Megherelu, G., and Vilag, V. A. (n.d.). Numerical Study of a Gas Turbine's Shaft Cooling. In *Sustainable Solutions for Energy and Environment, EENVIRO 2016,*. Energy Procedia.
23- Chai, F., Tang, Y., Pei, Y., Liang, P., & Gao, H. (2016). Temperature field accurate modeling and cooling performance evaluation of direct-drive outer-rotor air-cooling in-wheel motor. *Energies, 9*(10), 818. doi:10.3390/en9100818
24- Pahl, G., Wallace, K., & Blessing, L. (2007). *Engineering design: A systematic approach* (3rd ed.). London: Springer.)
25- Venkatachalam, A. R., Mellichamp, J. M., & Miller, D. M. (1993). A knowledge-based approach to design for manufacturability. *Journal of Intelligent Manufacturing, 4*(5), 355-366. doi:10.1007/BF00123780
26- Venkatachalam A.R., Mellichamp J.M., Miller D.M. (1993) Automating design for manufacturability through expert systems approaches. In: Parsaei H.R., Sullivan W.G. (eds) Concurrent Engineering. Springer, Boston, MA
27- Wiess, J., George, C., & Walker, J. (2006). Redesigning an Appropriate Technology Shredder for Manufacture in a Developing Country. *International Journal for Service Learning in Engineering, 1*(1), 11-26. Retrieved May 8, 2018.
28- Kerbrat, O., Mognol, P., & Hascoët, J. (2011). A new DFM approach to combine machining and additive manufacturing. *Computers in Industry, 62*(7), 684-692. doi:10.1016/j.compind.2011.04.003
29- Ong, S. K., Sun, M. J., & Nee, A. Y. C. (2003). A fuzzy set AHP-based DFM tool for rotational parts. *Journal of Materials Processing Tech, 138*(1), 223-230. doi:10.1016/S0924-0136(03)00076-1
30- Boothroyd, G. (1987). Design for assembly The key to design for manufacture. *The International Journal of Advanced Manufacturing Technology*. doi:10.1007/BF02601481
31- Ashley, S. (1995, March 1). Cutting costs and time with DFMA. *Mechanical Engineering-CIME*.)
32- Gerhardt, D. J., Hutchinson, W. R., & Mistry, D. K. (1991). Design for manufacture and assembly: Case studies in its implementation. *The International Journal of Advanced Manufacturing Technology, 6*(2), 131-140. doi:10.1007/BF02601436)
33- Rao, S. S. (2018). *The finite element method in engineering* (Sixth ed.). Oxford, United Kingdom: Butterworth-Heinemann, an imprint of Elsevier.
34- Logan, D. L. (2017). A first course in the finite element method (Sixth, SI. ed.). Andover: Cengage Learning.
35- Ansys. (2006, December). Heat Transfer Modelling. Retrieved May 8, 2018, from http://www.engr.uconn.edu/~barbertj/CFD Training/Fluent/6 Heat Transfer Modeling.pdf

36- Patankar, S. V. Spalding, D. B. (1972) A Calculation Procedure for Heat, Mass and Momentum Transfer in Three-Dimensional Parabolic Flows, Heat and Mass Transfer, vol. 15, pp: 1787 – 1806
37- Venkatakrishnan, V. (1993) "On the Accuracy of Limiters and Convergence to Steady State Solutions", Technical Report, American Institute of Aeronautics and Astronautics, vol. 93, pp: 880
38- Nagaraja, D. (2001). *LASER CUTTING MACHINE: JUSTIFICATION OF INITIAL COSTS* (Master's thesis, University of North texas). University of North texas.
39- British Standards Institution (1994). BS5500: Specification for Unfired Fusion Welded Pressure Vessels
40- British Standards Institution (2015). BS7608: Guide to fatigue design and assessment of steel products. Retrived from (https://www.bsigroup.com/PageFiles/435651/BS%207608%202014%20preview.pdf)
41- Temperature limits. (n.d.). Retrieved from http://www.skf.com/uk/products/bearings-units-housings/ball-bearings/self-aligning-ball-bearings/temperature-limits/index.html
42- Dargie, P.P., Parmeshwar, K., and Wilson, W.R.D. MAPS-1: Computer-aided design system for preliminary material and manufacturing process selection, ASME Trans., 104, 126–136, January 1982.